Distinct types of intramitochondrial protein aggregates protect mitochondria against proteotoxic stress

vom Fachbereich Biologie

der Rheinland-Pfälzischen Technischen Universität Kaiserslautern-Landau

zur Verleihung des akademischen Grades Dr. rer. nat. genehmigte

Dissertation

von

Lea Tamara Bertgen, M.Sc., geb. in Neustadt/ Weinstraße

Mündliche Prüfung: 18.12.2023

Dekan: Prof. Dr. Stefan Kins

Promotionskommissionsvorsitzender: Prof. Dr. Matthias Hahn

Berichterstattende: Prof. Dr. Johannes M. Herrmann

Prof. Dr. Tanja Maritzen

D 368

EIDESSTATTLICHE ERKLÄRUNG

Hiermit erkläre ich, dass die vorliegende Arbeit ohne unzulässige Hilfe Dritter und ohne Benutzung anderer als der angegebenen Hilfsmittel von mir persönlich angefertigt wurde. Die aus anderen Quellen übernommenen Daten und Konzepte sind unter Angabe der Quelle gekennzeichnet.

Ich habe nicht die entgeltliche Hilfe von Vermittlungs- beziehungsweise Beratungsdiensten in Anspruch genommen. Niemand hat von mir unmittelbar oder mittelbar geldwerte Leistungen für Arbeiten erhalten, die im Zusammenhang mit dem Inhalt der vorgelegten Dissertation stehen.

Die Arbeit wurde bisher weder im In- noch im Ausland in gleicher oder ähnlicher Form einer anderen Prüfungsbehörde vorgelegt.

Die Bestimmungen der Promotionsordnung des Fachbereichs Biologie der Universität Kaiserslautern sind mir bekannt. Insbesondere weiß ich, dass ich vor Vollzug der Promotion zur Führung des Doktortitels nicht berechtigt bin.

Lea Tamara Bertgen

Kaiserslautern, den 24.10.2023

Darlegung des Eigenanteils

Die Messung aller massenspektrometrischen Daten (Abb. 13, 19, 33, 34) wurden von Markus Räschle, Center for MS Analytics, RPTU Kaiserslautern, durchgeführt. Die Probenvorbereitung für die co-Immunoprezipitation der Pim1-Mutanten (Abb. 19) erfolgte gemeinsam mit Tim Schneckmann im Rahmen seiner Masterarbeit. Alle statistischen Auswertungen zu diesen Experimenten wurden von Jan-Eric Bökenkamp durchgeführt und die Daten wurden von Christian Koch mit Hilfe von R Studio geplottet. Die Analyse des Hefe-Proteoms in Bezug auf die Aminosäure-Anteile wurde von Timo Mühlhaus durchgeführt (Figure 23B).

Die vorliegende Einschätzung über die erbrachte Leistung von Dritten wurden mit den genannten Personen einvernehmlich abgestimmt.

Lea Tamara Bertgen   Prof. Dr. Johannes M. Herrmann

Kaiserslautern, den 24.10.2023

DARLEGUNG ALLER BENUTZTEN HILFSMITTEL UND HILFESTELLUNGEN

Zur Erstellung dieser Arbeit wurde das Microsoft Office 365 Softwarepaket (Word und Excel) genutzt. Das Literaturverzeichnis und Literaturverweise wurden mittels Citavi erstellt. Alle statistischen Analysen erfolgten mittels Microsoft Excel oder R Studio. Alle gezeigten Abbildungen wurden mit Hilfe der Corel Technical Suite 2020 erstellt. Strukturdarstellungen wurden mittels ChimeraX visualisiert. Mikroskopische Aufnahmen wurden mit dem Softwarepaketen Fiji und Leica LasX analysiert. Zur Quantifizierung aller Western Blot Experimente wurde die Software ImageQuant genutzt. Zur Überprüfung des Textes wurde die Software Grammarly verwendet.

Lea Tamara Bertgen

Kaiserslautern, den 24.10.2023

LIST OF PUBLICATIONS

2023   **Bertgen L.**, Bökenkamp J., Schneckmann T., Koch C., Räschle M., Storchova Z., Herrmann J.M., Distinct types of intramitochondrial protein aggregates protect mitochondria against proteotoxic stress, submitted

2023   Schilling S., Pradhan A., Heesch A., Helbig A., Blennow K., Koch C., **Bertgen L.**, Koo E.H., Brinkmalm G., Zetterberg H., Kins S., Eggert S., Differential effects of familial Alzheimer's disease-causing mutations on amyloid precursor protein (APP) trafficking, proteolytic conversion, and synaptogenic activity, Acta Neuropathol Commun., doi: 10.1186/s40478-023-01577-y.

2023   **Bertgen L.**, Flohr T., Herrmann J.M., Methods to Study the Biogenesis of Mitoribosomal Proteins in Yeast, Methods Mol Biol. Book series (MIMB, volume 2661: 143-161), doi: 10.1007/978-1-0716-3171-3_10

2020   **Bertgen L.**, Mühlhaus T., Herrmann J.M., Clingy genes: Why were genes for ribosomal proteins retained in many mitochondrial genomes?, Biochim Biophys Acta Bioenerg., doi: 10.1016/j.bbabio.2020.148275

TABLE OF CONTENTS

VIII

SUMMARY

Proteins need to be folded into their native conformation to fulfill their function. However, perturbations of the transport, folding, and assembly lead to the misfolding of proteins and challenge cellular protein homeostasis (proteostasis). Therefore, cells evolved an elaborate chaperone and protease network to deal with such conditions. Chaperone-mediated protein folding and proteasomal degradation clear the cytosol from misfolded proteins. Moreover, misfolded proteins can be sequestered into aggregates to lower the proteostasis network's workload and reduce toxic effects. Proteins imported into mitochondria fold and assemble only upon successful import and are, therefore, no longer subject to cytosolic quality control. Mitochondrial chaperones and proteases that are part of the mitochondrial proteostasis network have been identified and characterized. Still, factors that facilitate, control, and resolve aggregates for the sequestration of misfolded proteins are largely unknown.

In this study, I aimed to characterize the formation of protein aggregates in the mitochondrial matrix. On the one hand, I elucidated the role of the matrix disaggregase, Hsp78. Hsp78 associates with protein aggregates upon the induction of heat stress or when misfolded model proteins are imported into the mitochondrial matrix. By employing microscopy and proteomic analysis, I showed that Hsp78 interacts with protein aggregates and helps to recover from stress by refolding them. At the same time, non-productive refolding of aggregates leads to proteolytic degradation via the matrix master protease Pim1. On the other hand, I identified the mitochondrially encoded protein Var1 as a novel component of the matrix proteostasis network. Var1 is a mitochondrially encoded protein of the mitochondrial ribosome, but I discovered that Var1 has a second, independent function as it induces the formation of aggregates, which I named Var1 bodies. This aggregation-prone behavior is associated with the proteins' unusual sequence of many asparagine repeats. Hsp78 and Var1 bodies are distinct structures, absorbing different sets of proteins. Moreover, whereas Hsp78 aggregates form only transiently, Var1 bodies are persistent and are not resolved once stress conditions are over.

My findings show that the formation of aggregates in the matrix shows clear parallels to that in the cytosol: Hsp78, like Hsp104, binds various protein aggregates from which some get un- and refolded while others are degraded by the Pim1 protease. Var1, on the other hand, acts like the

cytosolic prion-protein Rnq1 that forms insoluble protein deposits that absorb and sequester other cellular proteins.

ZUSAMMENFASSUNG

Proteine müssen in ihre native Konformation gefaltet werden, damit sie ihre Funktion erfüllen können. Störungen des Transports, der Faltung und der Assemblierung führen zur Aggregation fehlgefalteter Proteine und stellen somit ein großes Problem für die zelluläre Proteinhomöostase (Proteostase) dar. Deshalb haben Zellen ein komplexes Chaperon- und Proteasen-Netzwerk entwickelt, um solchen Bedingungen effektiv entgegenzuwirken. Die durch Chaperone vermittelte Proteinfaltung und der proteolytische Abbau befreien das Zytosol von fehlgefalteten Proteinen. Darüber hinaus können fehlgefaltete Proteine in Aggregaten sequestriert werden, um die Last für das Proteostase-Netzwerks gering zu halten und gleichzeitig toxische Effekte zu reduzieren. Dies stellt allerdings ein Problem für die meisten mitochondrialen Proteine dar. Da die Faltung und der Zusammenbau innerhalb der Mitochondrien erfolgt, unterliegen importierte mitochondriale Proteine nicht mehr der zytosolischen Qualitätskontrolle. Mitochondriale Chaperone und Proteasen wurden bereits identifiziert und charakterisiert, aber Faktoren, die die Bildung von Aggregaten für die Sequestrierung fehlgefalteter Proteine erleichtern, kontrollieren und auflösen, sind weitgehend unbekannt.

In dieser Studie wollte ich die Bildung von Proteinaggregaten in der mitochondrialen Matrix charakterisieren. Zum einen habe ich die Rolle der Matrix-Disaggregase Hsp78 untersucht. Hsp78 assoziiert mit Proteinaggregate, die durch Hitzestress oder den Import fehlgefalteter Modellproteine in die mitochondriale Matrix, induziert werden können. Durch Mikroskopie und Proteom Analysen konnte ich zeigen, dass Hsp78 mit Proteinaggregaten interagiert und an der Erholung von Stress beteiligt ist, indem es einige Proteinaggregate entfaltet. Während Einschränkungen bei der Entfaltung von Proteinaggregaten zu deren proteolytischen Abbau durch die Masterprotease der Matrix, Pim1 führen. Andererseits konnte ich zeigen, dass das mitochondrial kodierte Protein Var1 eine neue Komponente des Matrix-Proteostase-Netzwerks ist. Var1 ist Teil des mitochondrialen Ribosoms und für die Translation mitochondrial kodierter Proteine essentiell. Ich habe herausgefunden, dass Var1 eine zweite, unabhängige Funktion hat, da es die Bildung von Aggregaten induziert, die ich hier als Var1-Bodies beschreibe. Ein sehr hoher Gehalt an Asparagin Resten in der Var1-Sequenz macht das Protein anfällig zur Bildung von Aggregaten. Hsp78- und Var1-Bodies sind unterschiedliche Strukturen und lassen sich durch unterschiedliche Zusammensetzung and Proteinen charakterisieren. Außerdem bilden

sich Hsp78-Aggregate nur vorübergehend, während Var1-Bodies persistent sind und nicht aufgelöst werden, sobald die Stressbedingungen vorbei sind.

Meine Ergebnisse zeigen, dass die Bildung von Aggregaten in der Matrix deutliche Parallelen zu der im Zytosol aufweist: Hsp78 bindet wie Hsp104 verschiedene Proteinaggregate, von denen einige ent- und wiedergefaltet werden, während andere durch die Protease Pim1 abgebaut werden. Var1 hingegen wirkt wie das zytosolische Prion-Protein Rnq1, das unlösliche Proteinablagerungen bildet, die andere zelluläre Proteine absorbieren und sequestrieren.

1 INTRODUCTION

Eukaryotic cells are divided into different biochemical compartments. These membrane-bound structures, or organelles, fulfill specialized functions and allow opposite reactions to take place at the same time. Most proteins required for these reactions are first synthesized in the cytosol and subsequently targeted to their cognate organelle. Cells employ an intricate network of chaperones, proteases, and other quality control factors to ensure that proteins reach their final destination and are properly assembled [1]. The model organism *Saccharomyces cerevisiae*, which will be further referred to as yeast, was vital in unraveling the components, functions, and regulations of the quality control system [2,3].

1.1 Protein homeostasis

Cells depend on a functional proteome, which is mediated by a process described as protein homeostasis (proteostasis) [4]. Insults on the intricate balance between protein synthesis, folding, and degradation lead to the accumulation of misfolded proteins, which can form protein aggregates [5]. The loss of proteostasis and the presence of protein aggregates are hallmarks of aging and neurodegenerative diseases [6–8]. Therefore, protein folding is a major interest in classical biochemistry.

1.2 Proteostasis network

After the synthesis of a protein, it needs to reach its proper three-dimensional topology to fulfill its function. The information for correct folding is encoded within the amino acid sequence, as described by Anfinsen's dogma, which states that proteins can spontaneously reach their native state [9]. Nevertheless, proteins can get stuck in folding intermediates or misfolded states, which are energetically favorable. These situations demand the assistance of other proteins (chaperones) to overcome such hurdles (Figure 1) [10]. Collapsed proteins can form globular structures that expose hydrophobic regions and can be stabilized via non-native interactions, also described as amorphous aggregates. More thermodynamically stable forms with defined β-sheets stacked on top of one another can grow from a single seed over oligomer soluble states into large, toxic fibrils when proteostasis fails [11]. These aggregates are problematic since they form in a concentration-dependent manner [12]. Therefore, cells evolved distinct strategies to

counteract protein aggregates. First is the presence of molecular chaperones that act in protein folding, restricting aggregate formation and promoting correct refolding [13,14]. The second strategy relies on the ubiquitin-proteasome system to degrade misfolded proteins and protein aggregates [15]. Under extreme stress conditions, a third defense strategy of sequestration becomes important [16].
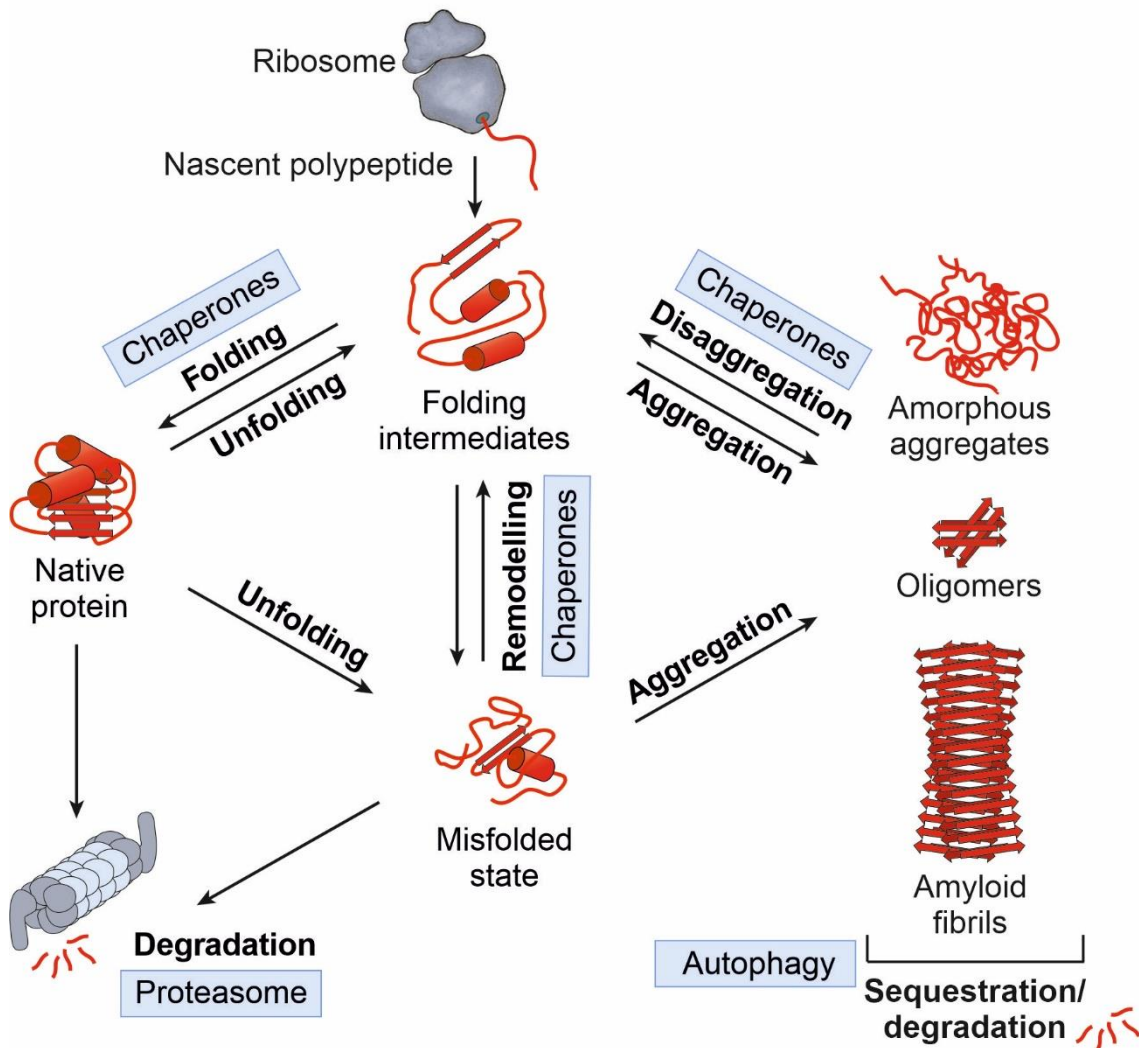
Figure 1:The proteostasis network. The proteostasis network describes the balance between protein synthesis, folding, and degradation. The nascent chain of newly translated proteins interacts with chaperones that help to find their native conformation. Chaperones either keep proteins unfolded or refold and disaggregate misfolded and aggregated proteins. Misfolded proteins can also be cleared via the ubiquitin-proteasome system or from larger aggregated structures sequestered into specific cellular sites. Modified from Hartl et al., 2011 [17].

1.2.1 Cytosolic chaperones and proteases

In the first line of defense against proteotoxic stress, chaperones mediate the correct folding and refolding without being part of the native protein, typically recognizing exposed hydrophobic regions of misfolded or aggregated proteins [18]. Many are upregulated in

response to stress conditions and are known as heat-shock proteins (HSPs) [19]. Different unrelated groups of HSPs exist, and the nomenclature (often) follows the molecular weight of these proteins (Hsp70, Hsp60, Hsp90; Hsp100, small Hsps) [20]. The protective role of chaperones can be divided into the prevention of aggregates by binding to unfolded chains, called holdases, and the active refolding of proteins, which is an ATP-dependent process mediated by foldases [21]. The major protein families of the proteostasis network, including the five chaperone classes and the proteasome, will be described in the following (Figure 2):

Hsp70 (DnaK) class proteins bind nascent chains to prevent misfolding. They have a combined foldase and holdase function. Substrate binding is mediated by another member of the chaperone network, namely the Hsp40 (DnaJ) family. Cycles of ATP binding, hydrolysis, and nucleotide release, mediated by a nucleotide exchange factor (NEF), lead to conformational changes in the carboxyl-terminal (C-terminal) domain of Hsp70. In the closed conformation, the substrate is held between a β-sandwich subdomain and the α-helical lid domain. This process stabilizes the unfolded substrate and prevents misfolding. Cycles of (re)binding and release allow proteins to reach their correct folding [22,23].

Downstream of the Hsp70 system, the Hsp90s control various cellular processes. Hsp90 forms dimers regulated via co-chaperones and other proteins, most interacting via tetratricopeptide repeats (TPR) with other proteins [24]. The C-terminal ends dimerize upon ATP-binding comprising a "molecular clamp" with their N-terminal ends. The inactive substrate gets wrapped with the individual Hsp90 monomers twisting around it. Cofactors stimulate or restrict this state before ATP hydrolysis is triggered, and the active substrate can be released [25].

The large octameric complex of the chaperonin group II is also located in the cytosol. In contrast to other chaperones, chaperonins enclose substrates, allowing them to fold in a chamber separated from their usual environment. The archaeal-derived CCT/ TriC forms a barrel made out of 8 identical subunits with apical finger-like domains that allow the enclosure of substrates inside the chamber of the double-sided ring. These segments also open and close in an ATP-dependent manner, enclosing and releasing the substrate [26].

Further components of the proteostasis network are found in the ATPases associated with diverse cellular activities (AAA+ protein) superfamily [27,28]. These proteins are characterized by a conserved ATPase domain, while additional modules provide them with extra functions

and the ability to interact with cofactors [29,30]. Hexamers form a central tunnel that processes substrates through interactions of aromatic residues in the pore loops with misfolded proteins. The ATPase domains are arranged in a pseudo-staircase configuration, matching the confirmation of the pore loops that intercalate with the substrate in an ATP-bound state [31]. In contrast, ADP and non-nucleotide subunits do not interact with substrates. This suggests hydrolyzation in the lowest subunit acting as a power stroke pulling the substrate through the central pore, like a hand-over-hand mechanism pulling a rope [32]. One major group (Type II ATPases) contains the Hsp100 family that consists of two staked rings in tandem. This includes the cytosolic Hsp104 that untangles and unfolds protein aggregates, also called disaggregase [33–35]. The N-terminal domain is responsible for recruitment and interaction with substrates; however, in the case of Hsp104, the interaction is mediated by the small heat-shock protein Hsp42 [36].

Other members of the AAA+ family include proteases that unravel and degrade proteins. The 26S proteasome of the cytosol has a proteolytic domain atop the ATPase domain [37–39]. Substrates are marked by ubiquitin chains covalently bound to proteins. [40]. These chains are later removed by deubiquitinating enzymes, which are associated with the proteasomal lid [41].
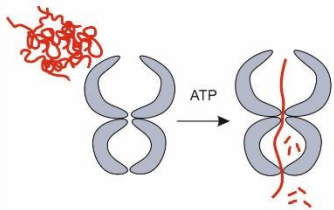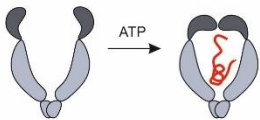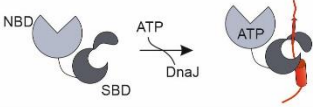
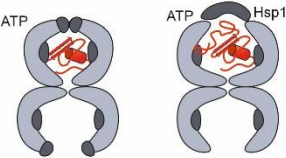| Protein Family	Topology	Cytosol	Mitochondria
AAA+ (Hsp100)		Hsp104 20S	Hsp78 Pim1 Mcx1
Hsp90		Hsp82 Hsc82	
Hsp70		Ssa1-4 Ssb1,2 Ssz1	Ssc1 Ssq1 Ecm10
Hsp60 Group I and II		Tric/ CCT	Hsp60 Tcm62
sHsps		Hsp42	

Figure 2: Topology of major protein families involved in protein folding and degradation in the cytosol and mitochondria. The schematic structure of different chaperone families and proteases are shown in order of size. Hsp100 proteins form hexameric double-ringed structures that disaggregate (Hsp104, Hsp78) and additionally cleave (20S proteasomal core subunit, Pim1) protein aggregates. Hsp90 proteins form dimers that hold unfolded substrates. HSP70s work with DnaJ/ Hsp40 proteins and nucleotide exchange factors (NEFs) to facilitate the folding of newly synthesized proteins in the cytosol and mitochondria and major energetic factors of protein import into mitochondria. Tric/ CCT forms an octameric complex in the cytosol with apical finger-like domains that allow substrate enclosure in a chamber. At the same time, the matrix of mitochondria uses the bacterial-derived heptameric complex made from Hsp60 and the lid Hsp10 to refold proteins. Small heat shock proteins (sHsps) come in many different flavors and act as nucleation factors. Examples of the different proteins from each family in the cytosol and the mitochondrial matrix are mentioned.

1.3 Protein misfolding and aggregation

If the chaperone and proteasome system is overloaded, the sequestration of misfolded proteins into aggregates becomes important [16]. Whereas some of these aggregates are benign and well-tolerated, others are toxic. However, it is often unclear whether these aggregates jeopardize proteostasis or their occurrence is the consequence of proteotoxic conditions. In yeast, these structures are categorized by their composition and localization within the cell [42].

Pathogenic aggregates are formed by a protein containing the disease-causing segment of human huntingtin's human polyglutamine (polyQ) region [43,44]. This protein gets sequestered by the yeast nucleation factor and endogenous polyQ protein Rnq1. This gives rise to insoluble protein aggregates (IPODs), which show a similar pathology to aggresomes found in humans, threatening cellular functions. However, whether the presence of IPOD-inducing Rnq1 increases or reduces fitness depends on the specific conditions; Rnq1 and similar nucleating factors often show cell-specific prion-like variability, presumably to allow an escape of individual cells from threatening conditions [45]. Other nucleation factors, like the small heat shock factor Hsp42, induce the formation of benign cytoQs or Q bodies that can grow into larger structures. Aggregates can be found associated with the nuclear envelope in the cytosol (juxtanuclear quality control aggregates, JUNQs) [42,46] or within the nuclear lumen (intranuclear quality control aggregates, INQs) [47]. Aggregates with a more specialized composition can be formed containing non-assembled proteasomal subunits [48], or for the instance of MitoStores, sequester non-imported mitochondrial precursor proteins [49,50].

1.4 Import into mitochondria

In the case of MitoStores, chaperones, such as the disaggregase Hsp104 and the proteasome, compete for the same substrates under challenging conditions [49]. With the proteasome degrading and Hsp104 disaggregating proteins for subsequent import and productive use after

storage. This is important because proteins need to be unfolded to allow their translocation into mitochondria [51]. Most matrix preproteins possess N-terminal matrix targeting signals (MTS) for efficient targeting [52–54]. The MTS gets recognized by the translocase of the outer membrane (TOM) and is guided through the complex, crossing the intermembrane space (IMS) and the inner mitochondrial membrane (IM) with the help of the translocase of the inner membrane (TIM) [55]. The MTS gets cleaved by the matrix processing peptidase (MPP), and the mature protein can be folded and fulfill its function [52]. The membrane potential across the IM and the ATP-powered import motor, including Ssc1 (an Hsp70 type protein) binding nascent chains, energetically drives the import process [56,57].

1.5 The mitochondrial genome of yeast

Many proteins imported into mitochondria are dedicated to maintaining the organelles' genome, revealing their prokaryotic ancestry [58,59]. However, genetic information was considerably changed during evolution, including substantial reductions. The loss and transfer of genes were driven by redundant genes, the advantages of the nuclear control of expression levels, and enhanced mutation rates in the mitochondrial genome (Muller's Rachet) [60,61]. Still, a small organellar genome comprising a set of tRNAs, rRNAs, and some protein-coding genes were retained. The number of mitochondrially encoded genes varies, ranging from 60 in a protist named *Andalusia godoyi* [62], to 8 in yeast [63] and 13 in humans [64]. These genes predominantly code for subunits of the respiratory chain (in yeast comprising *COX1*, *COX2*, *COX3,* and *COB*) and the ATPase (in yeast comprising *ATP6*, *ATP8,* and *ATP9*) that are polytopic IM proteins (Figure 3). Fungi, plants, and many unicellular organisms also retained additional genes for mitochondrial ribosomal proteins (MRPs) (in yeast *VAR1*) [63]. Most mitochondrial genomes are circular [65]. While the presence of the mtDNA is needed for respiratory growth, the mitochondrial genome is non-essential. Variances from the normal mtDNA (rho^+) are characterized by either extensive mutation or deletions (rho^-) [66] or the complete loss (rho^0) [67], both resulting in a respiratory deficient (petite) phenotype. Transcription occurs in a polycistronic fashion, and the resulting transcripts undergo

maturation. These transcripts are then translated by the organelle's mitochondrial ribosomes (mitoribosomes).
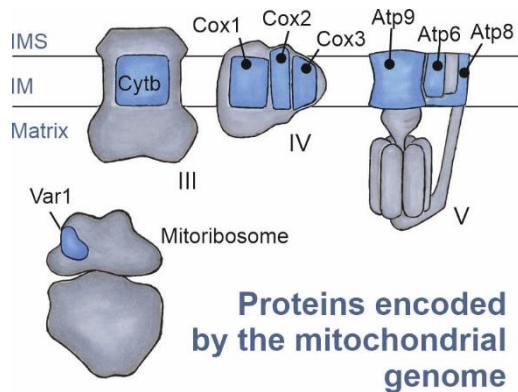
Figure 3: Mitochondrial encoded proteins in yeast. The mitochondrial genome encodes two rRNAs besides a set of tRNAs for eight proteins (blue). Those hydrophobic core components of the oxidative phosphorylation (Cytb, Cox1, Cox2, and Cox3) and the ATP synthase (Atp6, Atp8, and Atp9). The mitochondrial genome also retained the information for the S3 protein of the mitoribosome named Var1.

1.6 Evolution of mitoribosomes

Every eukaryotic group has its own mitoribosome specialized for translating its specific set of proteins. Throughout evolution, mitoribosomes gained several "supernumerary" proteins, along with a reduction of rRNA, making them larger and more protein-rich than their cytosolic counterpart. While humans have no MRPs in their mtDNA, other organisms retained a substantial number of mitoribosomal genes on their mtDNA. The largest number of mitochondrially encoded proteins is found in *Andalusia godoyi,* where 28 of 57 genes for MRPs were retained. Also, plants still contain many mitochondrially encoded MRPs [68]. Interestingly, plastid genomes often have similar sets of MRPs compared to their mitochondrial counterpart, suggesting a conserved pressure to anchor those genes [69,70]. Different factors may have influenced this evolution. Cytb and Cox1 are encoded by the mtDNA in all respiring organisms without exception. These extremely hydrophobic proteins are not import-competent, presumably because the hydrophobic regions are misinterpreted as an endoplasmic reticulum (ER)-targeting sequence [71]. Still, many integral membrane proteins make it as a precursor from the cytosol into mitochondria [72–74]. In contrast to the mitochondrial-encoded proteins, they have a very low abundance [73]. Overexpression of several of these proteins was reported to be toxic [53] and resulted in their mislocalization to the ER [47,48]. Thus, the toxicity of the respiratory chain subunits is probably caused by a combination of high abundance and high

hydrophobicity. This problem is avoided by maintaining the respective genes in organelles (Figure 8A).

Several mitochondrial proteins have the potential to be toxic in the cytosol. For instance, Atp25 is a nuclear-encoded mitochondrial factor that binds and inactivates mitochondrial ribosomes upon stress conditions [75,76]. In its mature form, this protein is highly toxic in the cytosol because it can also attach to the 80S ribosome, inhibiting cytosolic translation (Figure 4B). The synthesis of protein subunits for both the mitochondrial ribosome and the 80S ribosome in the cytosol might have posed a tricky challenge for early eukaryotes. Each ribosome contains about 80 positively charged proteins rich in RNA-binding sites. Potentially, it was the necessity of separating these two groups of ribosomal proteins that forced eukaryotes to relocate 80S ribosome assembly into the nucleus and to preserve the expression of problematic MRPs in mitochondria.

Assembly intermediates of the electron transport chain complexes can be highly harmful [77–81]. Organelles employ efficient feedback loops to avoid the accumulation of non-productive assembly intermediates by a relatively simple mechanism termed CES (control by epistasy of synthesis) that was initially identified in chloroplasts [82]. Protein synthesis in chloroplasts and mitochondria depends on nuclear-encoded control factors (translational activators in mitochondria), which competitively bind to ribosomes and assembly intermediates (Figure 4D). Accumulating non-assembled translation products sequester these factors and thereby switch off their synthesis. This principle was first discovered for the production of the cytochrome b6f complex in plastids of *Chlamydomonas reinhardtii* and later for translational control of the OXPHOS complexes in mitochondria [83–87]. Chloroplasts regulate many proteins by reversible redox modifications of cysteine residues [88,89]. These thiol switches are triggered by light conditions and photosynthetic activity and control protein functions and gene expression. Based on this observation, the CoRR (colocation for redox regulation) hypothesis was proposed, which suggested that organelle genes are co-located with their gene products to allow redox regulation of their expression (Figure 8C) [90,91].
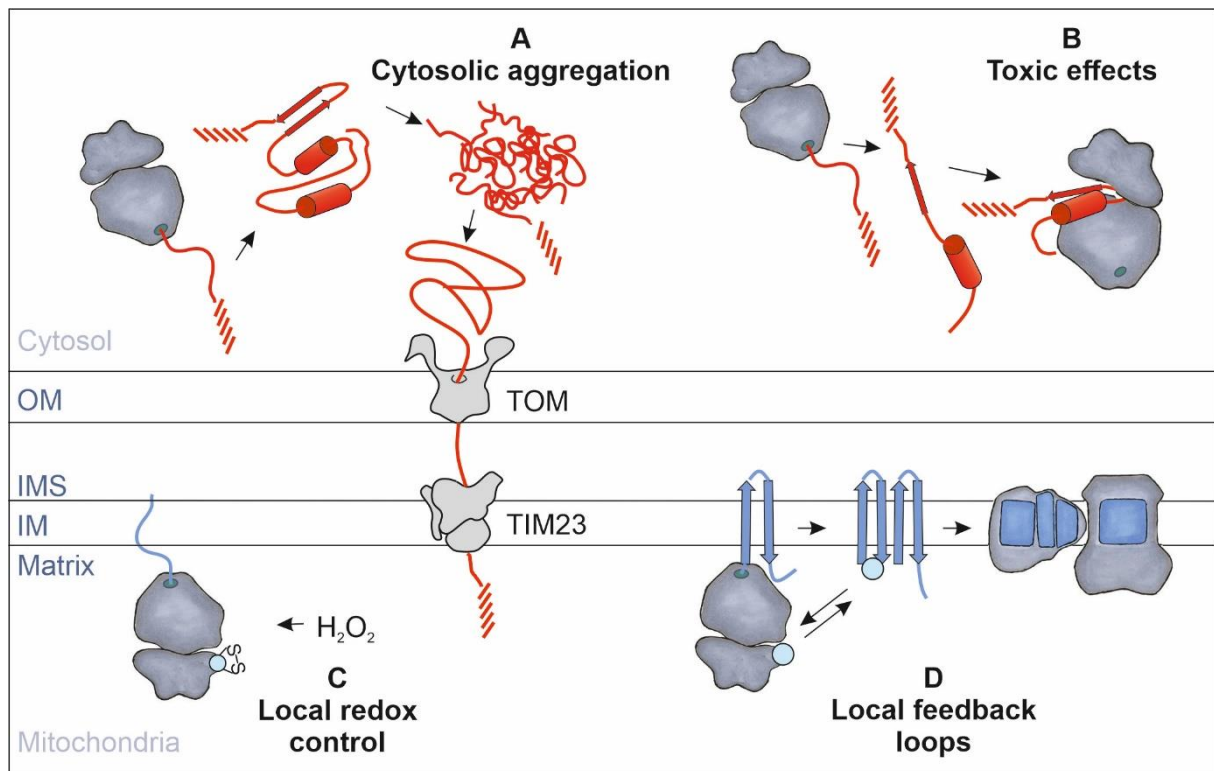
Figure 4: Reasons for the retainment of mitoribosomal genes in organellar DNA. The expression of proteins in the mitochondrial matrix offers several advantages: **A** The synthesis of aggregation-prone hydrophobic membrane proteins in the cytosol is avoided. **B** For example, some matrix proteins cause toxic effects in the cytosol because they interfere with the assembly or function of the cytosolic translation machinery. Expression of these proteins in the matrix prevents these problems. **C** The prevailing local redox conditions can rapidly regulate the expression of proteins in the matrix. **D** Feedback loops can avoid the accumulation of non-productive assembly intermediates, which can be highly toxic, particularly in the case of cofactor-containing reactive centers of redox enzymes.

Expression of yeast's mitochondrially encoded MRP, Var1, also requires a specific translational activator called Sov1 [92–94]. Sov1 is part of a recently described feedback loop that connects Var1 synthesis to mitochondrial ribosome assembly [95]. In the small ribosomal subunit assembly process, the addition of Var1 represents the final step [96]. If Var1 synthesis is switched off, almost complete small subunits accumulate as stable assembly intermediates in the matrix, lacking only three proteins (Var1/uS3m, Mrp2/uS14m, Rsm28/mS46). Upon re-expression of Var1, fully functional ribosomes are rapidly formed. In consistence with the potential role of Var1 as a critical component that determines cellular fitness, Sov1-mediated Var1 expression was reported to regulate the stress resistance and aging of yeast cells [97,98], but the underlying details remain unclear. Why the *VAR1* gene was retained in mitochondria is ambiguous since it was shown that a nuclear-encoded fusion protein with a mitochondrial targeting signal (MTS) is functional [93]. Sections of this paragraph (1.6) were adopted from my review [99].

1.7 The mitochondrial proteostasis network

As described before, matrix proteins only get folded after import is completed. This process is controlled by the chaperones of the mitochondrial proteostasis network. These chaperones, as well as mitochondrial proteases, are upregulated by the mitochondrial induced stress -response. A response that is launched upon insults in the mitochondrial import and the accumulation of precursors in the cytosol. Besides the upregulation of the synthesis of genes coding for mitochondrial chaperones and proteases, the synthesis of other mitochondrial proteins is downregulated to reduce the workload for the cell. [20] While many parts of the quality control system are dedicated to the degradation of precursors, storage of precursors [49], and clearance of the mitochondrial import pore [100], I will be focusing on the components and functions of the matrix proteostasis network.

Due to their proteobacterial ancestry, the composition of the mitochondrial proteostasis network differs from the cytosolic one. The lack of the proteasome is compensated by the presence of the master protease Pim1. Chaperones from only three of the five major chaperone families have been identified, including the Hsp60, Hsp70, and Hsp100, with their mode of action being conserved.

The matrix contains three different proteins encoded by genes of the Hsp70 family named *SSC1*, *SSQ1,* and *ECM10.* With Ssc1 being the most abundant and essential component of the chaperone system. Ssc1 not only drives the import of precursor proteins via its membrane-bound form in the presequence translocase-associated motor (PAM) [56,57]. But also folds proteins encoded by the mitochondrial genome. Ssc1 binds directly to newly synthesized complex V subunits and facilitates their assembly [101]. Showing that Hsp70 also plays a vital role in the biogenesis of mitochondrial complexes. The ATPase activity is controlled by the homolog of the bacterial DnaJ, Mdj1. While the loss is not lethal, protein aggregates are found to be accumulating independent of an import defect. Therefore, Hsp70, in conjunction with Mdj1, mediates protein folding inside the matrix [102]. Ssq1, together with Jac1, are associated with the biogenesis of iron-sulfur clusters [103]; the role of the low-abundant Ecm10 is more elusive. Nevertheless, all the Hsp70s share one nucleotide exchange factor and a homolog of the bacterial GrpE, named Mge1 [104].

The matrix has its own chaperonin complex (Hsp60), which is from bacterial ancestry and is formed in a homo-oligomeric fashion, with seven subunits forming each side of the double-ringed structure [105]. The chamber of Hsp60 allows for the folding of proteins up to 50 kDa and is enclosed by the cochaperone Hsp10 [106]. This process is vital for protein folding since mutants are found to accumulate misfolded proteins in the matrix and lack the ability to assemble active protein complexes. Additionally, Hsp60 is involved in protein translocation, acting in sequential order, following Hsp70 [107]. The matrix has a second protein, Tcm62, which exhibits sequence similarity to Hsp60. This largely uncharacterized chaperone is involved in complex biogenesis [108].

While the two chaperone classes described before act in protein import and folding of nascent proteins, the proteins of the AAA+ act downstream of those processes. The clearance of misfolded and aggregated proteins due to aging or other stress situations is handled by those machineries. The first members are Hsp100 proteins, including Hsp78, the homolog to the bacterial ClpB. Like Hsp104, this complex is associated with thermotolerance and works closely together with the matrix Hsp70. Both systems probably share similar functions since the overexpression of Hsp78 is able to counteract the effects of dysfunctional Hsp70 [109]. Recently, the interaction partners of the matrix disaggregase have been studied [110], and the role of folding of freshly imported proteins have been described [111]. An additional Hsp100 member of the matrix includes the uncharacterized yeast Mcx1. Its homology to bacterial ClpP suggests a role in proteolytic degradation and protein folding [112]. Nevertheless, mitochondria own a dedicated system for the proteolytic cleavage of matrix proteins that are also found in the AAA+ protein family. Besides the membrane-bound FtsH-like m-AAA protease (Yta12 and Yta10) of the inner membrane [113], the matrix has a soluble master protease, Pim1. This serin-protease is highly conserved to its bacterial homolog Lon [114]. The translocation from the pore loops in the first hexameric ring allows substrates to be subsequently degraded in the second hexameric ring with a conserved protease domain. This process has been identified to control the copy number of mtDNA and is vital for the maintenance of respiration. [115,116]

2 AIM

The cytosol of eukaryotic cells evolved an intricate and tightly regulated system to deal with the folding, assembly, misfolding, and degradation of proteins. Previous studies identified different arms of mitochondrial protein quality control, focusing on the regulation, targeting, and translocation of mitochondrial precursors [20,49,72]. However, after import, long-lived mitochondrial proteins are inaccessible to the quality control system of the cytosol. For this reason, analogous players of the proteostasis network exist in the mitochondrial matrix. But whether their interplay is governed by the same principles is still unclear.

In this thesis, I want to elucidate the protein quality control mechanisms of the mitochondrial matrix with a specific focus on protein aggregates in the context of refolding with the help of disaggregases, proteolytic degradation, and the gathering into specialized compartments via sequestration factors. To answer which kinds of protein aggregates are formed, I will induce their formation utilizing several stress conditions, e.g., heat stress and the import of misfolding model substrates, like the mutant version of the carboxypeptidase Y (CPY*). To understand the formation, clearance, and composition of these aggregates, I will use a combination of microscopic approaches as well as biochemical assays. To identify proteins bound to aggregates, I chose to investigate the matrix disaggregase Hsp78. Hsp78 was previously described as forming and binding to aggregates in the matrix upon stress conditions, which is phylogenetically related to the well-characterized cytosolic disaggregase Hsp104. Additionally, I want to investigate the mitochondrially encoded polyN protein Var1, which was indicated in the formation of aggregates upon insults to the matrix proteostasis network and might act similarly to the prion-like protein Rnq1. The help of fluorescently tagged versions of Var1 and Hsp78 will allow me to monitor aggregate formation. Moreover, the conjunction with mass spectrometry will allow me to isolate and characterize aggregates formed by these two proteins, as well as their substrate spectrum. Since the cytosol and nucleus exhibit a plethora of different protein aggregates with either benign or toxic effects, I want to study if this concept applies to the mitochondrial matrix. Therefore, I want to use fluorescence microscopy, biochemical aggregation assays, and viability assays to better understand the relevance of different types of aggregates for the cells' homeostasis.

Protein homeostasis, or proteostasis, is the balance between protein synthesis, folding, mediated via a chaperone network, and degradation of non-productive proteins. Protein aggregates in the cell can be differentiated by their composition, localization, and capacity to resolve after elevated stress. To investigate the formation of protein aggregates in the matrix of mitochondria, I studied the matrix disaggregase Hsp78 and the mitochondrial-encoded S3 protein Var1 in the context of proteostasis (Figure 5).
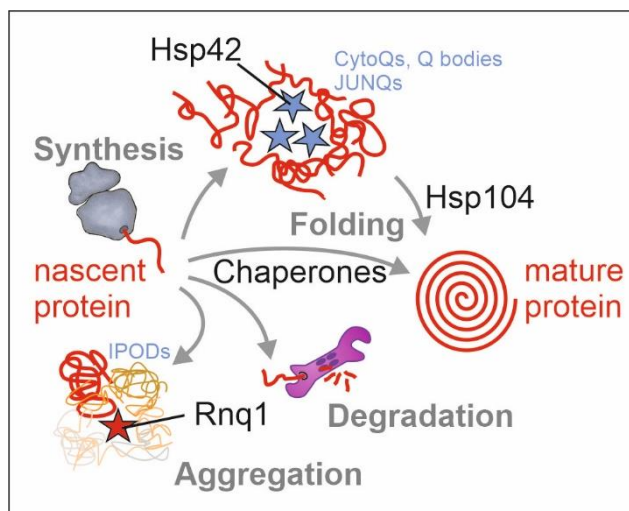
Figure 5: Schematic representation of the proteostasis network of the yeast cytosol. Chaperones facilitate the folding and assembly of newly synthesized proteins into their mature conformations. Protein folding is under the surveillance of the proteolytic quality control system, which degrades non-productive folding intermediates. If both the folding and degradation machinery are overwhelmed, such as the small heat shock proteins Hsp42 and Hsp26 and the polyQ protein Rnq1 can serve as nucleation factors that induce the formation of different types of aggregates. The disaggregase Hsp104 can disentangle proteins from certain types of aggregates and pass them on to the folding or degradation systems.

3.1 Hsp78 associates with mitochondrial aggregates

The yeast cytosolic chaperone Hsp104 and the bacterial ClpB are well-characterized chaperones that bind and resolve protein aggregates [34,35,117–119]. They belong to the ATPase with diverse cellular activities (AAA+) superfamily, featuring a conserved ATP binding domain known as Walker A motif and an ATP hydrolyzing domain referred to as Walker B motif (Figure 6A). 6 monomers assemble into a hexameric complex. The Hsp78 protein of the mitochondrial matrix is closely related to these proteins and shares the same architecture. I tagged Hsp78 with GFP using a constitutive promoter to express the fusion product. Additionally, I generated a trapping variant of Hsp78 with a mutation in the Walker A

motif (Hsp78[K149T]), which disrupts the ATPase activity in the first nucleotide-binding domain while still allowing for the formation of a hexameric complex (Figure 6B) [120]. Whether this alteration would result in a dominant negative phenotype or if the Hsp78[K149T] subunits change their aggregation propensity remains uncertain. However, the overexpression did not impact the growth of the cells at different temperatures and carbon sources. (Figure 6C).
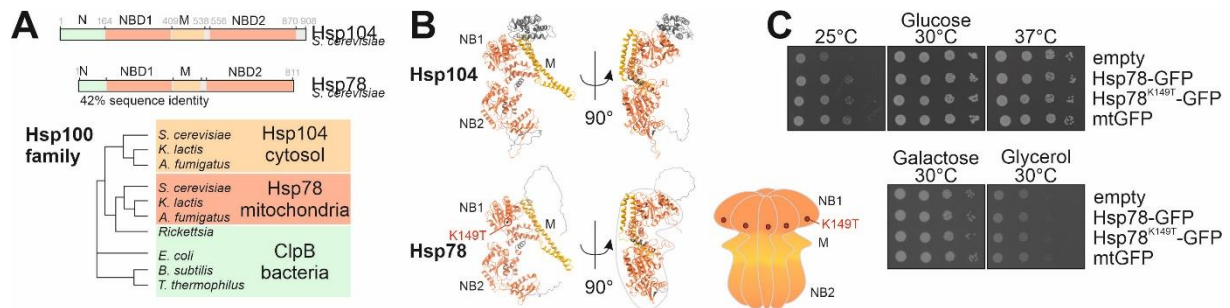
Figure 6: Hsp104 and Hsp78 are structurally and phylogenetically related members of the Hsp100 protein family. A They share the same overall structure. NBD, nucleotide-binding domain; M, middle domain. **B** AlphaFold predicted structure of monomers of Hsp104 (top) and Hsp78 (bottom) show the same folding [121]. These structures were created using ChimeraX [122]. Both form hexameric complexes *in vivo* (scheme, bottom right). **C** Wildtype (WT) cells of the indicated strains were grown to log phase in galactose medium before tenfold serial dilutions were dropped onto plates with the indicated carbon sources and incubated at the indicated temperatures.

GFP fusions to WT or trapping mutants of Hsp104 are established markers for the visualization of cytosolic protein aggregates that can be induced by subjecting cells to a short heat stress of 40°C for 30 min (Figure 7A). To study the distribution of proteins inside mitochondria, I visualized the mitochondrial network with mScarlet bound to the MTS of subunit 9 of the *Neurospora crassa* ATPase (Su9 MTS) (mt-mScarlet). Hsp78-GFP behaved similarly to Hsp104 with an equal soluble distribution in the matrix under non-stress conditions (Figure 7A, B). However, upon exposure of cells to acute heat stress conditions (40°C for 2 h), Hsp78-GFP formed punctate structures within mitochondria, indicating its association with intramitochondrial aggregates and confirming previous observations [110,111,123]. The Hsp78[K149T] variant showed a punctate distribution at all temperatures, presumably owing to its dysfunction and the diminished ability to release bound substrates (Figure 7C). To avoid possible artifacts by the non-physiological behavior of this mutant, I decided not to use it for further analysis.
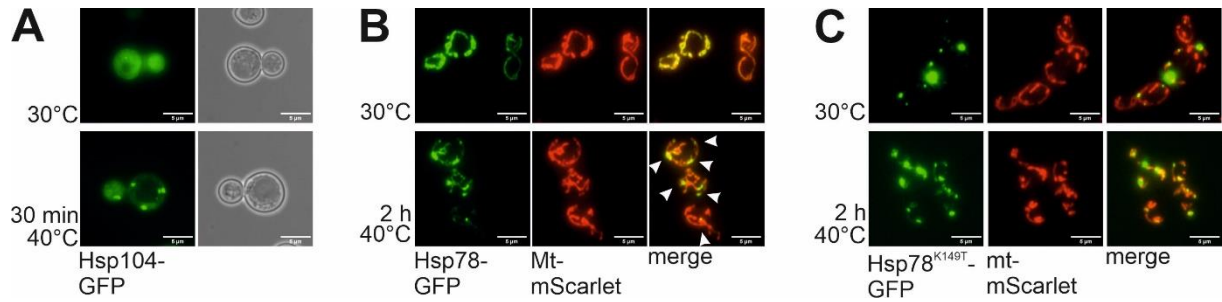
Figure 7: The disaggregase Hsp104 and Hsp78 associated with protein aggregates. A Hsp104-GFP was expressed in WT cells grown on galactose medium at 30°C (top) and shifted to 40°C for 30 min (bottom). The distribution of Hsp104 was visualized by fluorescence microscopy. **B** Cells expressing Hsp78-GFP and mitochondria-targeted mScarlet (mt-mScarlet) were grown to log phase in galactose medium at 30°C (top) and shifted for 2 h to 40°C (bottom). Arrowheads depict the Hsp78-bound aggregates that form upon heat shock. **C** Cells expressing Hsp78^{K149T}-GFP and mt-mScarlet were grown to log phase in galactose medium at 30°C (top) and shifted for 2 h to 40°C (bottom). The trapping mutant Hsp78^{K149T}-GFP was found to be aggregates independent of the temperature.

To test if this behavior can also be seen independent of the presence of the mitochondrial genome, I used *rho⁰* cells to study the distribution of Hsp78-GFP under conditions where the mitochondrial DNA is lost. The loss of mitochondrial DNA changes the assembly of many complexes in mitochondria since core components are no longer present. Many assembly intermediates still form and might be potential interaction partners. In *rho⁰* cells, the mitochondrial morphology was changed to a more collapsed state (Figure 8). Still, Hsp78 showed a mainly dispersed localization in mitochondria at 30°C and formed the same aggregates after heat stress treatment for 2 h at 40°C.
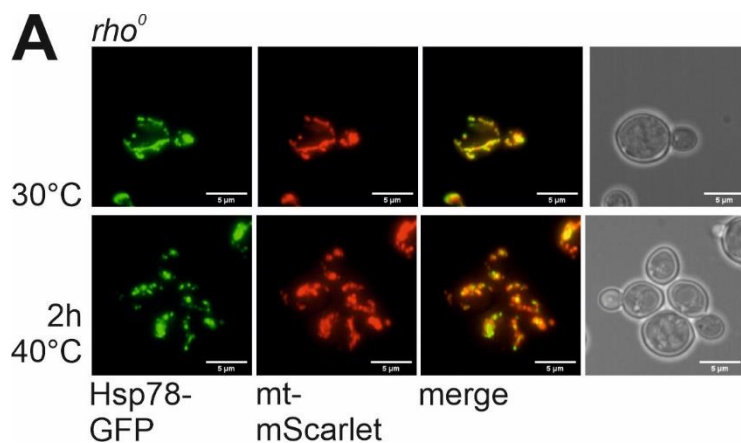
Figure 8: Hsp78 aggregates are formed independent of the presence of the mitochondrial DNA. *Rho⁰* cells expressing Hsp78-GFP and mt-mScarlet were grown to log phase in galactose medium at 30°C (top) and shifted for 2 h to 40°C (bottom).

Heat exposure has complex consequences on a molecular level, affecting proteins, lipids, and metabolites in all cellular compartments pleiotropically [124]. To challenge the

15

intramitochondrial protein folding more specifically, I fused the folding incompetent G255R mutant of carboxypeptidase Y (CPY*) [125] to the Su9 MTS (Figure 9A). This matrix-targeted mtCPY* protein strongly affected cellular growth at normal and increased temperatures (Figure 9B). Nevertheless, neither the import competence of mitochondria (Figure 9C) nor their ability to synthesize mitochondrial translation products was hampered (Figure 9D).
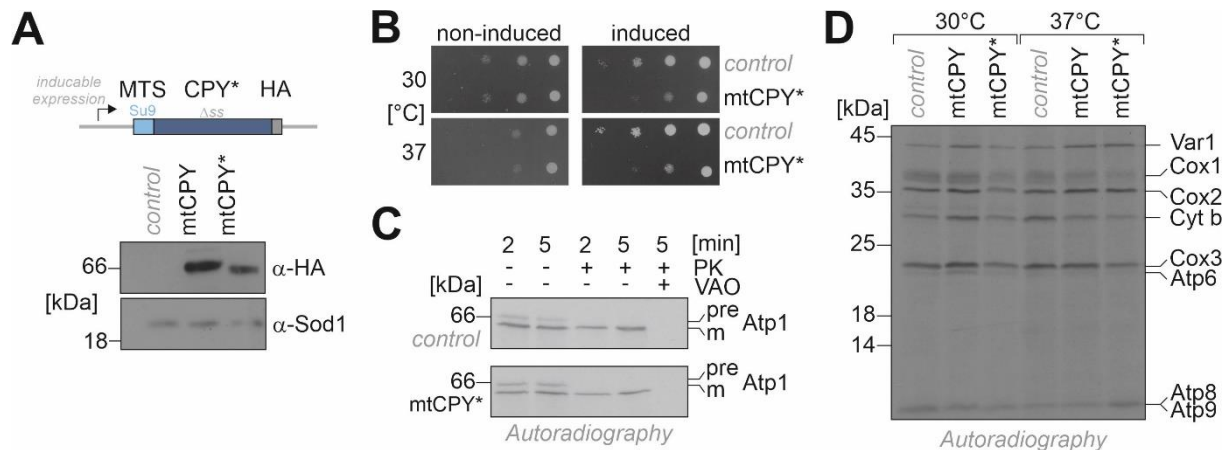
Figure 9: Expression of the mitochondrial-targeted CPY* preserves mitochondrial functions. A The protein levels of HA-tagged CPY and folding incompetent G255R CPY*, lacking its originals signal sequence (Δss), and instead fused to the Su9 MTS under the control of an inducible *GAL* promoter. An empty vector was used as a control. Samples were always taken after 4 h of induction. Sod1 is shown for control. **B** WT cells expressing mtCPY* or empty vector were grown to log phase on lactate medium. Serial dilutions were dropped on lactate (non-induced) or lactate with 0.5% galactose (induced) medium and grown at 30 or 37°C as indicated. **C** Radiolabeled Atp1 was synthesized in reticulocyte lysate in the presence of ^{35}S methionine and incubated with isolated mitochondria from WT cells after 4 h induction of mtCPY* or the control. After 2- and 5-min, the import was stopped, treated with (+) or without (-) proteinase K (PK) for 30 min on ice, and subjected to SDS-PAGE and autoradiography. As a negative control, the membrane potential was destroyed by adding valinomycin, antimycin, and oligomycin (VAO). **D** The indicated strains were grown in lactate medium, and mitochondria were isolated after 4 hours of induction with 0.5% galactose. Mitochondrial translation products were radiolabeled for 15 min with ^{35}S-methionine at 30 or 37°C. Radiolabeled proteins were visualized by SDS-PAGE and autoradiography.

To test whether the presence of Hsp78 induces the toxicity of aggregates, I generated knock-out strains of *HSP78* (Figure 10A) and expressed mtCPY*. The toxicity of the mtCPY* protein was not increased in mutants lacking Hsp78 (Figure 10B), indicating that Hsp78 does not repress the toxicity of this misfolded protein. To this end, I expressed mtCPY* as a fusion protein with mScarlet, resulting in puncta in WT and Δ*hsp78* cells, showing that the formation is an Hsp78-independent process (Figure 10C). Expression of the mtCPY*-mScarlet protein induced mitochondrial fragmentation, presumably owing to its proteotoxic effects.
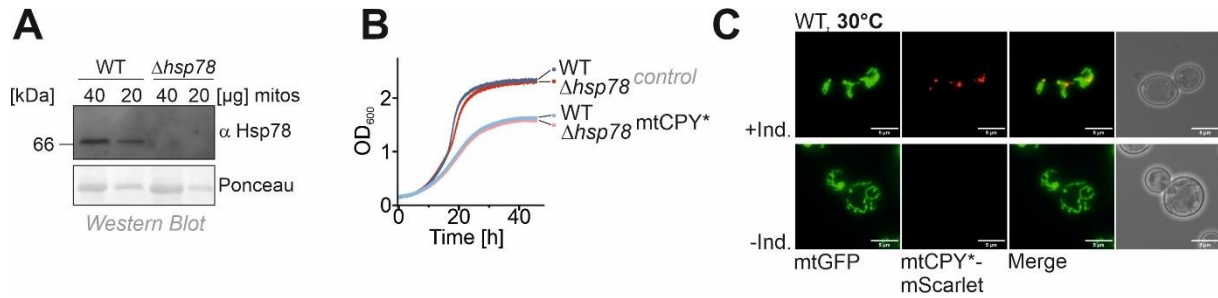
Figure 10: mtCPY* is toxic for cells independent of the presence of Hsp78. A The protein levels of Hsp78 were analyzed in WT and *Δhsp78* cells. The ponceau staining is shown for control. **B** The indicated strains were grown in galactose medium in a plate reader for 2 days, and the densities were recorded at 600 nm. **C** mtGFP and mtCPY*-mScarlet in yeast cells grown at 30°C in raffinose medium. The distribution of the fluorophores was visualized by microscopy in WT cells after 4 h with (top) or without (bottom) induction.

I tested whether Hsp78 binds to misfolded mtCPY*. The expression of mtCPY*-mScarlet resulted in 4-7 intramitochondrial puncta in WT and *Δhsp78* cells, showing that the formation is an Hsp78-independent process (Figure 11A, B). Co-expression of Hsp78-GFP showed a clear colocalization with mtCPY*-mScarlet, indicating that both proteins were part of the same aggregates. These Hsp78-CPY* aggregates were present even at 30 and 40°C as this highly aggregation-prone model protein cannot fold regardless of the temperature (Figure 11C, D) [125].
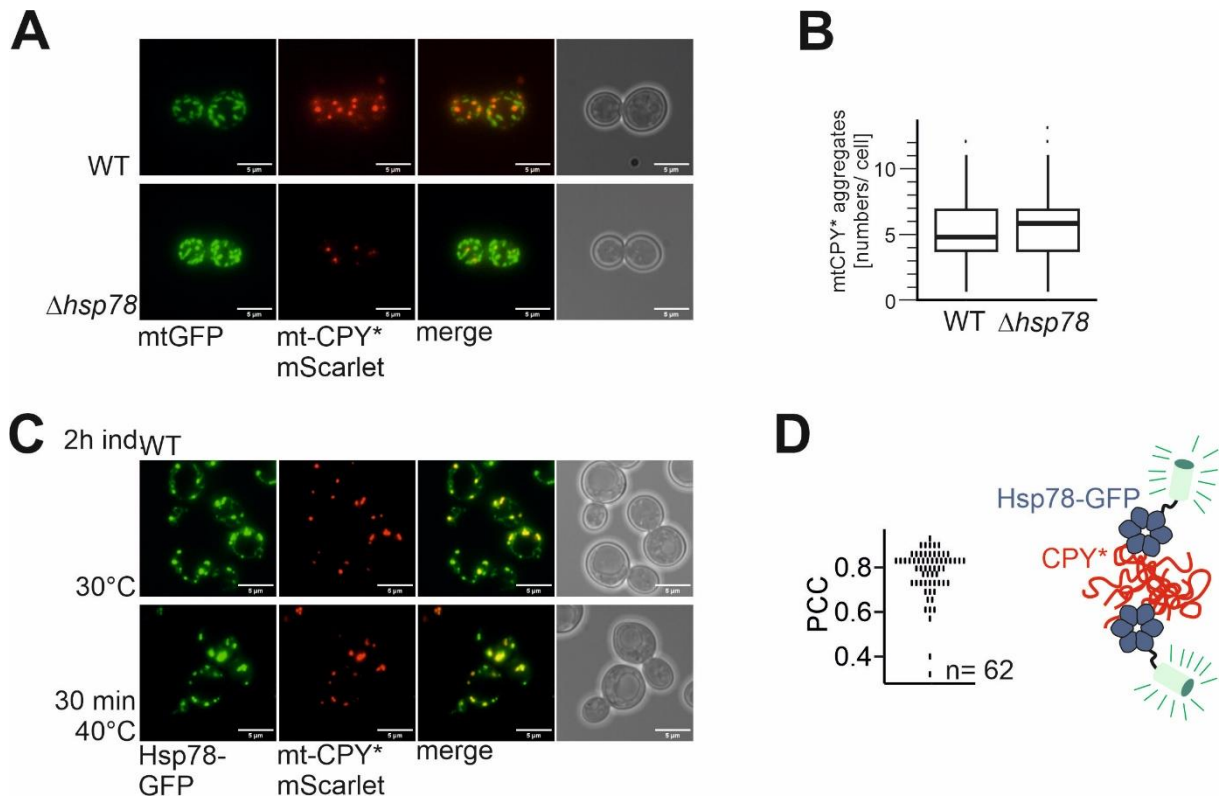
Figure 11: Hsp78-GFP interacts with mtCPY*-mScarlet aggregates A mtGFP and mtCPY*-mScarlet was expressed in yeast cells grown at 30°C in lactate medium. The distribution of the fluorophores was visualized by microscopy in WT and Δ*hsp78* cells after 2 h of induction. **B** Number of aggregates in WT and Δ*hsp78* cell after 4 h of induction. **C** Hsp78-GFP and mtCPY*-mScarlet were expressed in yeast cells grown in raffinose medium at 30°C (top) and after the shift to 40°C for 30 min (bottom). The distribution of the fluorophores was visualized by microscopy. **D** Person colocalization coefficient of Hsp78-GFP and mtCPY*-mScarlet after 4 h of induction at 30°C. A schematic representation of Hsp78-GFP binding to CPY* aggregates is shown.

To identify endogenous interaction partners of Hsp78, I isolated Hsp78-GFP, Hsp78^{K149T}-GFP, and mtGFP from yeast cells by sepharose-coupled nanobodies (GFP-Traps) and analyzed the bound proteins by immunoblotting. The pull-down showed the correct product in the eluate for the GFP fusions. However, I was not able to co-elute mtCPY* with Hsp78-GFP, which was exclusively found in the flowthrough, indicating that Hsp78 might quickly dissociate from bound substrates or only be transient in the mode of interaction (Figure 12A, B).

18
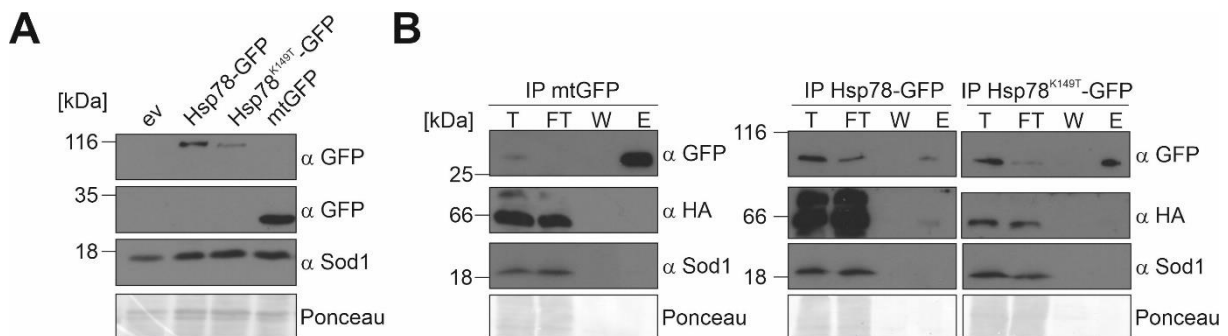
Figure 12: GFP-tagged Hsp78 can be isolated via GFP-Traps. A The protein levels of Hsp78-GFP, Hsp78^{K149T}-GFP, and mtGFP in WT cells grown in galactose media were analyzed. Sod1 and Ponceau staining are shown for control. **B** mtGFP, Hsp78-GFP, and Hsp78^{K149T}-GFP were purified after 4 h of mtCPY* induction in WT cells with GFP-Traps. T, Total lysate, FT, flow-through representing the non-bound fraction, W, wash I, E, eluate. The antibodies against GFP and HA were used. The signal for Sod1 and Ponceau staining are shown for control.

To identify substrates of Hsp78, I chose a more sensitive method for protein detection, mass spectrometry. To elucidate which proteins act as substrates independent of the presence of the mitochondrial genome, WT and *rho^0* cells were used for the co-immunoprecipitation (Figure 13A). The mass spectrometry was measured by Markus Räschle and statistically analyzed and imputed by Jan-Eric Bökenkamp. While Hsp78 was nicely enriched, only a few mitochondrial proteins were identified, including some mitoribosomal subunits (Figure 13B, C). I found many mitochondrial proteins, including many subunits of the mitochondrial ribosome, when mitochondrial DNA was lacking (Figure 13D, E). This might be due to the lack of rRNA, which MRPs usually can assemble onto. Still, this observation supports recent studies that proposed a function of Hsp78 as a binding partner of newly imported mitochondrial proteins [110,111].
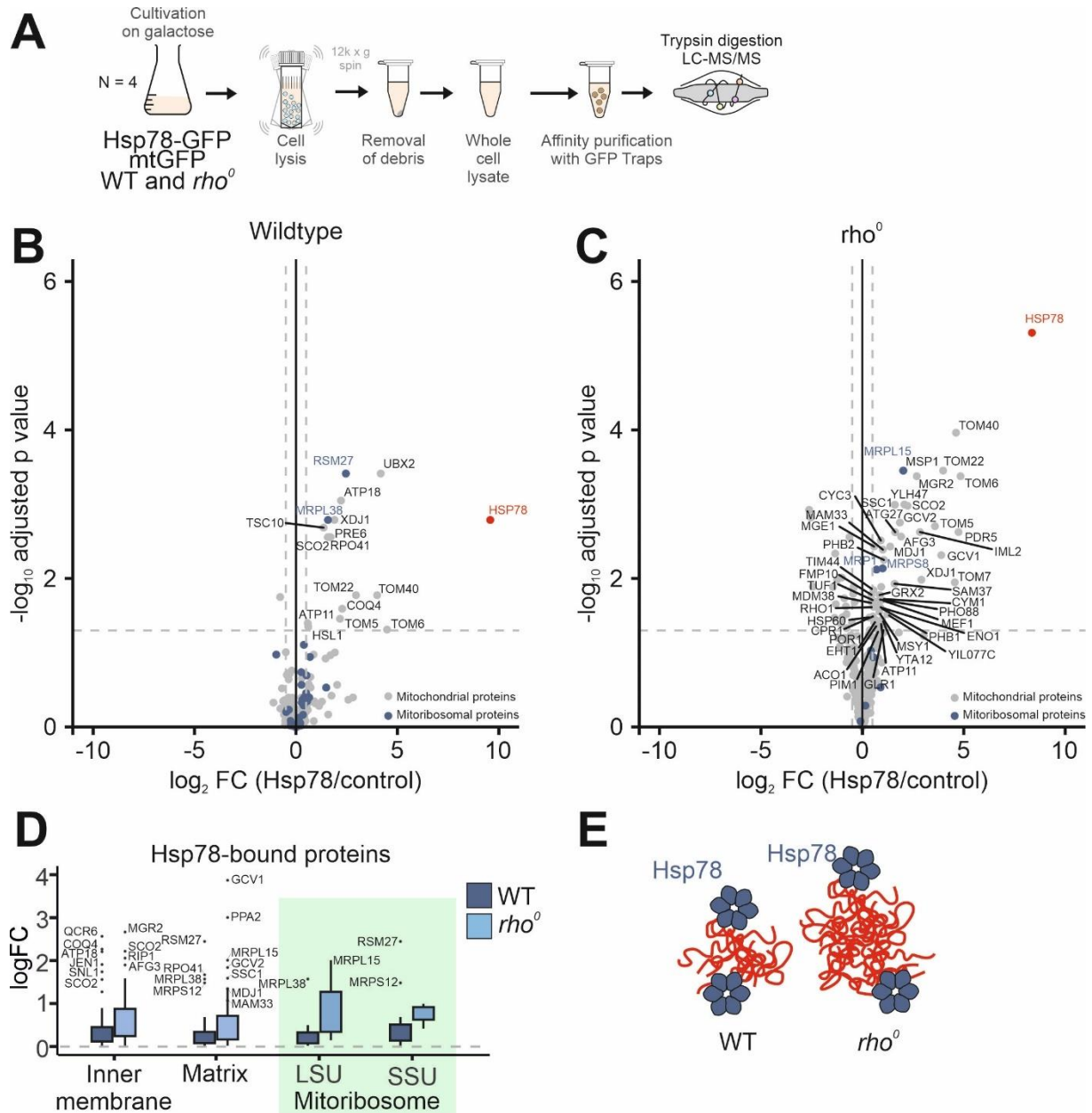
Figure 13: Hsp78 binds to matrix proteins. A Schematic representation of the Hsp78 purification that was used for mass spectrometry. WT or *rho⁰* cells expressing Hsp78-GFP or mtGFP were subjected to glass bead lysis. Proteins coeluting after affinity purification with GFP-Traps were then used for mass spectrometry **B**, **C** Comparison of the co-immunoprecipitation of Hsp78 in WT and *rho⁰* cells. Mitochondrial proteins [73] are indicated in gray. Mitoribosomal proteins are indicated in blue. **D** The relative enrichment (log2 fold change, log FC) of proteins in the Hsp78-GFP vs. GFP is shown for specific groups of proteins. LSU, large mitoribosomal subunit; SSU, small mitoribosomal subunit **E.** Schematic representation of the observation that Hsp78-GFP-bound proteins were much more prominent in *rho⁰* than in WT cells. Many of these proteins were subunits of the mitoribosome and complexes of the respiratory chain. Figures B, C., and D. were blotted in R Studio by Christian Koch.

In order to test whether Hsp78 would only bind to newly imported proteins, the synthesis of proteins in the cytosol and mitochondria was inhibited for 2 hours by the addition of cycloheximide (Figure 14A) or chloramphenicol (Figure 14B), respectively. Still, heat exposure

induced the formation of Hsp78-GFP-bound aggregates. Even in cells where the import was impaired for 2 hours via the expression of the rapid folding protein DHFR fused to the b_2 MTS, heat stress induced the formation of Hsp78 aggregates (Figure 14D). Here, the expression of cytosolic DHFR was used as a control for normal import (Figure 14C). The results suggest that aggregates are not exclusively formed from newly synthesized proteins.
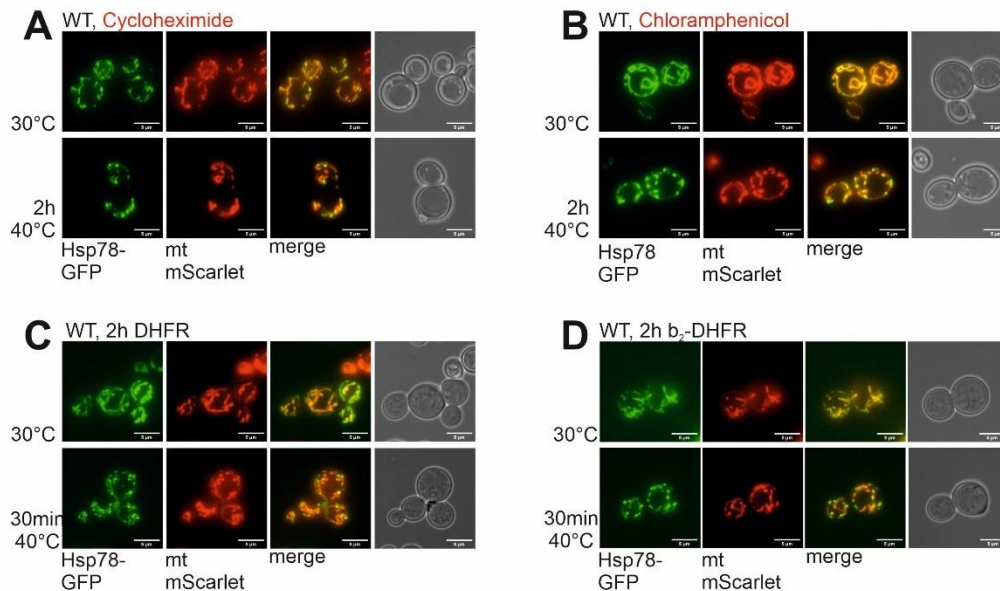
Figure 14: Hsp78 aggregates are not exclusively made up of newly imported and synthesized proteins. A WT cells expressing Hsp78-GFP and mt-mScarlet were grown to log phase in galactose medium and treated with cycloheximide (100 µg/ml) for 2 h before shifting cells to either at 30°C (left) or at 40°C (right) for 2 h. **B** WT cells expressing Hsp78-GFP and mt-mScarlet were grown to log phase in galactose medium and treated with chloramphenicol (2 mg/ml) for 2 h before shifting cells to either at 30°C (left) or at 40°C (right) for 2 h. **C, D** WT cells expressing Hsp78 and cytosolic DHFR (left) or b2-DHFR (right) for 2 h before shifting cells to either at 30°C (top) or at 40°C (bottom) for 30min.

In summary, Hsp78 is a protein of the mitochondrial matrix that forms or associates with aggregates under stress conditions and thus might be functionally equivalent to other AAA+ proteins such as Hsp104 or ClpB.

3.2 Hsp78 helps cells to recover from acute stress

What is the molecular function of Hsp78? To test if Hsp78 can resolve protein aggregates, the synthesis of mtCPY*-mScarlet was induced for 2 hours in WT and Δ*hsp78* cells (Figure 15A). Afterward, expression was stopped, and aggregates were followed over time. The mtCPY*-mScarlet aggregates were highly persistent and did not resolve when cells recovered even for 8 hours (Figure 15B, C).
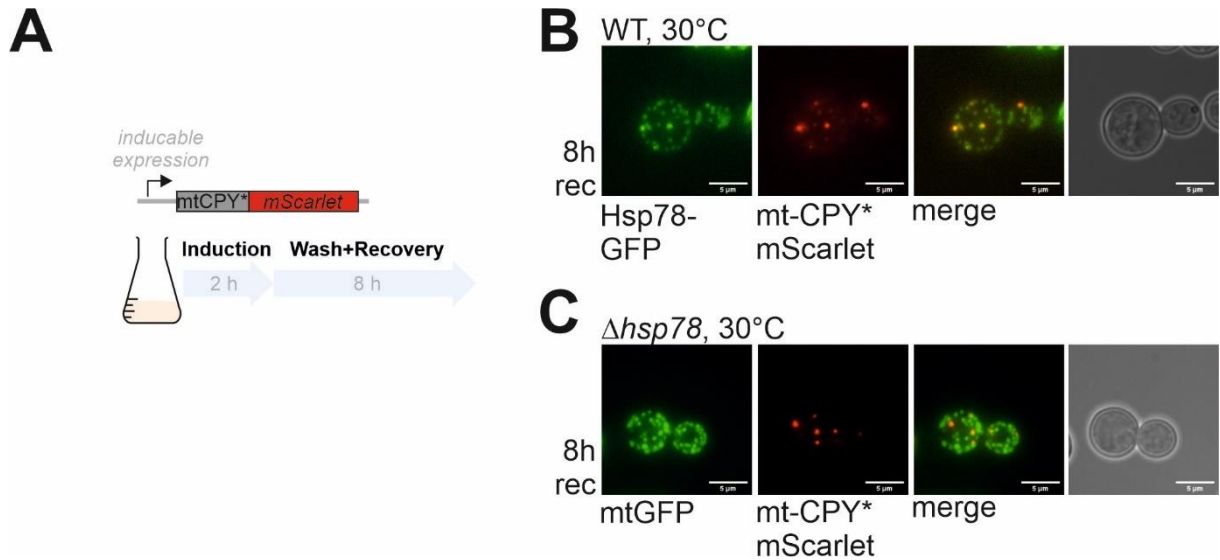
Figure 15: mtCPY* aggregates are not cleared from cells. A Schematic representation of the experimental set-up. The expression of mtCPY*-mScarlet was induced for 2 h. Afterward, cells were washed and resolubilized in media without galactose to stop mtCPY*-mScaret and incubated for a further 8 h at 30°C. **B**, **C** WT(top) and *Δhsp78* (bottom) cells expressing Hsp78-GFP and mtCPY*-mScarlet 2 hours after the synthesis was stopped and cells incubated for 8 h at 30°C.

Since mtCPY* did not resolve, I tested another misfolding model protein, DHRF[mut], [126] fused to the Su9 MTS and C-terminally tagged with mScarlet (Figure 16A). This fusion protein was dissolved in WT and *Δhsp78* cells at 30°C after 4 hours of induction (Figure 16B, C). But formed aggregates after 30 min at 40°C (Figure 16D, E). In WT cells, these Hsp78-bound aggregates were dissolved after heat shock but remained in punctate foci in *Δhsp78* cells (Figure 16F, G). Thus, Hsp78-bound aggregates can be transient or stable, dependent on the nature of the aggregated client proteins.
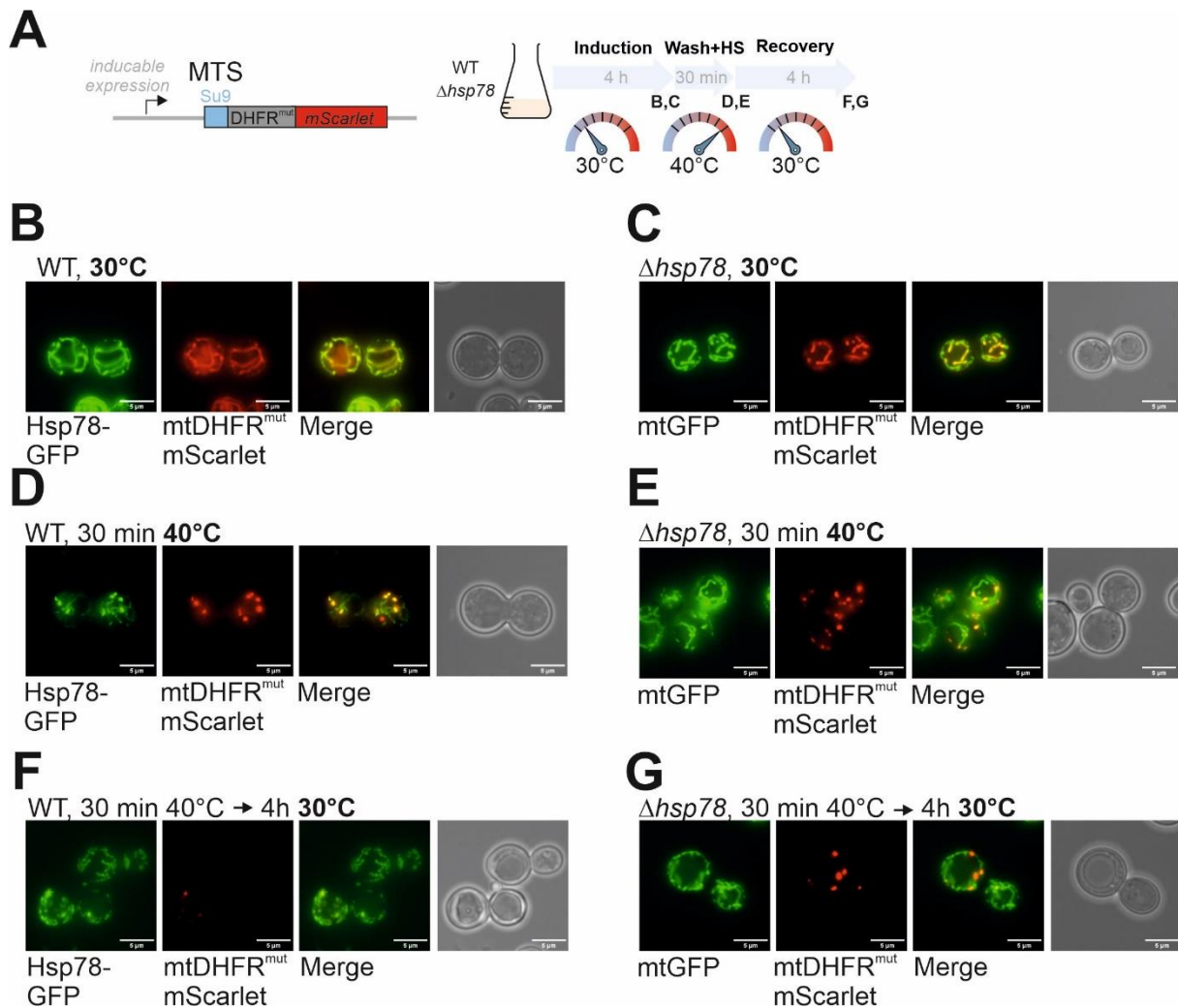
Figure 16: Hsp78 dissolves the aggregating model substrate mtDHFR^mut. A-G Schematic representation of the construct for the Su9-DHFR^mut-mScarlet fusion protein. Expression of this aggregation-prone protein in WT and *Δhsp78* cells was induced for 4 hours by the addition of galactose. Cells were resuspended in raffinose medium without galactose to prevent further Su9-DHFR^mut-mScarlet expression and subjected to a heat shock at 40°C for 30 min. Subsequently, cells were shifted to 30°C for 4 hours to allow recovery from heat stress. Samples were taken at the indicated time points and analyzed by microscopy.

In order to check if Hsp78 would also interact and resolve endogenous yeast proteins, I studied Aim17. The mitochondrial matrix protein Aim17 was previously found to form aggregates [49]. To this end, I expressed mCherry-tagged versions of Aim17 (Figure 17A). The protein showed a dispersed mitochondrial distribution at 30°C. However, 30 min to 40°C exposure formed intra-mitochondrial aggregates, which colocalized with Hsp78-GFP. When I reduced the growth temperature back to 30°C, the Hsp78-GFP aggregates disappeared again (Figure 17B). Likewise, Aim17 was reversible, and both proteins redistributed within mitochondria after the heat shock (Figure 17B). Interestingly, the dissociation of Aim17 was retarded in *Δhsp78* cells suggesting that Hsp78 can promote their dissociation (Figure 17C).
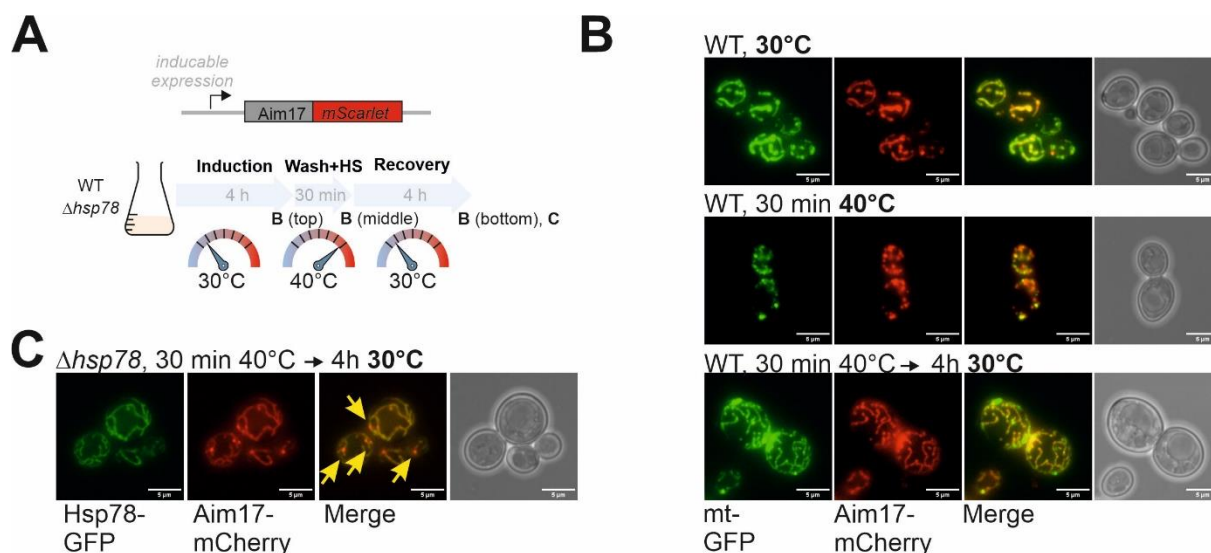
Figure 17: Hsp78 helps to refold matrix protein aggregates. A-C Cells expressing mtGFP or Hsp78-GFP were grown to log phase in raffinose medium at 30°C. Then, by the addition of 0.5% galactose, the expression of Aim17-mCherry was induced for 4 hours. Afterward, the expression was stopped, and cells were shifted to a heat shock (HS) at 40°C for 30 min. For the recovery phase, cells were shifted back to 30°C. In B, Aim17-mCherry aggregates are visible in WT cells after the heat shock. In C, the same cells were allowed to recover from heat exposure, resulting in the distribution of Hsp78 and Aim17. In C, *Δhsp78* cells were used instead of WT cells. Please note that Aim17 remained aggregated after the recovery phase, indicated with yellow arrows.

In consistency, I observed that *Δhsp78* cells were similarly vulnerable to acute heat exposure than WT cells (Figure 18A). However, WT cells recovered more quickly from acute heat stress (Figure 18B), again indicating that Hsp78 promotes the removal of damaged proteins but does not prevent protein aggregation per se.
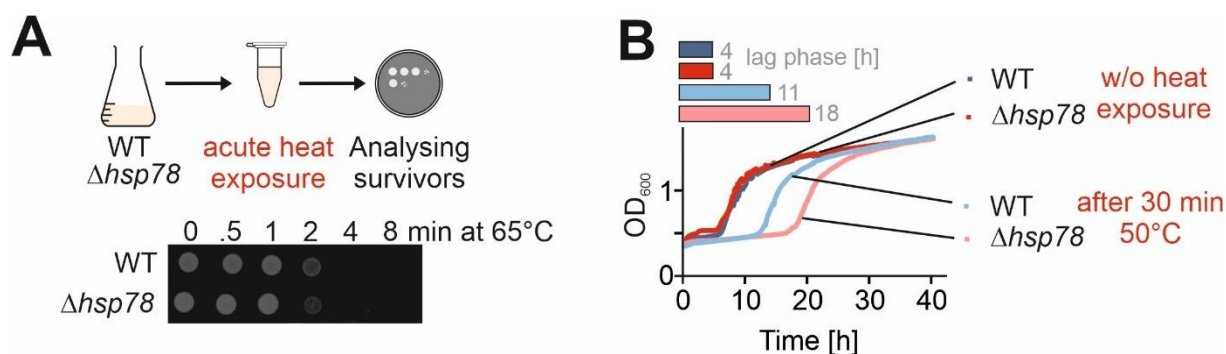
Figure 18: Hsp78 is vital to protect cells from acute heat stress. A WT and *Δhsp78* cells were grown to log phase in galactose medium at 30°C, pelleted, and diluted in medium of 65°C for the indicated time points. Then, 3 µl with an OD of 0.1 were dropped onto glucose plates, which were incubated for 2 days at 30°C. **B** Cells grown at 30°C were exposed to 50°C or 30°C for 30 min before their growth at 30°C was continuously measured for 2 days.

This inspired me to further look for a potential functional interaction of Hsp78 with Pim1. Pim1 is a homolog of the bacterial Lon protease and serves as the major protease of the mitochondrial matrix [116]. It was reported before that *in vitro*, overexpressed Hsp78 protects newly imported

model proteins from Pim1-mediated degradation [127]. The substrate spectrum of members of the Lon protease family was previously analyzed by co-isolation with a catalytically inactive mutant [128]. Following the same approach, I generated an S1015A point mutant in Pim1, which destroys the essential serine-lysine dyad of the protease's active site [114,129].

Tim Schneckmann expressed Pim1[S1015A] as an HA-tagged version in WT and *Δhsp78* cells, purified the protein from Triton X-100-lysed cell extracts, and performed mass spectrometry of the bound fractions (Figure 19A). The proteome was measured by Markus Räschle and statistically analyzed and imputed by Jan-Eric Bökenkamp. Pim1 was efficiently purified from both WT and *Δhsp78* cells. In addition, established interactors of Pim1, such as Mam33, Mrx6, and Pet20, were copurified (Figure 19B). Moreover, many mitochondrial proteins co-eluted with Pim1. Interestingly, from *Δhsp78* cells, many more proteins were coisolated with Pim1, indicating that Hsp78 indeed prevents proteins from Pim1-mediated degradation (Figure 19C).
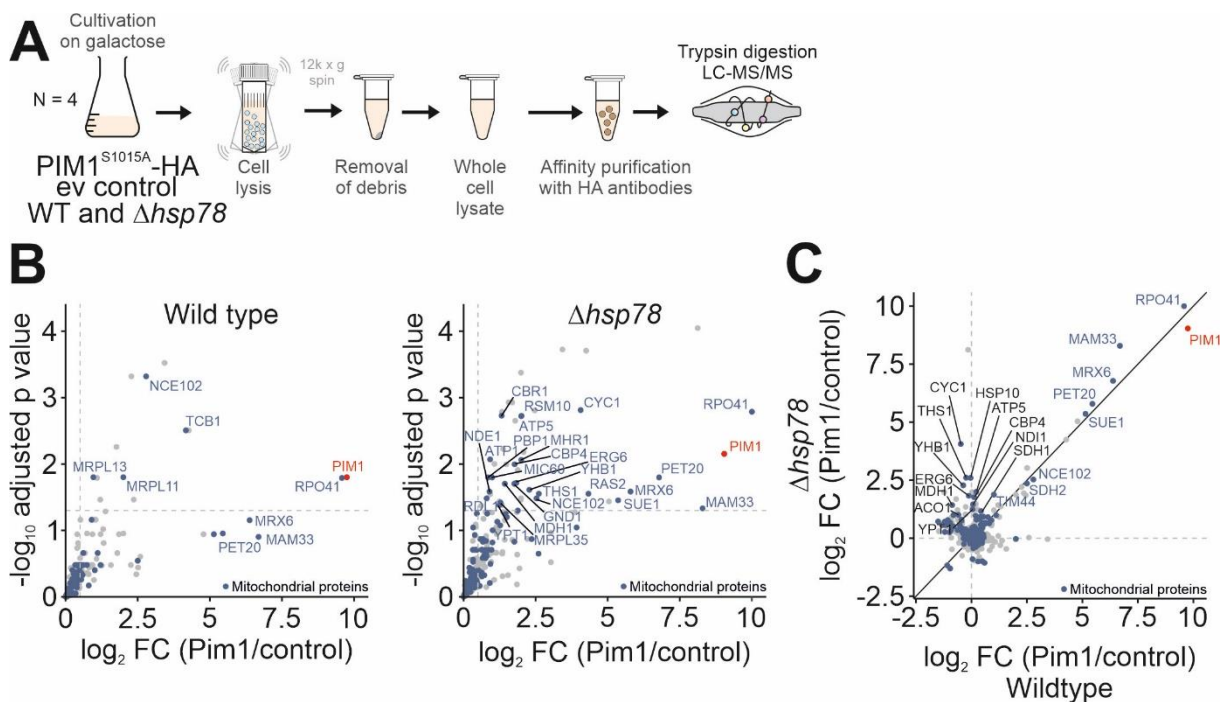
Figure 19: Hsp78 as a platform for proteins to protect them from proteolytic degradation. A Schematic representation of the Pim1 purification scheme used for mass spectrometry. WT and *Δhsp78* expressing either Pim1[S1015A]-HA or empty vector control were grown to log phase before cells were harvested. Cells were lysed using glass beads and Triton X-100. The co-immunoprecipitation was performed with Sepharose beads coupled to an HA antibody. **B** Proteomics of the proteins co-isolated with Pim1[S1015A]-HA from WT and *Δhsp78* cell extracts. Plotted proteins are more abundant in the Pim1-containing samples compared to the empty vector control. Mitochondrial proteins [73] are shown in blue. Names of the subunits of the Pim1-Mrx6-Mam33-Pet20 complex are indicated. **C** Correlation plot comparing the enrichment factors (log2 fold changes) of the Pim1 interactors of WT and *Δhsp78* cells. Graphs B and C were blotted in R Studio by Christian Koch.

These observations suggest that Hsp78 protects proteins against Pim1-mediated degradation in mitochondria, consistent with previous observations [127]. The underlying mechanisms will have to be analyzed in more depth in the future. Still, it appears likely that Hsp78 and Pim1 compete for the same misfolded substrates to either fold them into their native conformation (Hsp78) or degrade them (Pim1).

3.3 Mitochondrial protein synthesis protects against heat-induced proteotoxicity

Many nuclear-encoded mitochondrial proteins are substrates of Hsp78. However, no mitochondrial translation products were identified in the Hsp78 interactome. I, therefore, tested whether mitochondrial translation products are relevant for the resistance of cells against acute heat stress. To this end, WT cells were grown for 16 h with or without chloramphenicol, inhibiting mitochondrial protein synthesis but not the cytosolic translation machinery. Subsequently, cells were subjected to a short acute heat shock at 45 or 50°C for 5 min, and then surviving cells were counted after plating them onto glucose medium (Figure 20A, B).

I wondered which of the eight mitochondrially encoded proteins was relevant to stress resistance. The mitochondrial genome encodes for seven core subunits of respiratory chain enzymes and, in addition, for one ribosomal protein, Var1. Since the heat sensitivity was similar in WT and respiratory deficient mutants (Δcox18, Δcox20 Figure 20C), I reasoned that respiration per se is not critical for stress resistance (Figure 20C).
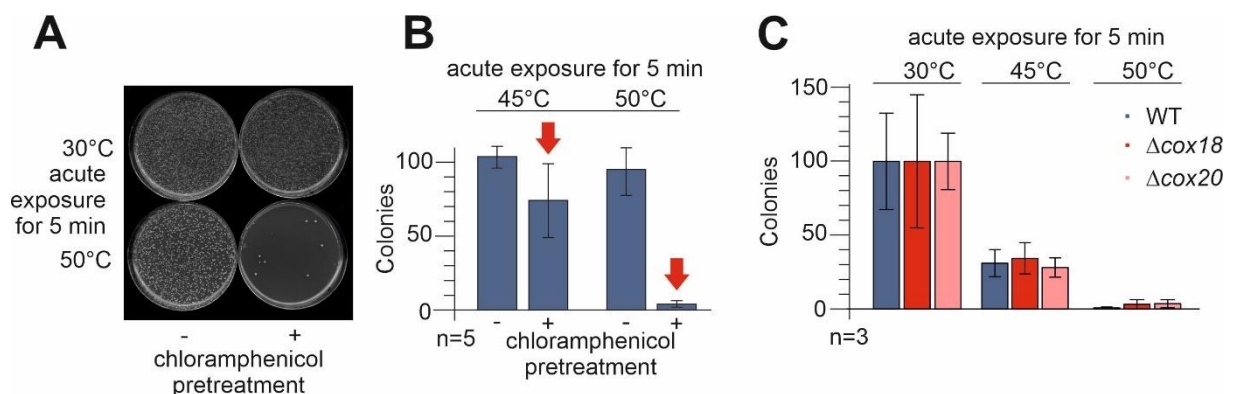
Figure 20: Mitochondrial protein synthesis protects cells from heat-induced stress. A, B WT cells were grown in galactose medium. The sample was split, and chloramphenicol (2 mg/ml final concentration) was added to one half. Cells were grown for 16 h at 30°C, the density was adjusted, and samples were exposed to 45 or 50°C for 5 minutes. Aliquots of samples were plated onto glucose medium and counted from 5 biological replicates. **C** WT, Δ*cox18,* and Δ*cox20* were exposed to 30, 45, or 50°C for 5 min. Aliquots of samples were plated to glucose medium and counted. Three biological replicates are shown.

To elucidate the role of Var1 independently of mitochondrial translation, I used MTS-Var1, a nuclear-encoded version of Var1 (Figure 21A). MTS-Var1 consists of the mitochondrial targeting signal of Cox4 fused to a Var1 sequence adapted to the universal genetic code rather than the mitochondria-specific code [93]. Upon expression in cells that lack the *VAR1* gene on the mitochondrial DNA, MTS-Var1 was targeted to mitochondria. The MTS-Var1 protein partially restored the respiration deficiency of *VAR1* mutants (Figure 21B) and their ability to synthesize mitochondrially encoded proteins (Figure 21C). However, the expression of MTS-Var1 reduced the fitness of non-respiring cells, indicating a translation-independent negative effect of this fusion protein. This dominant negative effect of MTS-Var1 was also observed in WT cells where the expression of MTS-Var1 repressed the synthesis of the mitochondrially encoded Var1 protein (Figure 21D), consistent with previous observations [95].
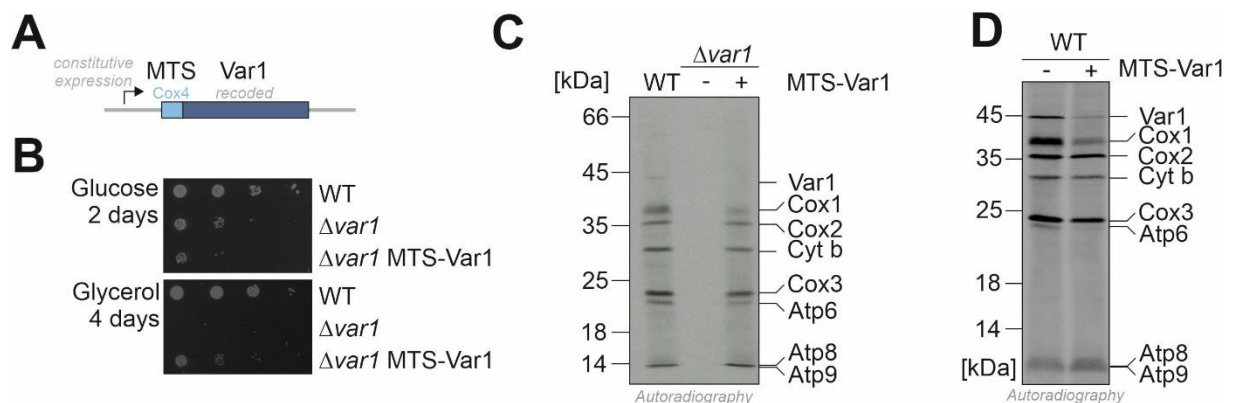
Figure 21: Allotopic expression of Var1 complements the mitochondrial loss of *VAR1*. A Schematic representation of yeast-optimized *VAR1* with N-terminal *COX4* MTS. **B** The indicated strains were grown to log phase in galactose medium at 30°C. 3 µl of the cell suspension was dropped onto glucose and glycerol plates, which were incubated at 30°C. **C** Mitochondrial translation products were radiolabeled in mitochondria of the indicated strains for 10 min at 30°C. Radiolabeled proteins were resolved by SDS-PAGE and visualized by autoradiography. In the MTS-Var1-expressing strain, no Var1 signal is visible since Var1 is not made in the mitochondria in that mutant. **D** The indicated strains were grown in galactose medium before the isolation of mitochondria. Mitochondrial translation products were radiolabeled for 15 min with ^{35}S-methionine at 30°C in the presence of cycloheximide to inhibit cytosolic translation. Radiolabeled proteins were visualized by SDS-PAGE and autoradiography.

The nuclear-encoded MTS-Var1 protein allowed to test a potential stress-protecting function of Var1. To this end, cells that contained the MTS-Var1 plasmid or an empty plasmid for control were grown in the presence of chloramphenicol for 16 hours before we exposed them to acute

heat stress. Please note that this construct was controlled by the *PSP2* promotor, allowing for expression at low protein levels [130]. I observed that the expression of MTS-Var1, which is not affected by chloramphenicol, strongly protected cells from heat toxicity (Figure 22A, B).
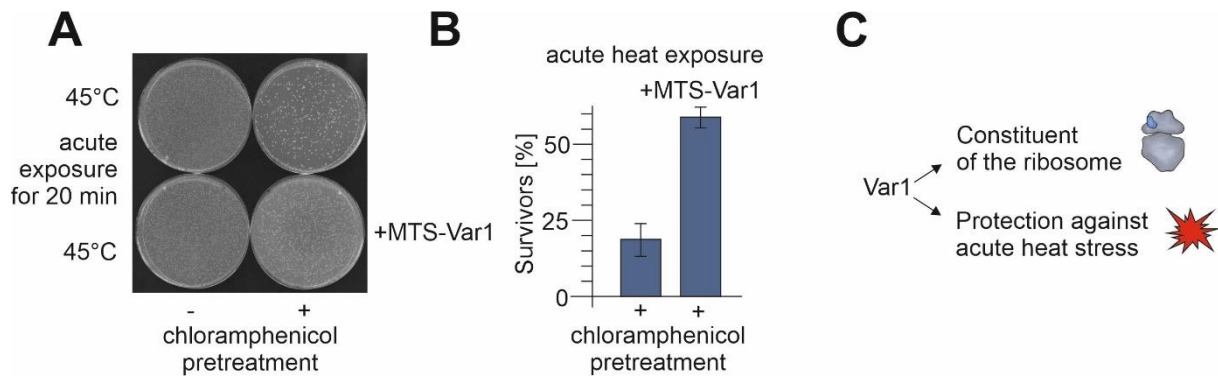
Figure 22: Low expression levels of MTS-Var1 protect cells against heat stress when mitochondrial translation is impaired. A, B Cells harboring an MTS-Var1-expression plasmid or an empty vector for control were grown in galactose medium. The sample was split, and chloramphenicol (2 mg/ml final concentration) was added to one half. Cells were grown for 16 h at 30°C, the density was adjusted, and samples were exposed to 45 (A) or 50°C (B) for 5 minutes. Aliquots of samples were plated onto glucose medium and counted from 3 biological replicates. **C** Scheme to illustrate the 2 distinguishable activities of Var1.

This shows that Var1 plays a crucial role in stress protection; this function is independent of the role of Var1 as a structural element of the mitochondrial ribosome as it remains protective in cells lacking mitochondrial DNA and, thus, mitochondrial rRNAs (Figure 22C).

3.4 Var1 is a polyN protein with aggregation protein propensity

Var1 belongs to the S3 protein family, members of which are universal and crucial constituents of small ribosomal subunits and are conserved among all kingdoms of life [131]. However, unlike other S3 proteins, Var1 is extremely rich in asparagine residues (Figure 23A). More than 30% of all amino acid residues in the Var1 sequence are asparagine residues. The analysis of the yeast proteome done by Timo Mühlhaus identified Var1 as the most N-rich protein (Figure 23B, C). PolyN and polyQ proteins are well-known for their aggregation-prone behavior [132]. While mitochondrially encoded Var1 homologs in fungi were consistently N-rich, nuclear-encoded S3 proteins (such as the mitochondrial S3 proteins of human cells) and bacterial S3 proteins have only a low, 'normal' asparagine content (Figure 23C, Appendix

Table 11).
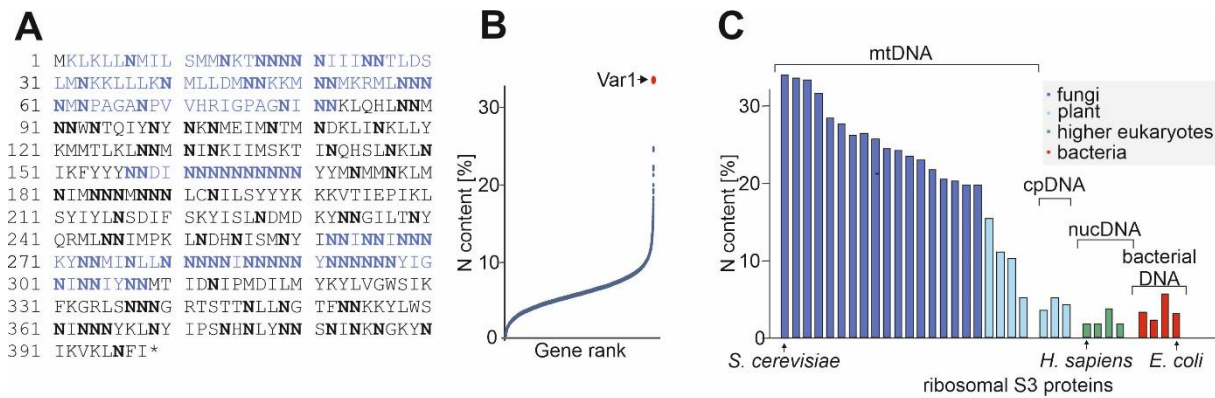
Figure 23: Mitochondrial encoded S3 proteins accumulated high asparagine amounts. A Primary structure of Var1. Insertions not present in bacterial S3 proteins are highlighted in blue, and all asparagine residues (N) are marked in bold. **B** The relative content of asparagine residues was calculated for all yeast proteins [133]. Var1 has the highest content, and its position is indicated. **C** The asparagine content in Var1 and other S3 proteins was calculated for proteins encoded by either the mitochondrial DNA (mtDNA), the chloroplast DNA (cpDNA), the nuclear DNA (nucDNA), or the genome of bacteria. See Appendix

Table 11 for details.

Var1 contains three loop-forming segments not found in other S3 proteins and represents continuous strings of asparagines. These loops largely contribute to the high asparagine content of Var1 (blue regions in Figure 23A and Figure 24A). These loops protrude from a structurally conserved core and are not found in the structures of bacterial S3 protein *Ec*-S3 and the human Mrps24.
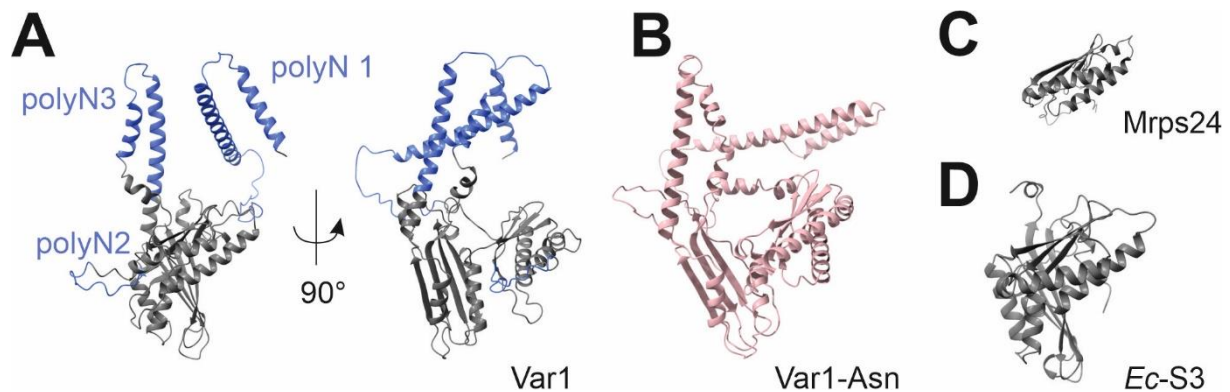
Figure 24: Protein structure of Var1 and S3 homologs. A AlphaFold prediction of Var1 with regions protruding from the conserved core colored in blue. **B** AlphaFold prediction of a synthetic Var1 variant with a lower asparagine content (Figure 39). **C, D** The structure of *Ec*S3 (top) and Mrps24 (bottom) as predicted by AlphaFold [121]. All structures were created using ChimeraX [122].

Due to the remarkable conserved structure of S3 proteins, as seen in the core from the ancestral S3, and in homologous found in other yeast with lower asparagine levels, I decided to test the complementation of Var1 with those homologous. I used a shuffle approach to exchange Var1

with different S3 homologous and a mutant containing lower asparagine levels of 18.5% (Figure 39, Figure 25B). To this end, I created a knock-out of the translational activator of Var1, named Sov1. A truncated version of Sov1 (aa 1-792) was expressed in this strain, allowing for late-stage assembly of the mitoribosome but hampering the translation of endogenous Var1 [95]. MTS-Var1 expressed from a *URA3* plasmid was replaced by the different S3- homologs via the addition of 5-Fluoroorotic acid (5-FOA). 5-FOA is metabolized to the toxic component 5-fluorouracil when the functional *URA3* gene is present, forcing cells to expel the initial MTS-Var1 plasmid. Despite the structural similarity, all homologous failed to restore mitochondrial translation, probably due to assembly constraints into the mitoribosome (Figure 25A).
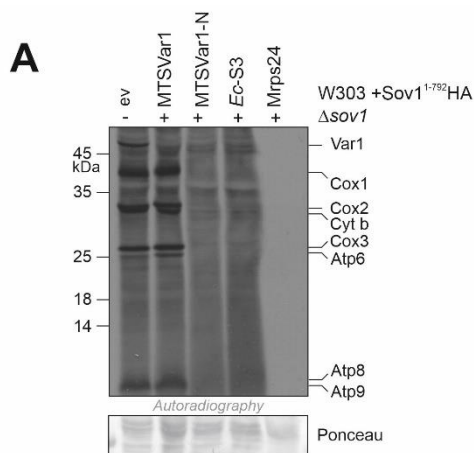
Figure 25: S3 homologs cannot rescue the translation by the loss of the mitochondrial Var1 protein. A Indicated strains were grown in galactose medium without methionine. Mitochondrial translation products were radiolabeled for 15 min with ^{35}S-methionine at 30°C in the presence of cycloheximide to inhibit cytosolic translation. Radiolabeled proteins were visualized by SDS-PAGE and autoradiography. The ponceau staining is shown as a loading control.

To reduce the asparagine content further but still allow electrostatic interactions with surrounding mitoribosomal subunits and rRNA, I decided to delete the loops found in Var1(Figure 24A) and try the same shuffle approach described above. Single deletions of L_1 and L_3 still retained their capacity for respiration, as seen when restreaked on glycerol plates. Interestingly, the deletion of L_2 and the triple knockouts prevented respiratory growth (Figure 25A, B). I used the same strains for a drop dilution assay to get a more quantitative impression of the respiration capacity. While the empty vector strain cells could not respirate due to the loss of endogenous Var1, there was a gradual loss of restored respiratory capacity in ΔL_1 and ΔL_3 (Figure 25C). ΔL_1 and ΔL_3 mutants showed a reduced and changed pattern of translation products in an *in organello* assay, indicating crucial roles of those amino acid stretches for translation (Figure 26D).
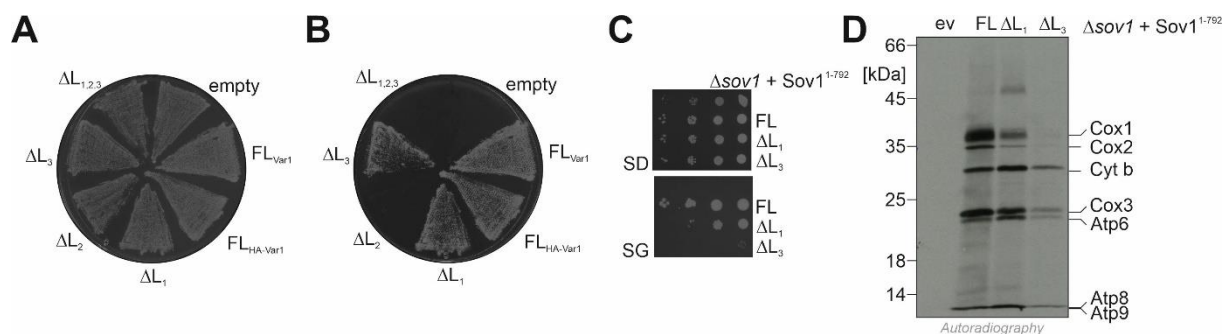
Figure 26: Truncated MTS-Var1 variants show reduced functionality. A Δ*sov1* with Sov1[1-792] expression with different *LEU* plasmids containing truncated Var1 versions, full length (FL, with and without N-terminal HA tag between the MTS and the gene of interest) Var1, and empty vector control restreaked on glucose media. **B** Strains as seen in A stamped onto glycerol media. **C** Cells of the indicated strains were grown to log phase in galactose medium before tenfold serial dilutions were dropped onto plates with the indicated carbon sources and incubated at 30°C. **D** Mitochondrial translation products were radiolabeled in isolated mitochondria of the indicated strains for 10 min at 30°C. Radiolabeled proteins were resolved by SDS-PAGE and visualized by autoradiography. In the MTS-Var1-expressing strain, no Var1 signal is visible since Var1 is not translated in mitochondria.

I next tested the aggregation behavior of Var1 directly. To this end, I performed *in organello* translation experiments during which mitochondrial translation products were radiolabeled. Subsequently, I lysed mitochondria and separated soluble from aggregated proteins via centrifugation. The expression of the misfolded mtCPY* and mtDHRF[mut], as well as their folding competent counterparts mtCPY and mtDHFR, induced Var1 aggregation to different extends (Figure 27A), while Var1 stayed soluble in the control. The identification of protein levels showed that the misfolding model substrates differed in their aggregation propensity. While mtCPY* and mtCPY (HA signal at 66 kDa) were exclusively found in aggregates, DHFR[mut] and DHFR (HA signal at 25 kDa) were only partially located in the pellet fraction (Figure 27B). This result is in accordance with the different behavior of mtCPY* and mtDHFR[mut] showing that these misfolding model substrates own different aggregation propensities. Surprisingly, Var1 was always soluble, suggesting that only newly synthesized Var1 protein was vulnerable to aggregation.
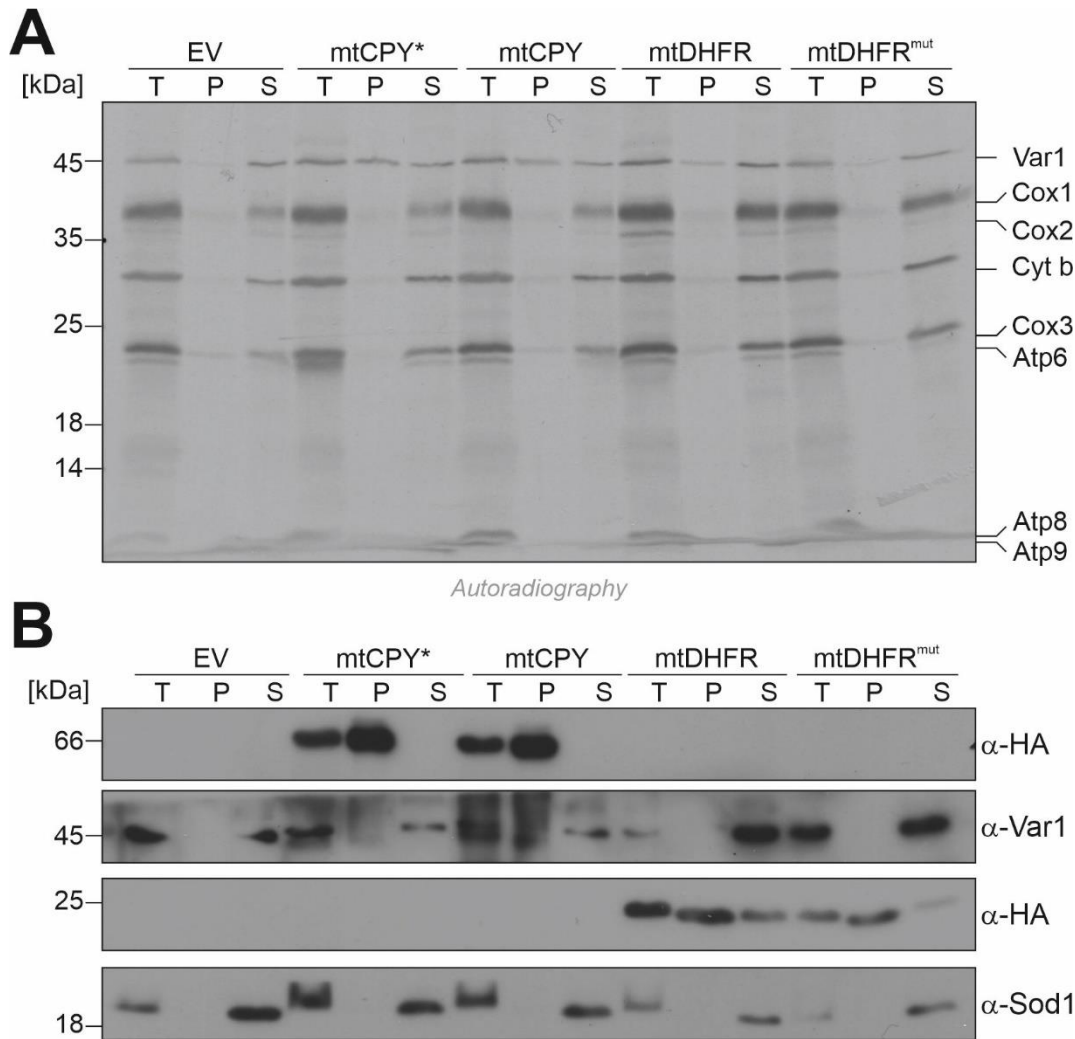
Figure 27: Newly synthesized Var1 is prone to aggregation. A Mitochondria were isolated from cells harboring plasmids to express mtCPY*, mtCPY, mtDHFR, mtDHFR^{mut}, or empty vector for control. Mitochondria were resuspended *in organello* translation buffer and incubated for 10 min at 25°C before mitochondrial translation products were radiolabeled for 20 min at 25°C. The sample was split, and one aliquot (T, total) was directly lysed in sample buffer. The other aliquot was incubated for 30 min at 37°C, lysed in Triton X-100 buffer, and separated into pellet (P) and soluble (S) fractions by centrifugation. Proteins from the supernatant were precipitated by the addition of trichloroacetic acid. Proteins were separated by SDS page and visualized by autoradiography. **B** The same membrane was used to check the protein levels of the indicated proteins. Sod1 was used as a loading control.

To see if the aggregated Var1 fractions are composed of partially or entirely assembled ribosomes, I isolated RNA from the fractions as described in the experiment above. Since ribosomes contain, besides all the other mitoribosomal subunits also, rRNA, I used quantitative real-time PCR (RT qPCR) with primers specific for the small (15S) and large (21S) rRNA. No rRNA was detectable in pellets with reinduced mtCPY*, suggesting that Var1 aggregates do not contain ribosomes (Figure 28A, B). Please note that the RNA was isolated from the same amount of mitochondria, and the RNA levels were not adjusted after the isolation, allowing only qualitative statements.
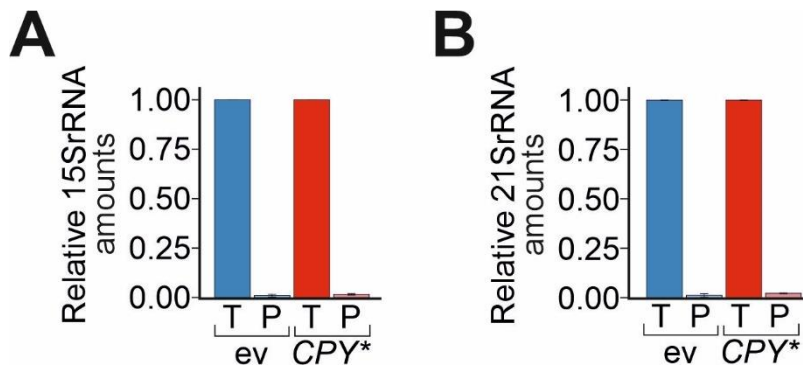
Figure 28: Ribosomes are not found in Var1 aggregates. A, **B** RNA was isolated from whole mitochondria (T) or pellet fractions (P) after Triton X-100 lysis. The levels of the indicated mRNAs were measured by RT qPCR. 15SrRNA (left) and 21SrRNA (right). Shown are the mean values of three biological replicates.

Using the possibility to express Var1 as a nuclear-encoded protein, I created an MTS-Var1-mScarlet construct with an inducible *GAL* promotor. This allowed me to visualize the Var1 aggregates within mitochondria. After 4 hours of expression in WT cells grown in raffinose media, MTS-Var1-mScarlet colocalized with the mitochondrial marker (mtGFP). Var1 was already forming small aggregates under these conditions. To ensure mitochondrial localization, expression of MTS-Var1 was stopped before exposing yeast cells to heat stress (30 min, 40°C), resulting in distinct Var1 foci (Figure 29A). Interestingly, the constitutive expression of MTS-Var1-eGFP showed extensive non-structured formations in WT cells (Figure 29B). The same construct in cells lacking endogenous VAR1 (Δ*var1*) led to a more dispersed signal in many small aggregates upon heat stress (Figure 29C). The difference found in WT and Δ*var1* cells might be due to the presence and inclusion of RNA into Var1 structures.
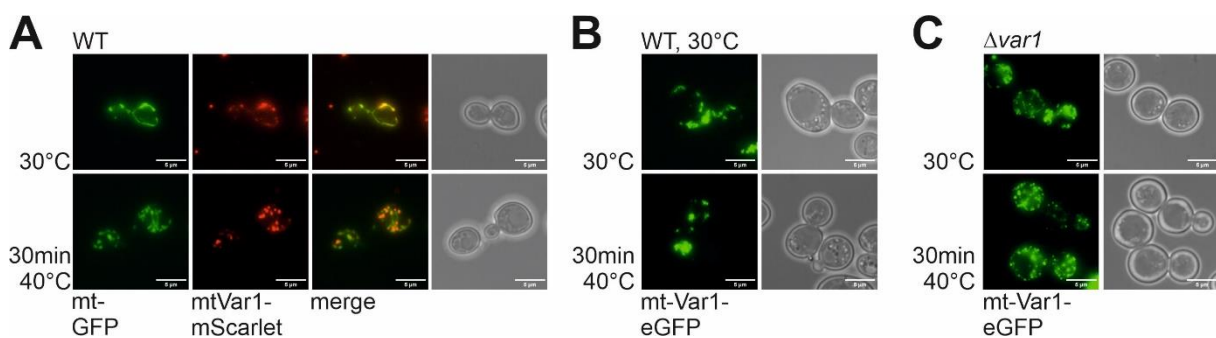
Figure 29: Var1 forms aggregates in mitochondria A WT cells were transformed with mtGFP and an inducible MTS-Var1-mScarlet under an inducible *GAL* promotor. Cells were grown in raffinose medium, with an additional 0.5% galactose for 4 hours (top). After the expression was stopped, cells were shifted to 40°C for 30 minutes and analyzed by microscopy (bottom). **B** WT and **C** Δ*var1* cells expressing MTS-Var1-eGFP with a constitutive *TEF* promotor were grown in raffinose medium at 30°C (top) and subsequently subjected to heat stress for 30 minutes at 40°C (bottom).

33

In summary, Var1 is an N-rich protein that forms intramitochondrial aggregates under stress conditions. In the following, I will refer to these Var1 aggregates as **Var1 bodies**.

3.5 Nuclear expression of Var1 leads to clogging of the TOM complex and triggers the mitoprotein-induced stress response

Why is Var1 mitochondrially encoded when it can be productively imported into mitochondria? To answer this question, I analyzed the consequences of expressing MTS-Var1 in WT cells, thus in cells with a normal, Var1-expressing mitochondrial genome. This allowed me to study the consequences of a nuclear Var1 expression, independent of its effects on mitochondrial gene expression. Expression of MTS-Var1 strongly compromised cell growth when the expression was induced from a *GAL* promotor (Figure 30A, B). The toxicity of Var1 was independent of the presequence as an expression of Var1 in the cytosol was likewise toxic. On the contrary, expression of the bacterial S3 protein of *E. coli (Ec*S3), thus an S3 variant of normal asparagine content, was not toxic, neither when it was expressed in the cytosol nor when it was targeted to mitochondria. Expressing other mitochondrial ribosomal proteins, such as Mrps24, had no toxic effect. Thus, nuclear expression of Var1 severely compromises cellular viability, explaining why the *VAR1* gene remained in the mitochondrial genome and was not transferred to the nucleus, even though the productive targeting to mitochondria of Var1 per se is possible.
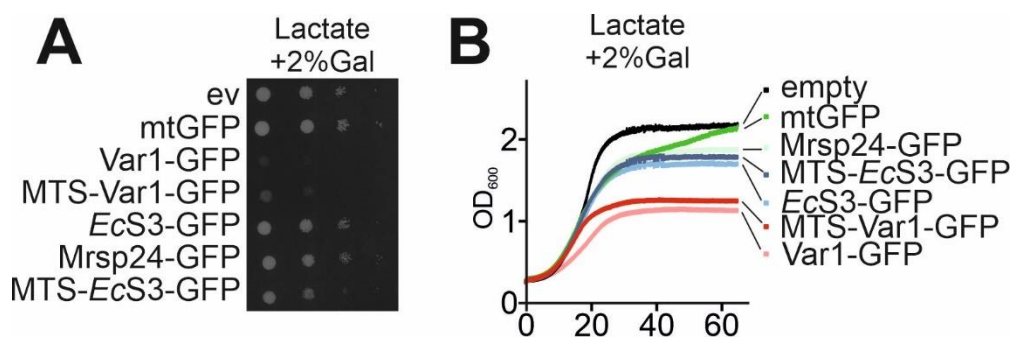
Figure 30: Expression of polyN S3 proteins is toxic for cells A The proteins indicated were expressed in WT cells from a galactose-inducible promoter. Tenfold serial dilutions of lactate-grown precultures were dropped onto galactose-containing lactate plates and further incubated at 30°C. **B** The growth of the cells shown in A was analyzed in a spectrometer under constant agitation.

To better characterize the consequences of MTS-Var1 expression, I analyzed the induction of stress response pathways by RT qPCR with primers specific for the yeast-optimized *VAR1*, *RPN4*, and *CIS1*. The expression of MTS-Var1 was comparable in WT and *rho⁰* cells. (Figure

31A). Still, MTS-Var1 induced the synthesis of *RPN4* mRNA, indicative of the mitoprotein-induced stress pathway [20][49]. Rpn4 is the master transcription factor for proteins of the ubiquitin-proteasome system [134], and its induction increases the proteolytic activity of yeast cells, a hallmark of UPR[am] (Figure 31B) [135]. In addition, I detected highly induced levels of *CIS1*, particularly in rho^0 cells (Figure 31C). Cis1 is the predominant target of the mitochondrial compromised protein import response (mitoCPR) [100], which, upon induction under stress conditions, recruits the AAA+ extractor Msp1 to the TOM complex to remove stalled import intermediates [3,136]. The induction of Cis1 indicates a strong effect of MTS-Var1 as a clogger of the import machinery. To test whether higher mRNA levels also lead to higher protein levels, reporter assays can be used. The promotor of a specific gene is placed upstream of a yellow fluorescent protein (YFP), which can be detected via photometry. I measured the expression of YFP under the control of the pleiotropic drug reporter element (PDRE). The PDRE also controls the expression of *CIS1*. This reporter assay also supported the strong induction of the mitoCPR (Figure 31D). The strong induction of the YFP protein from the PDRE confirmed that expression of the MTS-Var1 induces severe stress conditions in the rho^0 cells. The import of the aggregation-prone Var1 protein into mitochondria leads to problems at the TOM complex, presumably by clogging of the import pore. These problems are particularly pronounced in rho^0 cells, which already suffer from a reduced membrane potential and lower protein import efficiency.
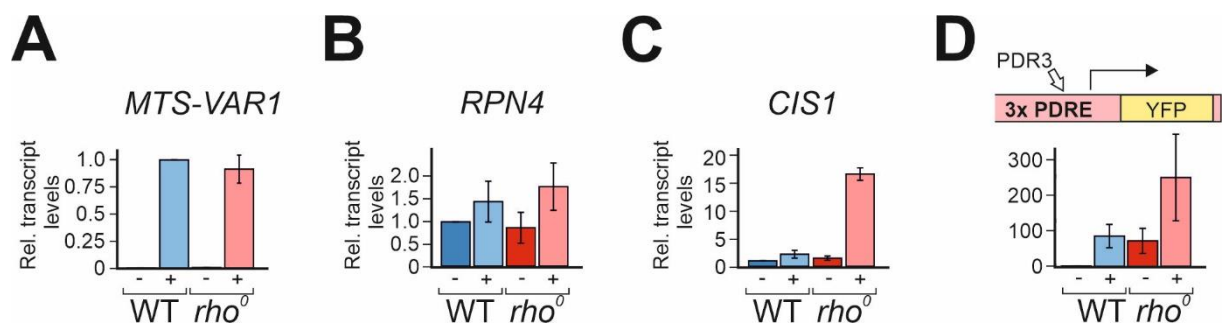
Figure 31: Allotopic Var1 expression induces mitoCPR. A-C The indicated strains were grown on galactose medium at 30°C. The levels of the indicated mRNAs were measured from cell extracts by RT qPCR. **D** The response from the pleiotropic drug response element was measured in the different strains using a genetically encoded chromosomally integrated sensor [137]. The data were quantified from three independent measurements of cells grown to log phase in galactose medium.

To compare the import competence of Var1 directly to other proteins, I tested the *in vitro* import of different S3 homologs. The bacterial S3 protein MTS-*Ec*S3 was imported without any problems. MTS-Var1 lysates showed only low amounts of imported protein. Still, a major part was always protected from protease treatment when the membrane potential was destroyed.

35

One reason might be that aggregated Var1 is inaccessible for PK (Figure 32A). I reasoned that due to the aggregation propensity of Var1, prolonged incubation before import could decrease efficient translocation. Indeed, incubating MTS-Var1 lysates in SH-buffer for a short time strongly decreased import efficiency, while Hsp60 lysate showed stable import rates over time (Figure 32B). Lost import competence could be due to the dilution of present chaperones in the lysate when added to the SH buffer.
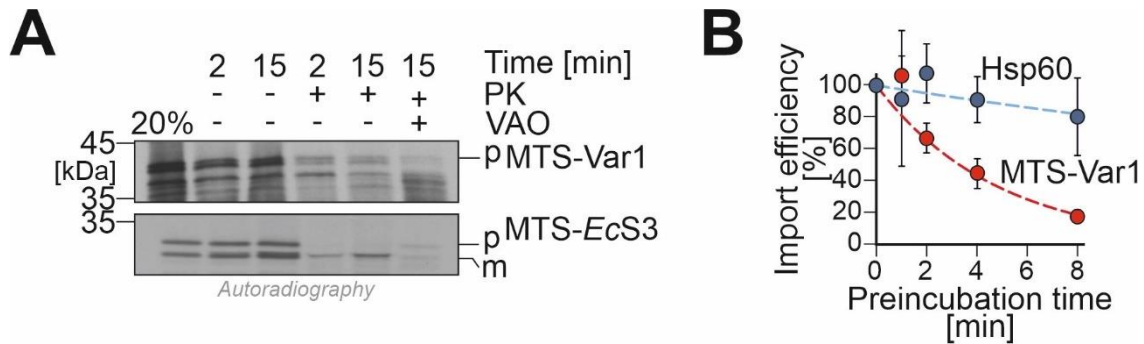
Figure 32: Var1 quickly loses import competence *in vitro*. A MTS-Var1 and MTS-*EcS3* were synthesized in reticulocyte lysate as radiolabeled proteins and incubated with isolated WT mitochondria for the indicated times. As a negative control, the membrane potential was destroyed via the addition of valinomycin, antimycin, and oligomycin (VAO). Non-imported protein was degraded by the addition of proteinase K (PK). The positions of precursor (p) and mature (m) forms are indicated. **B** Reticulocyte lysate containing radiolabeled precursors of MTS-Var1 and Hsp60 were mixed with import buffer and incubated for indicated times. Mitochondria were added, and the amount of imported mature proteins was quantified. Whereas the Hsp60 precursor remained import-competent over time, the MTS-Var1 precursor rapidly lost its ability to be imported into mitochondria, presumably owing to its aggregation-prone nature.

To identify the interactors of MTS-Var1, I constitutively expressed MTS-Var1-GFP in Δ*var1* cells as well as the mitochondrial protein Atp1-GFP in WT cells or used an empty vector for control. Mitochondria were purified from the cells and lysed with Triton X-100. Proteins were isolated with magnetic GFP-Traps and subjected to mass spectrometry (Figure 33A). The mass spectrometry samples were measured by Markus Räschle and analyzed by Jan-Eric Bökenkamp. The interactome of Var1 contained was highly enriched for proteins of the small subunit of the mitochondrial ribosome (Figure 33B, C), confirming the productive assembly of the nuclear-encoded MTS-Var1 protein into the ribosome. Proteins of the large subunit were also recovered, however, to a lesser extent. In addition, the MTS-Var1-GFP coisolated efficiently subunits of the TOM complex (Tom5, Tom6, Tom7, Tom20, and Tom22), and none of these was recovered with the Atp1-GFP or empty vector control (data not shown). This confirms the tight association of MTS-Var1 with the import pore. Intriguingly, MTS-Var1 also recovered a third group of proteins, namely mitochondrial chaperones and proteases (Figure 33B, D). The whole complement of chaperones was recovered with MTS-Var1, including the

mitochondrial Hsp70 proteins Ssc1 and Ssq1, the J protein for matrix protein folding Mdj1, the chaperonin Hsp60 as well as the poorly characterized chaperones Tcm62 and Mcx1. Also, the Pim1 and the mAAA protease of the inner membrane with its subunits Yta10/Afg3 and Yta12. Interestingly, Hsp78 was not recovered with MTS-Var1, suggesting that Hsp78 and Var1 do not physically interact. This strong association is not just the consequence of its folding in the matrix, as it was not seen for other proteins such as Atp1, which is similar abundant, of similar size as Var1 and also needs assembly after its import into the matrix [138] (data not shown).
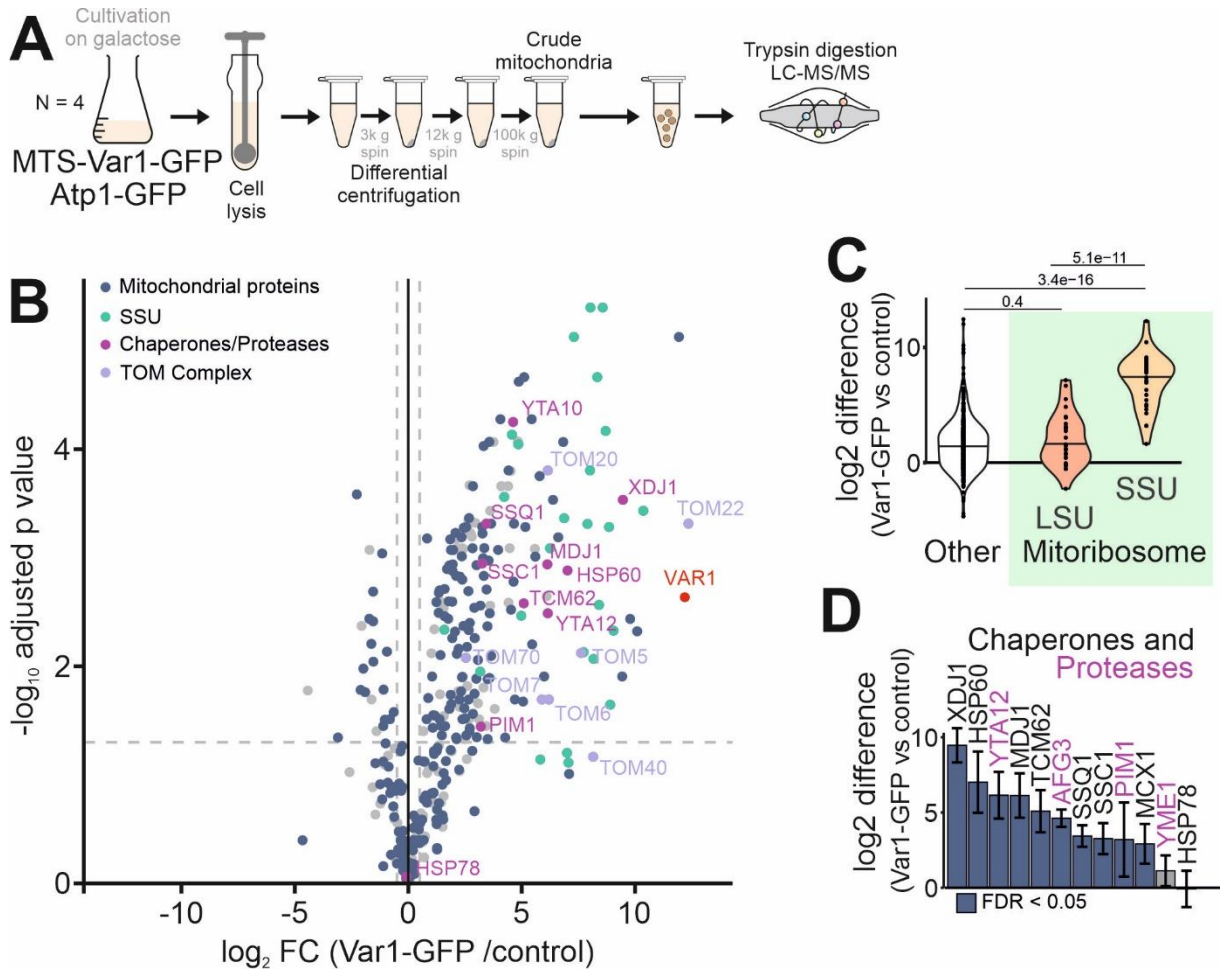
Figure 33: Co-immunoprecipitation of Var1 strongly interacts with the mitochondrial proteostasis network.
A Scheme of the detection of Var1 interactors by mass spectrometry. Mitochondria of Δ*var1* cells expressing either MTS-Var1 or MTS-Var1-eGFP and WT cells expressing Atp1-GFP were isolated from cells grown in galactose media. Mitochondria were lysed with Triton X-100 and proteins were isolated via a co-immunoprecipitation with GFP-Traps. **B** Proteins identified with Var1-GFP or control cells were detected. The volcano plot shows the proteins co-isolated with Var1 on the right-hand side. The positions of chaperones and TOM subunits are indicated. **C** Violine plot showing the relative enrichment (log2 fold change) of different protein groups with the Var1-GFP over the control sample. **D** Enrichment of mitochondrial chaperones and proteases with Var1-GFP over control. The IMS protease Yme1 and Hsp78 were not recovered with Var1. Graphs B, C, and D were plotted in R by Christian Koch.

Thus, my data show that Var1 is a highly aggregation-prone protein that is difficult to import and interacts with many components of the mitochondrial proteostasis network once it reaches the matrix.

3.6 Are Var1 bodies distinct from Hsp78 aggregates?

The observed aggregation propensity of Var1, its interaction with chaperones and proteases, and its ability to protect rho^0 cells against acute heat stress resembles the features that are known for the polyQ protein Rnq1 and other aggregate-nucleating factors of the cytosol [139,140]. They absorb and buffer misfolded proteins during transient periods of proteotoxic insults. This motivated me to test whether Var1 influences the mitochondrial proteome even in cells that lack a mitochondrial genome and, thus, mitochondrial ribosomes. To this end, I grew WT and rho^0 cells on a galactose-based medium containing an MTS-Var1 expression plasmid or an empty vector for control. Galactose allows the growth of the cells by fermentation but, unlike glucose, does not repress mitochondrial proteins [73]. Cellular extracts from 4 biological replicates were subjected to mass spectrometry (**Figure** 34A). The expression of MTS-Var1 left a characteristic footprint on the proteomes of these cells (**Figure** 34B). In both strains, the expression of MTS-Var1 increased the relative abundance of mitochondrial proteins in these cells (**Figure** 34C, D). This was particularly pronounced in rho^0 cells, even though these cells do not contain functional mitochondrial ribosomes due to the absence of mitochondrial rRNA. This shows that the ribosome-independent function of Var1 improves mitochondrial biogenesis.
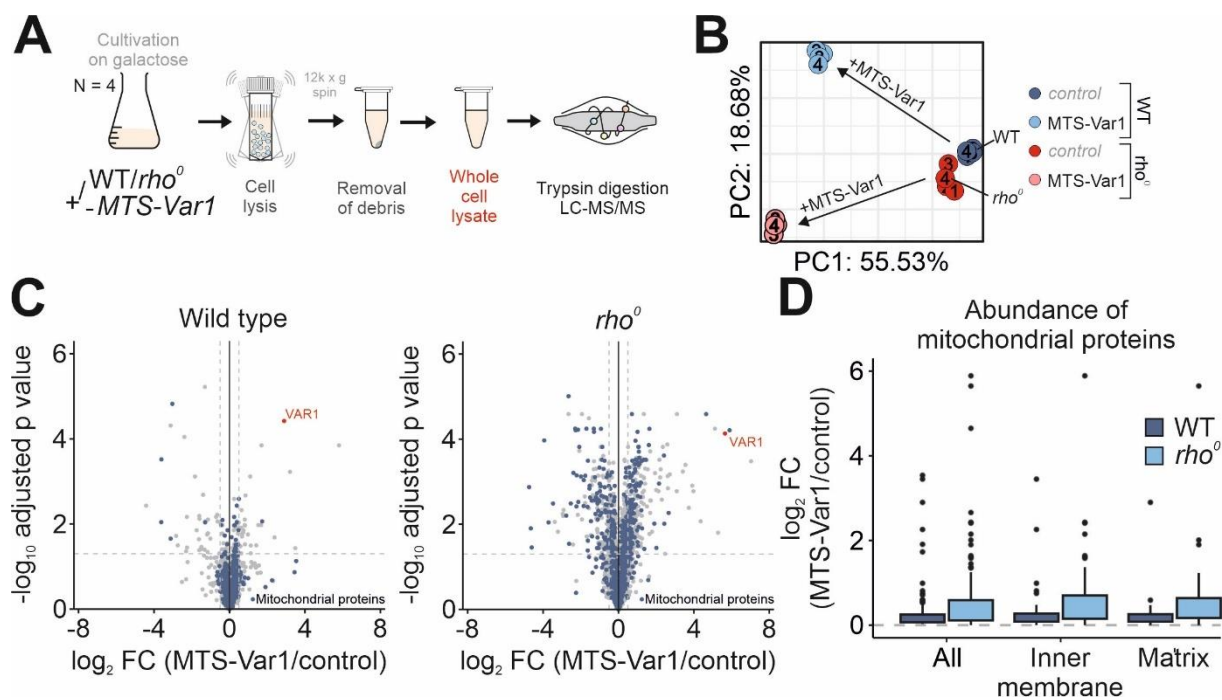
Figure 34: Allotopic MTS-Var1 expression has a strong effect on cells. A Scheme of the proteomic assessment of WT and *rho⁰* cells that express the nuclear-encoded MTS-Var1. **B** The principal component analysis (PCA) shows a strong footprint of Var1 expression on cells independent of the presence of a mitochondrial genome. The analysis is based on 2924 different proteins between any condition (ANOVA F-statistic p-value < 0.05). **C** Volcano plot of the whole cell proteomes of WT and *rho⁰* cells showing the effect of MTS-Var1 expression. **D** Expression of MTS-Var1 increased the levels of many mitochondrial matrix and inner membrane proteins. Markus Räschle measured the proteomics data, which was subsequently statistically analyzed and imputed by Jan-Eric Bökenkamp. Graphs shown in B, C, and D were plotted in RStudio by Christian Koch.

Finally, I tested whether the Var1 bodies behave differently from Hsp78 aggregates. To this end, Hsp78 induced aggregates from heat stress mainly resolved after 4 hours of recovery (Figure 35A). Are Var1 bodies also of a transient nature and resolved once cells recover from stress conditions? I grew cells expressing mtGFP at 30°C and induced the expression of MTS-Var1-mScarlet for 4 h. In these strains, MTS-Var1 was expressed from a *GAL1* promoter. After the expression of MTS-Var1-mScarlet was stopped, the cells were subjected to heat shock for 30 min at 40°C. Still, the Var1 bodies persisted after 4 hours of recovery (Figure 35B).
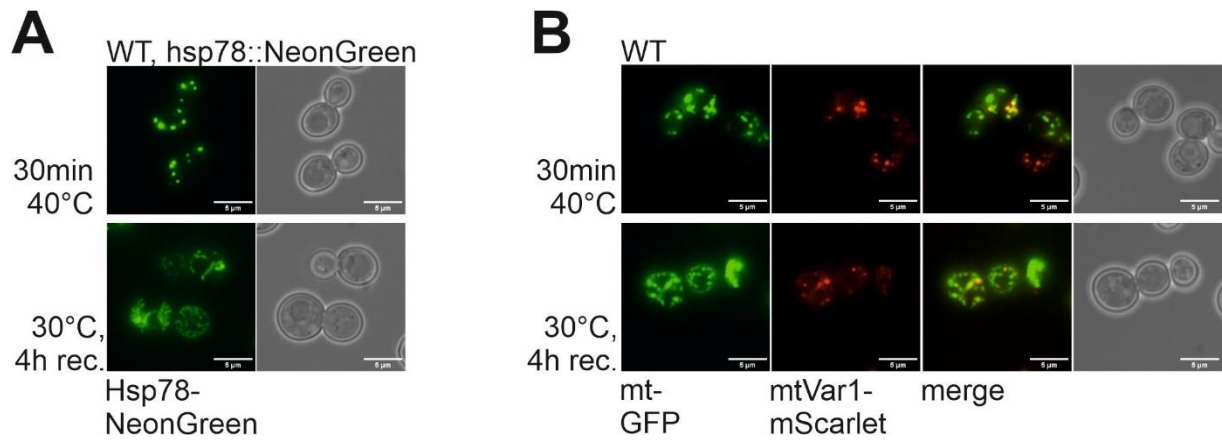
Figure 35: Var1 bodies do not resolve similarly to Hsp78. A Genomically tagged *HSP78* with mNeonGreen after 30 min 40°C (top) and after 4 h of recovery at 30°C (bottom) **B** Cells expressing mtGFP and Var1-mScarlet (top) were transiently exposed to a short heat shock for 30 min (top). After recovery, Var1 bodies persisted (bottom).

Then, I induced MTS-Var1mScarlet expression in cells expressing genomically tagged *HSP78*-mNeonGreen (Figure 36A). Hsp78 was dispersed and showed a uniform distribution in mitochondria, while Var1 formed foci under these conditions (Figure 36B). I shifted the cells to galactose-free raffinose medium to stop MTS-Var1 expression and for 30 min to 40°C. After this heat shock, both proteins punctate distribution. However, all Var bodies also contained Hsp78 (Figure 36 C). When we reduced the temperature to 30°C and cultured the cells for 4 more hours in raffinose, Var1 maintained its punctate distribution, whereas Hsp78 largely dispersed again (Figure 36 D).
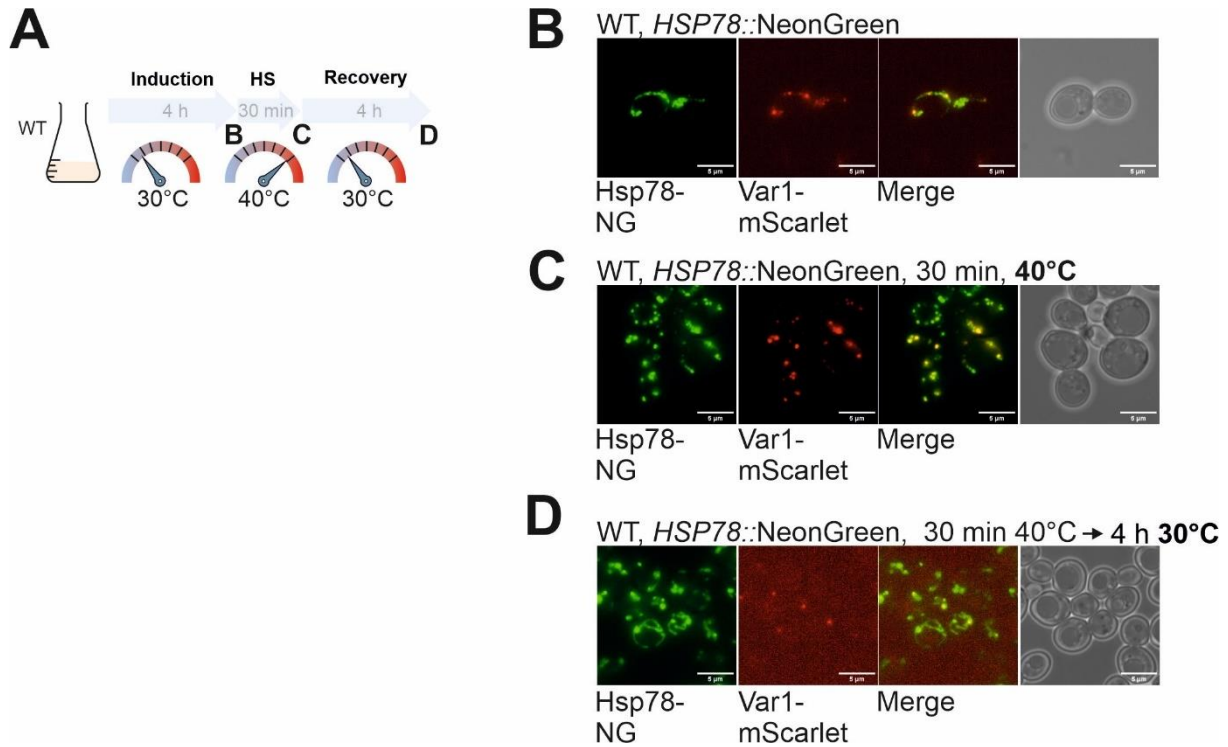
Figure 36: Var1 bodies formed by overexpression are Hsp78 positive A Schematics of the experimental setup. **B** WT with the induction of Var1-mScarlet for 4 h together with genomically tagged *HSP78* with NeonGreen (NG). **C** Cells were transiently exposed to a short heat shock for 30 min. Both proteins formed puncta during the heat induction. Please note that Var1 bodies were also positive for Hsp78; however, Hsp78 is also bound to structures that do not contain Var1. **D** After recovery, Hsp78 was removed from these Var1-negative structures, whereas Var1 bodies persisted (bottom).

Finally, I grew cells lacking the gene for mitochondrially encoded Var1 expressing MTS-Var1-GFP and Hsp78-mScarlet, both expressed from constitutive promoters at 30°C. Hsp78 was predominantly dispersed and showed a uniform distribution in mitochondria, whereas MTS-Var1 was largely part of punctate foci (Figure 37B). Both proteins did not colocalize. Then, I shifted the cells to 40°C for 30 min, which induced the formation of Hsp78-bound aggregates (Figure 37C). Most of the Hsp78-positive aggregates were distinct from Var1 bodies, showing that Hsp78 binds also client proteins that are not associated with Var1. When I reduced the temperature to 30°C and cultured the cells for 4 more hours, Var1 maintained its punctate distribution, whereas most of the Hsp78 dispersed again (Figure 37D).
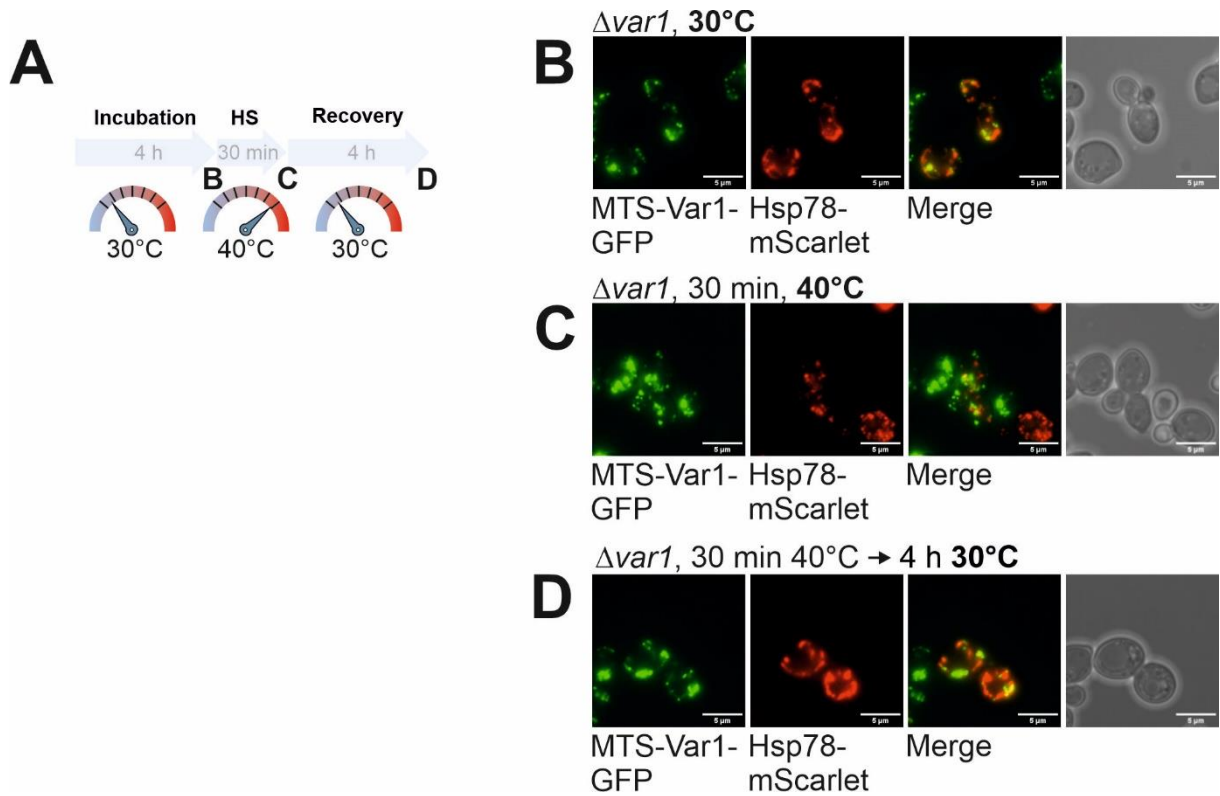
Figure 37: Hsp78 and Var1 form distinct aggregates. A-D *Δvar1* cells expressing MTS-Var1-GFP (*TEF* promoter) and Hsp78-mScarlet (*TPI* promoter) were grown at 30°C (B) and transiently exposed to a short heat shock at 40°C for 30 min (C). Subsequently, cells were brought back to 30°C and grown for 4 h (D).

Two conclusions can be drawn from this experiment: First, the Var1 bodies represent a subfraction of mitochondrial protein aggregates, and second, Var1 bodies are relatively stable and cannot be quickly resolved, whereas other Hsp78-bound aggregates are more transient and can be resolved. The activity of Hsp78 as a disaggregrase likely directly promotes the release of aggregated proteins from these transient aggregates (Figure 38).

4 DISCUSSION

The controlled induction of protein aggregation is a powerful strategy to sequester potentially harmful proteins [16,141]. A well-studied example is the formation of inclusion bodies in bacteria. These amorphous aggregates considerably reduce protein toxicity, allowing an even higher overexpressing of proteins [141–143]. Chaperones of the Hsp100, Hsp70, and Hsp60 protein families, such as ClpB, GroEL, and DnaK, do not prevent inclusion body formation in the first place but have been shown to disassemble these aggregates by releasing their proteins [144–147]. In the cytosol and nucleus of eukaryotic cells, several distinct types of protein aggregates have been characterized, which have ambivalent consequences for cellular physiology: on the one hand, they can sequester potentially harmful misfolded proteins and increase stress resistance; on the other hand, they also can be detrimental by impairing the function of cellular proteins and membranes [148–150]. The formation of intra-mitochondrial aggregates has been reported in the past [111,151–154], but their relevance for mitochondrial proteostasis has mainly remained elusive. My thesis aimed to study the formation of protein aggregates in the mitochondrial matrix of yeast cells. Indeed, I could demonstrate that protein aggregates form upon proteotoxic stress that can either be induced via a general response to heat stress or, more specifically, overload of the matrix via the import of misfolding model substrates. This results in aggregates that can be visualized by the mitochondrial disaggregase Hsp78 or the mitochondrial encoded protein Var1, with both forming distinct aggregate types. In the following, I would like to discuss the presence of different aggregate structures with regard to the mitochondrial proteostasis network and the relevance for higher eukaryotes.

4.1 Hsp78 as a marker for matrix aggregates

Using fluorescently tagged versions of Hsp78 was crucial to visualize intramitochondrial protein aggregates. Upon shift from non-stress to heat-stress conditions, Hsp78-GFP formed punctae, which colocalized with the mitochondrial network (Figure 7). This heat-induced aggregate formation of Hsp78 has been studied before [111] and is especially associated with the folding of newly imported proteins. However, as shown by the appearance of aggregates in import defective cells or with a blocked translation, the substrate spectrum must be more extensive than described before (Figure 14). The association of Hsp78 to substrates was confirmed by microscopy with the misfolding model substrates and the yeast protein Aim17.

Aggregates induced by the misfolding mtCPY* resulted in the formation of permanent aggregates, presumably owning the intrinsically misfolded nature of the protein [46]. The misfolding mtDHFR^{mut} behaved differently by forming aggregates only upon heat shock (Figure 16) and persisted in Δ*hsp78* cells, similarly to Aim17 (Figure 17). Two conclusions can be drawn from that: (1) since the misfolding model substrates behave differently, Hsp78 can bind aggregates with different features. (2) the refolding depends on the characteristics of aggregated protein contained in these structures (Figure 38). This also mirrors the binding of Hsp104 to different cytosolic protein aggregates. While the toxic INQs are labeled by Hsp104 and not resolved, stress granules like the JUNQs, INQs, and MitoStores get resolved via Hsp104 [49]. While Krämer and colleagues successfully co-immunoprecipitated Hsp104 to identify the disaggregase substrates, the analogous Hsp78 pull-down was inefficient. The proteomic analysis showed only minor enrichment of the possible matrix and inner membrane substrates (Figure 13). This indicates that either the interaction of Hsp78 to its substrate is not particularly strong or the hexametric complex of Hsp78 is not as stable as that of Hsp104. The Hsp78 substrates identified by Jaworek and colleagues also showed similarly low enrichment, significance values, and number of proteins identified [110]. Each ring of the Hsp78 owns a Walker A and B motif for ATP binding and hydrolyzation. Mutations in each motif limit their function, resulting in the trapping of substrates. However, I decided not to use the Walker A variant K149T since it displayed non-physiological behavior. While it is unclear if trapping mutant E216Q/E614Q, used by Jowarek et al., still assembles properly, Krzewska and colleagues showed that K149T can still form a hexamer [120]. Still, mutations of both Walker B motifs did not improve the quality of their proteomics data. Besides minor changes in the hits identified, it is not clear whether this displays the physiological substrate range. Interestingly, Hsp78 substrates in *rho⁰* cells showed a more significant enrichment of MRPs in the MS experiment. Those might be orphaned upon loss of mitochondrial rRNA, suggesting that non-assembled proteins serve as substrates of Hsp78 even under non-stress conditions. All in all, I could probe the substrate spectrum of Hsp78, which includes freshly imported proteins and non-assembled- /disassembled proteins from complexes, which is especially relevant for cells to recover from intense stress conditions.

4.2 Hsp78 and Pim1 compete for substrates

Pim1, the master protease of the matrix, is known to prevent protein aggregates in the matrix [155]. Therefore, I decided to further investigate its role in the context of disaggregation. In the presence of Hsp78, only a few mitochondrial proteins were bound to the non-catalytic mutant of Pim1 (Figure 19). However, in *Δhsp78* mutants, the number of Pim1-bound proteins was strongly increased (Figure 19), suggesting that sequestration or refolding by Hsp78 and degradation by Pim1 are competing outcomes of protein misfolding in mitochondria. It has been reported before that the Pim1-mediated degradation of model substrates is slowed in *Δhsp78* mitochondria [156]. This led to the proposal that Hsp78 promotes protein degradation via Pim1. However, it is also possible that the decreased degradation of the tested model substrate is due to the competition with other substrates that bind to Pim1 in *Δhsp78* mitochondria. In addition to substrates on Pim1, We found several proteins that efficiently co-eluted with Pim1, such as Mam33, Mrx6, and Pet20. These three proteins were recently reported to be permanent complex partners of Pim1 and involved in controlling the copy number of mitochondrial genomes [157]. Interestingly, we found two similar enriched proteins: Sue1, a protein required for the degradation of the IMS protein cytochrome *c* [158], and Rpo41, the mitochondrial RNA polymerase. The interaction of Pim1 with the RNA polymerase is unexpected and exciting, as it could explain the crucial role of Pim1 in mitochondrial genome stability [116]. The primers for transcription, generated by Rpo41, are also used for mtDNA replication. While it is not the only available option, since *rho⁻* genomes are also replicated without the presence of Rpo41 [159], it is tempting to speculate that Pim1 might control the mtDNA copy number directly via the amount of Rpo41 present or indirectly by further needed for replication. This function of Pim1 seems to be conserved, as a recent genome-wide study showed that single point mutants and indels in the gene for the human Pim1 homolog are critical determinants of mitochondrial DNA copy number in humans [160]. It will be exciting to study the relevance of this Pim1-Rpo41 complex in the future.

4.3 Var1 as a component of the mitochondrial proteostasis network

To study the sequestration of intra-mitochondrial aggregates, I investigated the mitochondrially encoded protein Var1(S3, rps3, uS3m). Var1 has an extremely high asparagine content. Studies have found that the elongation of amino acids affects proteins' behaviors and favors their aggregation [161]. Still especially polyN and polyQ proteins show a high propensity to

aggregate, and many diseases are associated with polyQ protein aggregates. [132] Those stretches often form tandem repeats (TRs), leading to intrinsically disordered regions (IDRs). These describe an unstable three-dimensional structure in parts of the protein that can transition to an ordered conformation upon binding with ligands or complexes. Indeed, Var1 is known to be very aggregation-prone. Mutants of mitochondrial chaperones induce the aggregation of newly synthesized Var1, a phenomenon that was observed in strains deficient in the matrix Hsp70 protein Ssc1 [101], in the matrix J protein Mdj1 [162], as well as in the chaperonins Hsp60 [106] and Tcm62 [95,163]. Ssc1 and Mdj1 directly interact with newly synthesized Var1, maintain its solubility, and facilitate its assembly into the small subunit of mitochondrial ribosomes [101,162]. I could show that proteotoxic stress in the matrix, induced via the induction of misfolded model substrates, could also induce the aggregation of newly synthesized Var1 (Figure 27). Interestingly, their folding competent analogs (mtCPY, mtDHFR) also induced Var1 body formation. The changed physiological conditions found in the matrix, with a lower pH, might hamper their proper folding. Aggregates in the matrix lead to a redistribution of the chaperones as an early response, and Ssc1 moves away from the import motor [164,165]. Similarly, stress conditions presumably recruit the chaperones to other binding sites, thereby inducing Var1 aggregation (Figure 38). Besides the MRPs and proteins of the matrix proteostasis network, a plethora of other matrix proteins were identified, which might be substrates that get sequestered together with Var1. It remains unclear whether this sequestration of proteins causes the beneficial effects of the allotopic Var1 expression when the mitochondrial translation is blocked with chloramphenicol (Figure 22). Cells might benefit from a changed baseline expression of quality control factors induced by the Var1 expression. This effect was observed by high constitutive expression under the control of the *TEF1* promotor, which is already compromised *rho^0* cells, the mtCPR (Figure 31). The WT cells combined with the low Var1 expression under the control of the *PSP2* promotor [130] might still allow import without clogging the import pores. Therefore, the induction of a stress response prior to the experiment seems unlikely. Thus, not only the positive effects observed in this experiment but also the aggregation of Var1 induced by several proteotoxic stress conditions, along with its close interaction with chaperones and proteases, makes Var1 a newly identified protein of the mitochondrial proteostasis network in yeast.

4.4 Why was Var1 retained in the mitochondrial genome?

Relocalization of the *VAR1* gene to the nucleus can restore respiration and translation (Figure 21). This raises the question of why the *VAR1* gene was retained in the mitochondrial genome. For some fungi species, the gene localization of *VAR1* in the essential *rnl* (gene coding for the large subunit of the ribosomal RNA) intron might have hampered the gene transfer to the nucleus. However, *S. cerevisiae* has a free-standing *VAR1* gene and does not explain the retainment [166]. The different Var1 analogs vary in size, attributed to the number of AT-rich repeats [167], which might have influenced the asparagine accumulation. The thereby obtained aggregation propensity of Var1 might explain why the gene was not transferred to the nuclear genome. The aggregation makes Var1 toxic when accumulating in the cytosol (Figure 30) and complicates it's *in vitro* import (Figure 32). Additionally, Var1 blocks the import pore of mitochondria *in vivo*, as seen in the co-immunoprecipitation of many components of the TOM complex. This induces stress for the cell, and it needs the mitoCPR to extract Var1 stuck in the pore. So, jeopardizing the cytosolic chaperone network is prevented by mitochondrial expression. Since Var1 is quite strongly expressed, protein levels might have also played into a similar direction of gene retention. Supersaturation describes the phenomenon when the local protein concentration exceeds the solubility threshold. Increasing at the same time the risk of aggregation and the dependence on the proteostasis network. Direct assembly of a portion of Var1 into mitoribosomes might be beneficial to control the free Var1 protein pool. So after the *VAR1* gene did accumulate these high levels of asparagine codons, the `cost` of relocating it to the nucleus was likely too high [99].

4.5 Distinct types of intra-mitochondrial aggregates

Bruderek and colleagues also used a mitochondrial-targeted mutant of GFP-DHFR to induce intramitochondrial aggregates named intramitochondrial protein quality control (IMiQ). Surprisingly, they found aggregates located near the nucleus [153]. While the DHFR[mut] constructs had a different MTS sequence and a changed order of domains, this might be sufficient to change aggregation behavior and localization within the cell. Other intramitochondrial aggregates induced by a non-folding luciferase version (MitoFLuc) were recently described and named DUMPs (deposits of unfolding mitochondrial proteins) [154]. DUMPs seem likely identical to Var1 bodies since they are inherited from mother to daughter cells. Interestingly, DUMPs are also found to be Hsp78 positive. The same result can be seen

in my experiments with the overexpression of Var1 and Hsp78. These previous results show that Hsp78 aggregates and Var1 bodies are not exclusively located in distinct sites of mitochondria, as observed in the overexpression of both proteins in my experiments. Still, the stability, composition, and different localization in Δ*var1* cells clearly make these two aggregates distinguishable.

In general, the situation in the mitochondrial matrix resembles the situation known from the yeast cytosol: Hsp78, similar to Hsp104, binds to aggregates that can have a transient or stable nature [34,35,46]. It promotes the disassembly of these structures, if possible. The polyN protein Var1 serves as a nucleation factor for stable aggregates. It thus has an analogous role to Rnq1, a prion controlling aggregate formation as an extra-genetically inheritable trait [45].
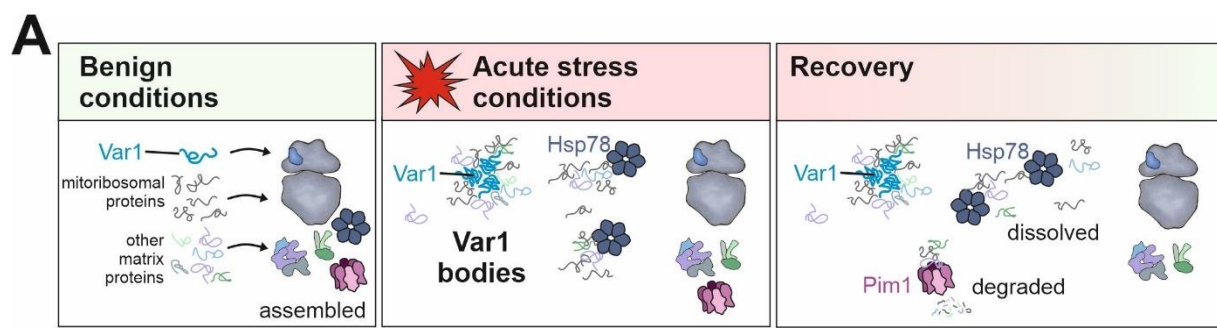
Figure 38: Model for the Var1-induced aggregate formation in mitochondria. Acute stress conditions lead to the misfolding of non-assembled mitochondrial proteins. The formation of Var1 bodies sequesters these proteins and reduces their toxicity. Hsp78 and Pim1 can resolve mitochondrial aggregates and refold or degrade the entangled proteins, respectively.

4.6 How do mammalian cells regulate protein sequestration?

In cells of higher eukaryotes, neither Hsp78 nor Var1 can be found. How is proteostasis controlled without a sequestration factor and a disaggregase? Hsp104 and Hsp78 act in nonmetazoans to disentangle protein aggregates. Recently, a human mitochondrial ClpB, named Skd3, has been identified. The activity of the IMS AAA+ is increased by the cleavage by PARL [168]. Its activity is critical for human health since mutations in Skd3 are linked to a rare disease, MGCA7, leading to neurologic deterioration, neutropenia, and infant death [169,170]. Showing that proteostatic control of intramitochondrial aggregates via the disaggregases is crucial for health. Proteostasis load might be changed in humans since α-synuclein, an aggregation-prone protein in Parkinson's, is also found aggregating on the OMM and the IMS but not in the mitochondrial matrix [171,172]. Additionally, eukaryotic cells possess a different way to disentangle protein aggregates. Hsp70-like proteins, or HSP110

proteins work together with the Hsp70 and Hsp40s to disaggregate proteins [173] even though with a lower efficiency than the Hsp104 [174]. Since chaperones often rely on backup pathways, other proteins which are part of the AAA+ family might also be able to act as disaggregases in eukaryotic cells. For example, ATAD3A and ATAD3B are located in the IM of human cells but are more associated with mtDNA nucleoids, possibly assisting aggregation or replication of mtDNA [175,176]. Also, the role of the Hsp100 protein ClpX is still largely unknown. It targets proteins to be degraded via the ClpP but is also known to act independently of ClpP as a chaperone and can unfold proteins in an ATP-dependent manner [177].

Human cells also express an S3 homolog, Mrps24, part of the 28S mitoribosomal subunit. The nuclear-encoded S3 protein has an average asparagine content and likely has only a singular function in translating the 13 human mitochondrial-encoded proteins. Nevertheless, polyN proteins are not a feature solely found in fungi. They are also found in more primitive nonvertebrates, such as nematodes and flies [155], as well as in humans. While polyA and polyQ are more common, one-third of the human proteome has IDRs. Those proteins are associated with different functions, ranging from DNA and protein binding to transcription, translational regulation, and cell cycle control [178,179]. Some of these IDRs display conservation, with functional important residues being more important [180]. Taken together, the enrichment of asparagine seems specific for mitochondrial and, more precisely, for fungal S3. Still, the accumulation along with the IDRs might not only be coincidental but associated with a gain of function in the proteostasis network. So, analyzing the mitochondrial proteome should also show a plethora of poly amino acid-containing proteins that could behave similarly to Var1 I humans.

While the players of Var1 and Hsp78 might not have direct analogs in humans, the demand for protein sequestration and disaggregation in the matrix will also have to evolve different strategies to build similar pathways.

5 OUTLOOK

In this study, I provided insight into the conditions and proteins that form intramitochondrial aggregates in yeast cells. In addition to the formation of Hsp78 foci that resolve, I could identify Var1 bodies. These are persisting protein aggregates formed by the mitochondrial-encoded protein Var1. However, the nature of the aggregate formation, biophysical properties, the relevance for survival, and the components of the different aggregate types still have not been elucidated.

The co-immunoprecipitations of Hsp78 could be improved, and while the mutation of the Walker B motifs makes an increased affinity for substrates, non-physiological behavior might change the substrates. Therefore, adding non-hydrolyzable ATP analogs or a crosslinker before pull-downs is possible.

The drivers of protein aggregation in the matrix could be identified through various methods: Single knock-outs and -downs with screening for Hsp78-GFP aggregation could be employed. Since yeast genetics are well established, a synthetic genetic array (SGA) could be used to screen for such factors unbiased [181]. A genomically tagged Hsp78 with a fluorophore would be crossed with a library of mitochondrial deletion and knock-down strains. The expression of a mitochondrially misfolding protein in the mitochondria, such as mtCPY*, would allow for automated screening of a soluble and mitochondrial Hsp78 signal.

Co-immunoprecipitations only give information about stable interaction partners. However, this is not sufficient to identify which proteins are aggregated. Different studies used proteomics to look into protein aggregates. Isolation of aggregates from *C. elegans* identified protein aggregates and the changed composition while aging. Walther and colleagues compared the measurement of aggregates to a standard channel that could quantify protein aggregates [182]. A different approach directly compared total, aggregated, and soluble proteins to study aggregates upon heat stress [183]. Hydrophobic proteins cannot be identified as efficient because they do not stay in a solution easily [184]. Therefore, measuring the increase of aggregated and the loss of proteins from a soluble mitochondrial fraction would improve the data obtained. To reduce the background of cytosolic proteins, mitochondria should be isolated from yeast cells with and without previous stress induction via one of the used misfolding model substrates. Subsequent fractionation and isolation of aggregates combined with multiplexing

could be used to compare proteins found under different conditions directly. Since the aggregated fraction of proteins only comprises a subpopulation of proteins, identification might be hampered by low protein amounts. Measuring the same samples in the presence of a channel with higher protein content would increase the identification rate, as described before as a booster channel [185].

To further characterize protein aggregates, their biophysical characteristics can be determined in more detail. Dynamic light scattering (DLS) is used to monitor protein aggregation in solutions by measuring fluctuations in the light intensity scattered by a protein. This depends on the size of proteins, temperature, and solvent viscosity but also can be used to identify interaction partners of proteins [186]. Also, cryo-electron microscopy (cryo-EM) or cryo-EM tomography could be applied to look for the formation of different aggregate forms. For example, this would allow checking if ribosome intermediates or whole subunits are found in Var1 bodies. Another characterization factor of protein deposits is the speed at which proteins diffuse in and out of these structures. Fluorescence recovery after photobleaching (FRAP) is used to determine the mobility of structures formed by liquid-liquid phase separation (LLPS) [187]. Additionally, fluorescent dyes can be used to get a more in-depth insight into the characteristics of protein aggregates. This depends on the ability of a specific dye to interact with a particular type of aggregate. Nevertheless, interaction with dyes might influence the aggregation behavior of proteins [188]. Another problem is the uptake of such dyes into yeast since many components are not permeable to their cell wall.

It is unclear whether the aggregates formed by Var1 have a protective effect. The toxic impact of nuclear-encoded Var1 makes it challenging to distinguish the toxicity of expression and targeting from a possible positive intramitochondrial effect of Var1 bodies. Distinguishing between the function of Var1 in translation and proteostasis would be vital to answer this question. A mutant, assembly competent, and functional in translation initiation but with a changed amino acid composition that makes Var1 soluble could be generated and expressed in a strain lacking endogenous Var1. This will allow screening if Var1 bodies are beneficial or toxic for cells under various stress conditions.

Fluorescent microscopy is a valuable tool to check for the localization and distribution of molecules in cells. Nevertheless, it has resolution limits. Confocal microscopy can reduce the background measured since only molecules in a specific plane are excited. Simulated emission

depletion microscopy (STED) uses a second doughnut-shaped laser surrounding the excitation beam, increasing resolution. This allows us to go to a subcellular level, differentiating between the localization of proteins in sub-compartments of mitochondria and studying the interaction of single components of aggregates and their separation in more detail.

The formation of aggregate deposits is associated with beneficial effects for cells. One reason for that is the cells' ability to retain certain proteins in the mother to generate healthy offspring by a process called asymmetric inheritance. The concentrated protein aggregates remain in the mother, creating a "rejuvenated" daughter cell free of misfolded proteins [8]. While this process is studied for cytosolic protein aggregates, it is also found in mitochondria [154]. The sequestration of protein aggregates together with asymmetric fission could allow for an alternative pathway besides mitophagy, to generate a functional mitochondrial network. It will be interesting to study if this process is driven by specific aggregate types and characteristics and thereby does provide benefits for the whole cell.

6 MATERIAL AND METHODS

Unless mentioned otherwise, all reagents were ordered at Sigma, Roth, Diagonal, Thermo Scientific, or Sarstedt.

6.1 Genetic Methods

6.1.1 *E. coli* strains

For plasmid purification and isolation, the bacterial *Escherichia coli* (*E.coli*) strains MH1 and DH5α were used [189,190]. The strains are described in Table 1.

Table 1: Bacterial strains used in this study. Listed are the used *E. coli* strains with genotype and their references.

Strain	Genotype	Reference
MH1	MC1061 derivative; araD139, lacX74, galU, galK, hsr, hsm+, strA	[189]
DH5a	K12 derivative; F- φ80dlacZΔM15, Δ(lacZYAargF)U169, deoR, recA1, endA1, hsdR17(rk- mk+), phoA, supE44, λ -, thi-1, gyrA96, relA1	[190,190]

Bacterial plasmids used for *in vitro* translation and bacterial protein expression are shown in Table 2.

Table 2: Bacterial plasmids used in this study.

Plasmid	Characteristics	Reference
pGem4-MTS-Var1	Yeast-optimized Var1 with N-terminal Cox4MTS, in vitro expression	This study
pGem4 MTS-EcS3	RpsC from K12 *E. coli*, *in vitro* expression	This study
pGem4 Hsp60	Hsp60, *in vitro* expression	
pGem4 Oxa1	Oxa1, *in vitro* expression	
pET21 Var1$_{FL}$	Var1 bacterial expression	This study
pET21 Var1$_{1-230}$	Var1 bacterial expression	This study
pET21 Var1$_{236-395}$	Var1 bacterial expression	This study

6.1.2 Transformation of chemo-competent *E. coli* cells

50 µl chemically competent *E. coli* cells were transformed to amplify plasmid DNA. Therefore, the cells were thawed slowly on ice, and 2-10 µl of a ligation or 2 µl plasmid DNA was added. The mixture was incubated on ice for 30 min, subjected to heat shock treatment (42°C) for 65 s, and cooled down on ice for 2 min. Next, 1 ml LB medium was added to the cells, followed by incubation for 45 min at 37°C and 1,000 rpm. Transformed cells were plated onto LB agar plates containing 100 µg/ml ampicillin (Amp), 25 µg/ml chloramphenicol (Cam), or 30 µg/ml kanamycin (Kan) depending on the used resistance cassette and incubated overnight at 37°C.

6.1.3 *S. cerevisiae* strains, plasmids, and primers

Saccharomyces cerevisiae (*S. cerevisiae*) strains are stored in glycerol stocks and were plated onto agar plates. Cultures were inoculated from plates in liquid media and cultivated shaking at 130 rpm and 30°C. Temperature-sensitive mutants were grown at 25°C. Continuous growth under heat stress conditions was done at 37°C, and for acute heat stress, cultures were incubated for the short indicated time points at 50°C. The strains and plasmids used in this study are shown in Table 2 and Table 3.

Table 3: Overview of *S. cerevisiae* strains used in this study. Listed are the background strains, strains obtained by homologous recombination and by transformation, together with their phenotype and references.

Strain	Genotype	Reference
YPH499 Δ*arg* pYX142 Hsp104-GFP pYX233 cyt-DHFR	*MATa ura3-52 lys2-801_amber ade2-101_ochre trp1-Δ63 his3-Δ200 leu2-Δ1 Darg4* +pYX142 Hsp104-GFP + pYX233 cyt-DHFR	[49]
YPH499 Δ*arg* pYX142 Hsp104-GFP pYX233 b₂-DHFR	*MATa ura3-52 lys2-801_amber ade2-101_ochre trp1-Δ63 his3-Δ200 leu2-Δ1 Darg4* +pYX142 Hsp104-GFP + pYX233 b₂-DHFR	[49]
W303	MATα *leu2-3,112 trp1-1 can1-100 ura3-1 ade2-1 his3-11,15*	[191]
W303 pYX142 Hsp78-GFP, cHHYTK284	W303 + pYX142 Hsp78-GFP, cHHYTK284 mt-mScarletI	This study

W303 pYX233 empty	W303 + pYX233 empty	This study
W303 pYX233 mtCPY*-HA	W303 + pYX233 mtCPY*-HA	This study
Δ*hsp78*	W303 HSP78::Nat$_{NT2}$	This study
Δ*hsp78* pYX233 empty	W303 HSP78::Nat$_{NT2}$ + pYX233 empty	This study
Δ*hsp78* pYX233 mtCPY*-HA	W303 HSP78::Nat$_{NT2}$ + pYX233 mtCPY*-HA	This study
W303 pYX142 Hsp78-GFP, pYX113 mtCPY*-mScarletI	W303 + pYX142 Hsp78-GFP + pYX113 mtCPY*-mScarletI	This study
W303 pYX142 Hsp78-GFP	W303 + pYX142 Hsp78-GFP	This study
W303 pYX142 mtGFP	W303 + pYX142 mtGFP	This study
W303 *rho^0* pYX142 Hsp78-GFP	W303 *rho^0* + pYX142 Hsp78-GFP	This study
W303 *rho^0* pYX142 mtGFP	W303 *rho^0* + pYX142 mtGFP	This study
W303 pYX142 Hsp78-GFP, pYX113 mtDHFR^{mut}-mScarletI	W303 +pYX142 Hsp78-GFP + pYX113 mtDHFR^{mut}-mScarletI	This study
W303 pYX142 mtGFP, pYX113 mtDHFR^{mut}-mScarletI	W303 +pYX142 Hsp78-GFP + pYX113 mtDHFR^{mut}-mScarletI	This study
Δ*hsp78* pYX142 Hsp78-GFP, pYX113 mtDHFR^{mut}-mScarletI	W303 HSP78::Nat$_{NT2}$ +pYX142 Hsp78-GFP + pYX113 mtDHFR^{mut}-mScarletI	This study
Δ*hsp78* pYX142 mtGFP, pYX113 mtDHFR^{mut}-mScarlet	W303 HSP78::Nat$_{NT2}$ +pYX142 Hsp78-GFP + pYX113 mtDHFR^{mut}-mScarletI	This study
W303 pYX142 Pim1^{S1015A}-HA	W303 +pYX142 Pim1^{S1015A}-HA	This study
Δ*hsp78* pYX142 Pim1^{S1015A}-HA	W303 HSP78::Nat$_{NT2}$ +pYX142 Pim1^{S1015A}-HA	This study
Δ*var1* p416 empty	*MATα trp1 ura3 leu2 cyh2 [rho$^+$]* + p416 empty	This study

Δ*var1* p416 MTS-Var1	*MATα trp1 ura3 leu2 cyh2 [rho⁺]* + p416 MTS-Var1	This study
W303 pYX112 empty	W303 +pYX112 empty	This study
W303 cHHYTK200 MTS-Var1	W303 +cHHYTK MTS-Var1	This study
Δ*var1*	22-2D *MATa trpl ura3 leu2 cyh2 rho⁰*	[93]
ATF3	22-2D *MATa trpl ura3 leu2 cyh2 rho⁰* + MTSVar1	[93]
ssc1-3	*MATα;ade2-101, lys2, ura3-52, leu2-3, Dtrp1 ssc1-3(LEU2)*	[192]
Δ*pim1* SUP	YPH500 PIM1::His3 + YEp13-SUP	[116]
W303 p416 MTS-Var1-eGFP	W303 p416 MTS-Var1-eGFP	This study
Δ*var1* p416 MTS-Var1-eGFP	*MATα trp1 ura3 leu2 cyh2 [rho+]* + p416 MTS-Var1-eGFP	This study
W303 pYX223 empty	W303 + pYX223 empty	This study
W303 pYX223 mtGFP	W303 + pYX223 mtGFP	This study
W303 pYX223 Var1-GFP	W303 + pYX223 Var1-GFP	This study
W303 pYX223 MTS-Var-GFP	W303 + pYX223 MTS-Var1-GFP	This study
W303 pYX223 *Ec*S3-GFP	W303 + pYX223 *Ec*S3-GFP	This study
W303 pYX223 Mrps24-GFP	W303 + pYX223 Mrps24-GFP	This study
W303 pYX223 MTS-*Ec*S3-GFP	W303 + pYX223 MTS-*Ec*S3-GFP	This study
W303 p416 empty	W303 + p416 empty	This study
W303 p416 MTS-Var1	W303 + p416 MTS-Var1	This study
W303 *rho⁰* p416 empty	W303 *rho⁰* + p416 empty	This study
W303 *rho⁰* p416 MTS-Var1	W303 *rho⁰* + p416 MTS-Var1	This study

W303 pYX122 Atp1-GFP	W303 + pYX122 Atp1-GFP	[193]
W303 pYX142 Hsp78^{K149T}-GFP	W303 + pYX142 Hsp78^{K149T}-GFP	This study
W303 pYX142 empty	W303 +pYX142 empty	This study
W303 pYX142 Hsp78-GFP, cHHYTK284 + pYX233 cyt-DHFR	W303 + pYX142 Hsp78-GFP, cHHYTK284 mt-mScarletI +pYX233 cyt-DHFR	This study
W303 pYX142 Hsp78-GFP, cHHYTK284 +pYX233 b$_2$-DHFR	W303 + pYX142 Hsp78-GFP, cHHYTK284 mt-mScarletI +pYX233 b$_2$-DHFR	This study
W303 pYX233 mtCPY-HA	W303 + pYX233 mtCPY-HA	This study
W303 pYX142 mtGFP pYX233 mtCPY*-HA	W303 + pYX233 mtCPY*-HA + pYX142 mtGFP	This study
W303 pYX142 Hsp78-GFP pYX233 mtCPY*-HA	W303 + pYX233 mtCPY*-HA + pYX142 Hsp78-GFP	This study
W303 pYX142 Hsp78 ^{K149T}-GFP pYX233 mtCPY*-HA	W303 + pYX233 mtCPY*-HA + pYX142 Hsp78^{K149T}-GFP	This study
W303 pYX142 Hsp78-GFP pYX113 Mam33-mCherry	W303 + pYX142 Hsp78-GFP + pYX113 Mam33-mCherry	This study
W303 pYX142 Hsp78-GFP pYX113 Aim17-mCherry	W303 + pYX142 Hsp78-GFP + pYX113 Aim17-mCherry	This study
Δ*var1* p416 MTS-Var1	Δ*var1* p416 MTS-Var1	This study
W303 pYX142 Hsp78-GFP pYX113 MTS-Var1-mScarletI	W303 pYX142 + Hsp78-GFP + pYX113 MTS-Var1-mScarletI	This study
W303 pYX142 mtGFP pYX113 MTS-Var1-mScarletI	W303 pYX142 + mtGFP + pYX113 MTS-Var1-mScarletI	This study
W303 *HSP78::*NeonGreen	W303 *HSP78::*NeonGreen Nat$_{NT2}$	This study
W303 *HSP78*::NeonGreen	W303 *HSP78::*NeonGreen Nat$_{NT2}$ + pYX113 MTS-Var1-mScarlet	This study

Table 4: Yeast plasmids used in this study. Listed below are the plasmids used in this thesis. The selection marker for yeast and the restriction sites used for inserting PCR fragments are given.

Nr.	Plasmid	Description	Reference
1	pYX142 Hsp104-GFP	ARS/CEN, *TPIP*, LEU2, AmpR	[49]
2	pYX142 Hsp78-GFP	ARS/CEN, TPIP, LEU2, AmpR	This study
3	pYX142 Hsp78^{K149T}-GFP	ARS/CEN, TPIP, LEU2, AmpR	This study
4	cHHYTK274 Su9-mScarletI	INT, pTEF1, YPRCΔ15, KanR-ColE1	This study
5	pYX233 empty	2μ, *GAL1P*, TRP1, AmpR	[20]
6	pYX233 mtCPY*HA	2μ, *GAL1P*, TRP1, AmpR	This study
7	pYX113 mtCPY*-mScarletI	ARS/CEN, *GAL1P*, URA3, AmpR	This study
8	pYX113 mtDHFR^{mut}-mScarelt	ARS/CEN, *GAL1P*, URA3, AmpR	This study
9	pYX142 mtGFP	ARS/CEN, *GAL1P*, URA3, AmpR	[194]
10	pYX142 Pim1-HA	ARS/CEN, *GAL1P*, URA3, AmpR	This study
11	pYX142 Pim1^{S1015A}-HA	ARS/CEN, *GAL1P*, URA3, AmpR	This study
12	p416 empty	ARS/CEN, *TEF3P*, URA3, AmpR	[195]
13	p416 MTS-Var1	ARS/CEN, *TEF3P*, URA3, AmpR	This study
14	cHHYTK200 MTS-Var1	CEN6/ARS4, *pPSP2*, URA3, AmpR-ColE1	This study
15	pYX223 empty	2μ, *GAL1P*, HIS3, AmpR	[194]
16	pYX223 mtGFP	2μ, *GAL1P*, HIS3, AmpR	[194]
17	pYX223 Var1-GFP	2μ, *GAL1P*, HIS3, AmpR	This study

18	pYX223 MTS-Var1-GFP	2μ, *GAL1P*, HIS3, AmpR	This study
19	pYX223 EcS3-GFP	2μ, *GAL1P*, HIS3, AmpR	This study
20	pYX223 Mrps24-GFP	2μ, *GAL1P*, HIS3, AmpR	This study
21	pYX223 MTS-*Ec*S3-GFP	2μ, *GAL1P*, HIS3, AmpR	This study
22	pNH605-PDRE-YFP	INT, pCYC1_4xPDRE-YFP, LEU2	[137]
23	p416 MTS-Var1-eGFP	ARS/CEN, *TEF3P*, URA3, AmpR	This study
24	pYX122 Atp1-GFP	2μ, *TPIP*, HIS3, AmpR	[193]
25	pYX113 MTS-Var1-mScarletI	ARS/CEN, *GAL1P*, URA3, AmpR	This study
26	pYX233 cty-DHFR	2μ, *GAL1P*, TRP1, AmpR	[20]
27	pYX233 b$_2$-DHFR	2μ, *GAL1P*, TRP1, AmpR	[20]
28	pYX233 mtCPY-HA	2μ, *GAL1P*, TRP1, AmpR	This study
29	pFA6a–natNT2	pFA6a–natNT2	[196]
30	pYX113 Mam33-mCherry	ARS/CEN, *GAL1P*, URA3, AmpR	[49]
31	pYX113 Aim17-mCherry	ARS/CEN, *GAL1P*, URA3, AmpR	[49]
32	cHHYTK303 Pim1	SP6, AmpR	This study
33	cHHYTK303 Pim1^{S1015A}	SP6, AmpR	This study
34	pYX142 MTS HA Var1	ARS/CEN, *TPIP*, LEU2, AmpR	This study
35	pYX142 MTS HA Var1 ΔL$_1$	ARS/CEN, *TPIP*, LEU2, AmpR	This study
36	pYX142 MTS HA Var1 ΔL$_2$	ARS/CEN, *TPIP*, LEU2, AmpR	This study

37	pYX142 MTS HA Var1 ΔL$_3$	ARS/CEN, *TPIP*, LEU2, AmpR	This study
38	pYX142 MTS HA Var1 ΔL$_{1,2,3}$	ARS/CEN, *TPIP*, LEU2, AmpR	This study
39	pYX142 MTS HA Var1 ΔL$_{1,3}$	ARS/CEN, *TPIP*, LEU2, AmpR	This study
40	pYX142 MTS Var1	ARS/CEN, *GAL1P*, URA3, AmpR	This study
41	pYX142 MTS Var1-N	ARS/CEN, *GAL1P*, URA3, AmpR	This study
42	pYX142 MTS RpsC	ARS/CEN, *GAL1P*, URA3, AmpR	This study
43	pYX142 Mrps24	ARS/CEN, *GAL1P*, URA3, AmpR	This study

Table 5 lists primers used in this study to create the strains above.

Table 5: Primers used in this study. Listed below are the names and sequences of the primers used in this thesis. The template DNA, as well as a short description, are also shown. fwd, forward primer; rev, reverse primer; n/a, no information available.

Primer	Sequence [5' - 3']	Usage
TFA2 fwd	CGATTCTTCAAAGTTGCTTTGGGCGAC	qPCR SYBR Green
TFA2 rev	GTTCCGAAGGGGAATGGACATCGTA	
RPN4 fwd	GCAACAAGAGCAACACCAAGAGGAG	qPCR SYBR Green
RPN4 rev	CTGTCCATGTTAGAGTCAACGTAACTG	
CIS1 fwd	ATCAGTAATTGTCCCATCGGGTTAGTTTC	qPCR SYBR Green
CIS1 rev	CCTGGGCAGCCTTGAGTAAATCATATC	
15S rRNA fwd	GTTAATC ATAATGGTTT AAAGGATCCG TAGAATG	qPCR SYBR Green
15S rRNA rev	GGTATCGAATCCGTTTCGCTACTCTAG	

21S rRNA fwd	GTTTGC AGATAGCTGG TTTTCTATGA AATATATG	qPCR SYBR Green
21S rRNA rev	GGAACTTTATATCTTAATCTGGGCTGTTTCC	
VAR1 syn. fwd	GAAACTGAAACTGCTGAAC	qPCR SYBR Green
VAR1 sny. rev	GTTGTTGATGTTACCAGCC	
KO SOV1 fwd	GTTTCTAACGAAAAAATTTGACTTGAATATTGATTACG ATTTGAGT CGTACGCTGCAGGTCGAC	SOV1 knock-out
KO SOV1 rev	GTACACGTATAGCTAAAATTATATAAAATGCATCCGTT TTTTTA ATCGATGAATTCGAGCTCG	
KO HSP78 fwd	CCAGGAACCCTGAAACAAGCGAGTGAAAATCTTTCAA GGTTAAATATGCGTACGCTGCAGGTCGAC	HSP78 knock-out
KO Hsp78 rev	GTTTATATATGTATTTTCTTGGGAATTTATTATTCATAA ACCGCTTGTGCAGTTAATCGATGAATTCGAGCTCG	
LB9 Var1 fwd. EcoRI	GGG GAATTC ATGAAACTGA AACTG	Cloning of Plamsid 13
LB12 Var1 Synt rev. SalI	GGG GTCGAC TTAAATGAAGTTCAGTTTAAC	
LB16 fwd BamHI COX4MTSEcoRI	GGGGGATCCATGCTTTCACTACGTCAATCATAAGATTT TTCAAGCCAGCCACAAGAACTTTGTGTAGCTCTAGATA TC TGCTT GAATTC CCC	
LB17 revEcoRI COX4MTS BamHI	GGGGAATTCAAGCAATATCTAGAGCTACACAAAGTTCT TGTGGCTGGCTTGAAAAATCTTATAATTGACGTA GTGAAAGCAT GGATCC CCC	
LB13 Var1 Synth rev.	GGGGTCGACTTAAATGAAGTTCAGTTTAACTT	

SalI ohne STOP	62	Cloning of Plamsid Nr. 23
LB14 eGFP fwd SalI	GGG GTCGAC ATGGTGAGCAAGG	
LB15 eGFP rev XhoI	GGG CTCGAG TTACTTGTACAGCTCGTC	
LB224 hsp78o.STOP_fwd	acacatacagATGTTAAGACAAGCTACAAAAG	Cloning of Plasmid Nr. 2
LB225 Hsp78o.STOP_rev	tggtacccggCTTTTCAGCTTCCTCTTC	
LB226 GFP_fwd	agctgaaaagCCGGGTACCAGATCTATG	Cloning of Plasmid Nr. 2,3
LB227 GFP_rev	gcaggtgtctagaactagtgTTATTTGTATAGTTCATCCATGC	
LB228 Hsp78_till 466_fwd	acacatacagATGTTAAGACAAGCTACAAAAGCAC	Cloning of Plasmid Nr. 3
LB229 Hsp78_till 466_rev	aagggcggttGTACCGACACCAGCTCGAC	
LB230 Hsp78_467 _end_fwd	gtgtcggtacAACCGCCCTTATTGATGG	
LB300 mScarlet rev	attcagttagctagctgagcTTATTTATACAATTCATCCATTCC	Cloning of Plasmid Nr. 7, 8, 25

LB301 Su9 fwd	ggagaaaaaaccccggatcgATGGCCTCCACTCGTGTC	Cloning of Plasmid Nr. 7, 8, 25
LB302 Su9 rev	gcaatgagatAGATCTGGTACCCGGGGATC	Cloning of Plasmid Nr. 7
LB303 CPY* fwd	taccagatctATCTCATTGCAAAGACCG	
LB304 CPY* rev	ctttactaacTAAGGAGAAACCACCGTG	
LB305 mScarlet fwd	tttctccttaGTTAGTAAAGGTGAAGCTG	
LB40_CPY*_fwd	gaagcgcgcctactcttccggaatgatctcattgcaaagac	Cloning Plamsid Nr. 6, 28
LB41_CPY*_rev	gatacccgggtcgacgcgtattataaggagaaaccaccg	Cloning Plamsid Nr. 6, 28
TS5 Pim1 G. fwd	actacaaaaaacacatacagatgctaagaacaagaaccac	Cloning of Plamsid Nr. 10, 11
TS6 Pim1 G. rev	gatacccgggtcgacgcgtaagcttgtccttttcctttttagcatcc	
TS7 Pim1 1-3024 rev	tgacacctgcagctggaccatctttaggggtag	Cloning of Plamsid Nr. 11
TS8 Pim1 3046-3399 fwd	ggtccagctgcaggtgtcactatggcc	
LB290_P3b_Var1_fwd	gcatcgtctcatcggtctcattctAAACTGAAACTGCTGAACATG	Domestication of Cox4MTS

LB291_P3b_Var1_rev	atgccgtctcaggtctcaggatccAATGAAGTTCAGTTTAACTTTGATGTT	part for Plasmid Nr. 14
LB293_P3a_Cox4MTS_fwd	TCGGTCTCATATGATGCTTTCACTACGTCAATCTATAAGATTTTTCAAGCCAGCCACAAGAACTTTGTGTAGCTCTAGATATCTGCTTTTCTTGA	Domestication of Var1 part for Plasmid Nr. 14
LB294_P3a_Cox4MTS_rev	GGTCTCAAGAAAAGCAGATATCTAGAGCTACACAAAGTTCTTGTGGCTGGCTTGAAAAATCTTATAGATTGACGTAGTGAAAGCATCATATGAGA	
LB182 Var1synt for	agaagcgcgcctactcttccATGAAACTGAAACTGCTG	Cloning of Plamsid Nr. 18
LB65 Var1synt rev	ctcatagatctggtacccggAATGAAGTTCAGTTTAACTTTG	
LB187 RpsC_fwd	agaagcgcgcctactcttccATGGGTCAGAAAGTACATC	Cloning of Plamsid Nr. 21
LB75 RpsC K12 rev	ctcatagatctggtacccggTTTACGGCCTTTACGCTG	
LB64 Var1synt fwd:	actacaaaaaacacatacagATGAAACTGAAACTGCTG	Cloning of Plamsid Nr. 17
LB65 Var1synt rev	ctcatagatctggtacccggAATGAAGTTCAGTTTAACTTTG	
LB72 Var1 Mrps24 fwd	actacaaaaaacacatacagATGGCTGCATCTGTTTGTTC	Cloning of Plamsid Nr. 20
LB73 Var1 Mrps24 rev	ctcatagatctggtacccggCAAGTATTTATAAACAACTTTTGATGGAAC	

LB74 RpsC K12 fwd	actacaaaaaacacatacagATGGGTCAGAAAGTACATC	Cloning of Plamsid Nr. 21
LB75 RpsC K12 rev	ctcatagatctggtacccggTTTACGGCCTTTACGCTG	
TS1 Pim1 fwd	gcatcgtctcatcggtctcatatgCTAAGAACAAGAACCACAAAG	Domestication of Pim1 and Pim1^{S1015A} part for Plasmid Nr. 32, 33
TS2 Pim 1 rev	atgccgtctcaggtctcaggatccGTCCTTTTCCTTTTTAGCATC	
LB76_rpsC fwd XbaI	GGG TCTAGA ATGGGTCAGAAAGTACATC	Cloning of pGem4 MTS-EcS3
LB77_rpsC rev SalI	GGG GTCGAC TTATTTACGGCCTTTACG	

6.1.4 *S. cerevisiae* transformation

S. cerevisiae cells were grown to exponential phase, and 1.5 ml culture was harvested by centrifugation for 1 min at 17,000 g at room temperature (RT). The cell pellet was washed with 1 ml ddH$_2$O. The cells were resuspended with 1 ml of 0.1 M lithium acetate and incubated for 10 min at 30°C and 1,000 rpm. After centrifugation (1 min at 17,000 g at RT), the cell pellet was resuspended in 74 µl ddH$_2$O, 5 µl salmon sperm DNA (ssDNA, denatured at 96°C for 10 min and cooled down), 5 µl 100 ng/µl plasmid DNA, 36 µl 1 M lithium acetate (final concentration 0.1 M) and 240 µl 50% (w/v) polyethylene glycol (PEG) 3350. The mixture was vortexed for 1 min and incubated for 30 min at 30°C, followed by a heat shock for 25 min at 42°C. For temperature-sensitive mutants, the incubation for the heat shock was done at 30°C. Afterward, the cells were pelleted (1 min at 17,000 g at RT) and resuspended in 100 µl sterile ddH$_2$O. The suspension was plated on selective media.

For homologous recombination to genomically integrate a DNA cassette, over one µg of DNA and 34 µl ddH$_2$O were used. The residual procedure was the same as described above. For

homologous recombination with antibiotic cassettes, the cells were first incubated overnight in 5 ml YPD medium at 30°C to allow the expression of the resistance cassette and afterward plated onto the selective media.

6.2 Molecular Biology Methods

6.2.1 Isolation of plasmid DNA from E. coli

Plasmid DNA was isolated from *E. coli* cells in small (Mini-prep) or large scale (Midi-prep). For small-scale isolation of plasmids, 5 ml selective LB$_{Amp/ Cam/ Kan}$-media were inoculated with a single bacterial colony and incubated overnight. To isolate plasmid DNA, 2 ml of culture was harvested, and the DNA was extracted using the NucleoSpin Plasmid-Kit (Macherey-Nagel) according to the manufacturer's instructions.

For large-scale isolation, 100 ml selective LB$_{Amp Cam/ Kan}$-media were inoculated with bacteria. The cells were cultured overnight before the plasmid DNA of the whole culture was isolated using the *PureYield^{TM}* Plasmid Midiprep System (Promega) as described by the manufacturer.

6.2.2 Determination of DNA concentration

The Spectrophotometer/Fluorometer DS-11 FX+ (DeNovix) was used to determine the DNA concentration and purity. After calibration with 1 µl of water, 1 µl of DNA was used for the measurement. The absorbance was measured at 230 nm, 260 nm, and 280 nm. The ratio of the absorbance at 260 and 280 nm indicates the degree of contamination with proteins (< 1.8) or RNA (> 1.8). The 260/230 values should be between 2.0 and 2.2. If the ratio is lower, it may indicate the presence of organic compounds.

6.2.3 Polymerase Chain Reaction

DNA amplification for homologous recombination of plasmid construction was achieved by polymerase chain reaction (PCR). One response had a volume of 50 µl containing 15 ng template DNA, 0.5 µM of each primer, 0.2 mM dNTPs (deoxyriboNucleoside Triphosphates), 1 U Q5® High-Fidelity (HF) polymerase and 1x Q5® reaction buffer.

Table 6 displays the PCR program for the amplification of DNA.

The insert length determined the elongation time, and the polymerase used (Q5: 1 kbp/20 sec).

Table 6: PCR Program. Protocol for DNA amplification by standard PCR.

Temperature [°C]	Time	Cycle Number	Reaction
98	30"		Initial denaturation of DNA and nuclease inactivation
98 50-72 72	10" 30" 20-30" s/kb	35x	DNA denaturation Primer annealing Elongation
72	2"		Final elongation
4	∞		Cooling

Colony PCR was used for the verification of successful homologous recombination. Therefore, one yeast colony was mixed with 20 µl of 20 mM sodium hydroxide (NaOH) and boiled for 10 min at 96°C. Afterward, cell debris and intact cells were pelleted using a small tabletop centrifuge for 30 seconds. 100 ng of the supernatant was added as template DNA to the PCR reaction described in Table 7 using the Q5® HF polymerase. The PCR program is described above in Table 6.

Table 7: Colony PCR. Listed are the reagents and their amounts used for performing a colony PCR.

	1x [µl]
H2O	30.5
5x Q5® reaction buffer	10
100% DMSO	1
dNTPs	1
Primer forward (10 µM)	2.5
Primer reverse (10 µM)	2.5
Q5® polymerase	0.5
Total	48

6.2.4 Restriction digest of DNA

Restriction digestion was performed to verify successful ligation or to prepare to insert DNA and vectors for ligation. The 100 µl reaction mix contained 15 U of the specific restriction

enzyme, specific restriction buffer, and 2 µg of DNA. The plasmid DNA's digest reaction also contained 1 U calf intestine alkaline phosphatase (CIP) to avoid the vector's self-ligation. The reaction mixture was incubated for 15-60 min at 37°C, analyzed by agarose gel electrophoresis, or directly purified using the NucleoSpin® PCR Clean-up kit (Macherey-Nagel) according to the manufacturer's instructions.

6.2.5 Ligation of DNA fragments with vectors

Insert fragments were ligated into vector plasmid DNA in a 20 µl reaction volume. Therefore, 3:1(5:1, if the length of the insert was smaller than 200 bp) molar ratios of the insert to vector (50-100 ng), 2 µl T4 DNA ligase, and 2 µ 10x ligase reaction buffer were mixed. The reaction was performed at 16°C overnight or at room temperature (RT) for one h. 10 µl of the ligation reaction was used to transform *E. coli* cells. Single colonies were selected and inoculated in a small volume (5 ml) of selective LB media and subjected to plasmid DNA isolation as described in 0 and analyzed in restriction digestion for successful ligation.

6.2.6 Agarose gel electrophoresis

Agarose gel electrophoresis was used for analytic (test of successful ligation) and preparative purposes (isolation of DNA fragments). This method allows the size-dependent separation of DNA fragments in an electric field. The negatively charged DNA migrates in an electrical field through a polysaccharide agarose matrix towards a positive electrode. To cast the gel matrix, 1% agarose (w/v) was dissolved entirely in TAE buffer (40 mM Tris, 1.14% acetic acid, ten mM EDTA pH 8.0) by heating the solution in the microwave. After cooling down the agarose solution, 0.5 µg/ml ethidium bromide was added to visualize DNA under ultraviolet light. Before loading, samples were supplemented with 6x loading dye (60 mM Tris/HCl pH 7.5, 30 mM sodium acetate, 12 mM EDTA, 60% (v/v) glycerol, 0.36% (w/v) orange G). A molecular weight ladder (a mix of DNA fragments of known lengths) was loaded alongside the samples to determine the size of the DNA fragments. The electrophoresis was performed in 1x TAE buffer at 10 V/cm. The separation of DNA fragments was analyzed under ultraviolet light. To isolate DNA fragments of interest (for preparative purposes), the respective DNA band was cut out using a scalpel and purified with the NucleoSpin® Gel Clean-up kit (Macherey-Nagel) according to the manufacturer's instructions.

6.2.7 Real-time quantitative polymerase chain reaction and RNA isolation

For total RNA extraction, yeast strains were cultivated in synthetic media to mid-log phase. 4 OD_{600} cells were harvested, or 100 µg isolated mitochondria were used–for RNA extraction using the RNeasy Mini Kit (Qiagen) in conjunction with the RNase-Free DNase Set (Qiagen) according to the manufacturer's instructions. Yield and purity of the obtained RNA was determined with a Spectrophotometer/Fluorometer DS-11 FX+ (DeNovix). According to the manufacturer's instructions, 500 ng RNA was reverse transcribed into cDNA using the qScript cDNA Synthesis Kit (Quanta Biosciences). The iTaq Universal SYBR Green Supermix (BioRad) was used with 2 µl of a 1:10 dilution of the cDNA sample to measure relative mRNA levels. The Luna Universal Probe One-Step RT-qPCR Kit (NEB) was used with 2 µl of RNA sample to assess rRNA in isolated mitochondria. Measurements were performed in technical triplicates with the CFX96 Touch Real-Time PCR Detection System (BioRad). The relative mRNA expressions were calculated using the 2-$\Delta\Delta$Ct method [197]. For normalization, the housekeeping gene *TFA2* was used due to its stability. See Table 5 for primer sequences.

6.3 Cell Biology Methods

6.3.1 E. coli cultivation media

E. coli cells were grown on LB-medium or LB plates. 1% bacto-tryptone, 0.5% yeast extract, and 1% sodium chloride were used for liquid culture. The pH was adjusted to 7.5 with NaOH, and 100 µg/ml ampicillin (amp) was used for plasmid selection. LB medium was supplemented with 2% bacto-agar (w/v) for agar plates and autoclaved. For plasmid selection, 100 µg/ml ampicillin was added to the pre-chilled (50°C) agar or to the liquid medium.

6.3.2 *S. cerevisiae* cultivation media

Yeast cells were grown in non-selective YP-media, containing 1% yeast extract and 2% peptone. The pH was adjusted to 5.5 with HCl, and the media was supplemented with 2% of the respective carbon source (D, glucose; Gal, galactose, G, glycerol, Raf, raffinose). For YP plates, 2% agar, 1% yeast extract, and 2% peptone (pH adjusted to 5.5 with HCl) were autoclaved and supplemented with 2% of the respective carbon source. For selection, 100 µg/ml G418, cloNAT, or hygromycin b were added.

Cells harboring plasmids were cultured in selective media (S-medium) or selective lactic acid-based (SLac-medium). For this purpose, 1,7 g/l yeast nitrogen base 5 g/l ammonium sulfate was mixed with a drop-out mix lacking auxotrophic markers and 2% of the respective carbon source (D, glucose; Gal, galactose; G, glycerol). For SLac medium, 1,7 g/l yeast nitrogen base, five g/l ammonium sulfate, and 2,2% lactic acid (90%(v/v)) were mixed with drop-out mix lacking auxotrophic markers and could be supplemented with 0.5% or 2% galactose to induce protein expression from a GAL-promotor. In table 7, the components of the 20x drop-out mix are listed. For plates containing selective media, ½ volume of water supplemented with 2% (w/v) agar was autoclaved. The agar solution was mixed with S-medium or SLac-medium, respectively, to 1 volume and poured into petri dishes.

6.3.3 Dropout-Mix

The dropout mix contains all amino acids. For plasmid selection, the respective amino acids were left out.

Table 8: Composition of the dropout-mix. Depending on the selection marker, amino acids were left out.

Amino acids/Nucleobase	20x (mg/ml)
L-adenine hemisulfate salt	400
L-Arginine	400
L-Histidine HCl Monohydrate	400
L-Isoleucine	600
L-Leucine	2000
L-Lysin HCl	600
L-Methionine	400
L-Phenylalanine	1000
L-Threonine	400
L-Tryptophan	400
L-Tyrosine	400
L-Uracil	400
L-Valine	3000

6.3.4 Growth Assays

Growth curves were performed in a 96-well plate using the automated ELx808^{TM} Absorbance Microplate Reader (BioTek$^{®}$). Yeast cells were grown to mid-log phase in liquid-rich or synthetic media before the growth curves started at 0.1 OD_{600}. The OD_{600} was measured every 10 min for 72 h at 30°C or 37°C respectively. The mean of technical replicates was calculated and plotted in R.

The respective yeast strains were grown in liquid-rich or synthetic media for drop dilution assays. Total yeast cells equivalent to 0.5 OD_{600} were harvested at mid-log phase. The cells were washed in sterile water and subjected to ten-fold serial dilutions. From each dilution, 3 µl were spotted on the respective media, followed by incubation at 30°C or 37°C. Pictures were taken after different days of the growth.

For survival assays, cells were grown in liquid media and optionally treated with chloramphenicol, which explicitly inhibits mitochondrial translation, for 16 h before an acute heat treatment with the indicated temperatures. The same OD_{600} cells were plated onto SD plates and counted colonies.

6.3.5 YFP reporter assay

The *PDRE-YFP* reporter genes were integrated into the *LEU2* locus of the yeast genome. Cells were grown to mid-log phase (OD_{600} 0.6 – 0.8). 4 OD_{600} cells were harvested by centrifugation (20,000 g, 3 min, RT) and resuspended in 400 µl H2O. In technical triplicates, 100 µl of cell suspension were transferred to flat-bottomed black 96-well imaging plates (BD Falcon, Heidelberg, Germany). Cells were sedimented by gentle spinning (30 g, 5 min, RT), and fluorescence (excitation 497 nm, emission 540 nm) was measured using a ClarioStar Fluorescence Platereader (BMG-Labtech, Offenburg, Germany). The corresponding wildtype strain not expressing YFP was used for background autofluorescence subtraction.

Fluorescence intensities were normalized to the value obtained from the wild type empty vector control in three independent biological replicates.

6.3.6 Isolation of mitochondria

For the isolation of mitochondria, cells were grown in selective media. In the exponential phase, cells were harvested (4,000 rpm, JA10 Beckmann rotor, 5 min, RT). After a washing step, cells were treated for 10 min with 2 ml per g wet weight MP1 buffer (10 mM Tris pH unadjusted and 100 mM DTT) at 30°C. After washing with 1.2 M sorbitol, yeast cells were resuspended in 6.7 ml per g wet weight MP2 buffer (20 mM KPi buffer pH 7.4, 1.2 M sorbitol, 3 mg per g wet weight zymolyase from Seikagaku Biobusiness) and incubated for one h at 30°C. Spheroplasts were collected via centrifugation at 4°C and resuspended in ice-cold homogenization buffer (13.4 ml/g wet weight) (10 mM Tris pH 7.4, 1 mM EDTA pH 8, 0.2% fatty acids free bovine serum albumin (BSA), 1 4 mM PMSF, 0.6 M sorbitol). Spheroplasts were disrupted by ten strokes with a cooled glass potter. Cell debris was removed via centrifugation at 3,300 rpm in a JA10 Beckmann rotor. The supernatant was centrifuged for 12 min at 10,000 rpm to collect mitochondria. Mitochondria were resuspended in 300 µl of ice-cold SH buffer (0.6 M sorbitol, 20 mM Hepes pH 7.4). The Spectrophotometer/Fluorometer DS-11 FX+ (DeNovix) was used to determine the protein concentration and purity. After calibration with 1 µl of SH-buffer, 1 µl of mitochondria was used for the measurement.

6.4 Protein Biochemistry Methods

6.4.1 Whole cell lysates

For whole cell lysates, yeast strains were cultivated in selective media to mid-log phase. 2 OD_{600} were harvested by centrifugation (17,000 g, 2 min at RT). Cells were washed with water and resuspended in 100 µl (50µl/OD_{600}) reducing loading buffer. Cells were transferred to screw-cap tubes containing 1 mm glass beads. Cell lysis was performed using a FastPrep-24 5G homogenizer (MP Biomedicals, Heidelberg, Germany) with three cycles of 30 s, speed 8.0 m/s, 120 s breaks, glass beads) at 4°C. Lysates were boiled at 96°C for 5 min, centrifuged (17,000 g, 2 min), and stored at -20°C until further use. An equal amount of OD_{600} was loaded on an SDS gel.

6.4.2 SDS-polyacrylamide gel electrophoresis

Sodiumdodecylsulfate polyacrylamide gel electrophoresis (SDS-PAGE) allows the separation of proteins by size [198]. In this method, proteins are denatured and negatively charged through the detergent SDS. This allows the migration through an electric field put on a polyacrylamide gel matrix. The network of acrylamide fibers leads to a slow migration of unfolded and large proteins. In contrast, small or partially folded proteins (for example, folded because of preserved disulfide bridges) run faster through the gel. In this study, a self-made vertical one-dimensional gel system was used. For the standard gel system, glass plates with a size of 160 x 180 mm and spacers with 1 mm thickness were sealed using a base gel, on top of which first the separation gel and then the stacking gel was placed. The concentration of acrylamide and bis-acrylamide in the separation gel depends on the molecular size of the proteins of interest. The composition of the gels is represented in Table 9. Before loading, samples were supplemented with reducing sample (Laemmli) buffer (50 mM Tris-HCl pH 6.8, 10% glycerin, 2% SDS, 0.01% bromophenol blue, 100 mM DTT). To determine the protein size, the unstained marker from peQLab was used. The electrophoresis was conducted at 25 mA for 2.45 h in SDS running buffer (25 mM Tris-HCl pH 8.3, 190 mM glycine, 0.1% SDS).

Table 9: Gel composition for SDS-PAGE. Composition of the running, stacking, and base gel.

Gel	Composition
Running gel	16% acrylamide 0.11% bisacrylamide 375 mM Tris-HCl pH 8.8 0.1% SDS 0.1% ammonium persulfate (APS) 0.03% N,N,N',N'-Tetramethylethylenediamine (TEMED)
Stacking gel	5% acrylamide 0.03% bisacrylamide 60 mM Tris-HCl pH 6.8 0.1% SDS 0.05% ammonium persulfate (APS) 0.1% N,N,N',N'-Tetramethylethylenediamine (TEMED)
Base gel	20% acrylamide

	0.13% bisacrylamide
	375 mM Tris-HCl pH 8.8
	0.1% SDS
	0.05% ammonium persulfate (APS)
	0.1% N,N,N',N'-Tetramethylethylenediamine (TEMED)

6.4.3 Transfer of proteins to a nitrocellulose membrane

Proteins separated by SDS-PAGE were transferred from a gel onto a nitrocellulose membrane using a semi-dry blotting method [199]. Therefore, the SDS-gel was placed onto a nitrocellulose membrane. It was covered with 2 Whatman papers below and one Whatman paper on top of it. The stack was soaked in blotting buffer (20 mM Tris, 150 mM glycine, 0.08% SDS, 20% methanol), arranged in this order on the anode transfer module, and covered with the cathode transfer module. The transfer of proteins from the gel onto the membrane was performed for 1.5 h at 1.3 mA/cm^2. To detect proteins on the nitrocellulose membrane, it was stained with Ponceau S solution (0.2% (w/v) Ponceau S, 3% (w/v) acetic acid) for 5 min.

6.4.4 Radioactive in vivo labeling of mitochondrial translation products

Cells were grown in galactose medium lacking methionine to exponential phase. ^{35}S-methionine (1 µl of an 11 µCi solution) was added to the cell suspension. Aliquots of 2 OD$_{600}$ cells were withdrawn after 5 min incubation at 30°C. The incorporation of radioactive methionine was quenched by adding 8 mM cold methionine. Cells were lysed with 0.3 M NaOH, 1% β-mercaptoethanol, and three mM PMSF. Proteins were precipitated with 12% trichloroacetic acid and analyzed by SDS–PAGE and autoradiography.

6.4.5 Radioactive in organelle labeling of mitochondrial translation products

Isolated mitochondria (100 µg) were incubated in 1.5x *in organello* translation buffer (ioTL buffer, 20 mM Hepes/KOH pH 7.4, 15 mM KPi, 0.6 M Sorbitol, 150 mM KCl, 12.66 mM MgSO$_4$, 12.13µg/ml Amino acid mix, 66.66µM Cys, 12.13 µg/ml Tyrosine, 7.5 mM Phosphoenolpyruvate, six mM ATP, 0.75 mM GTP, five mM α-Ketoglutarate, 10 µg/ml Pyruvat-Kinase) together with 1µl ^{35}S-methionine (of a 11 µCi solution) and incubated at 30°C for 10 min shaking at 600 rpm. The incorporation of radioactive methionine was quenched by adding 8 mM cold methionine, and the reaction was stopped by adding 1 ml ice-cold SH buffer

(0.6 M Sorbitol, 20 mM Hepes). Mitochondria were pelleted by centrifugation (20000 x g, 10 min, 4°C), resuspended in loading buffer, and analyzed by SDS-PAGE and autoradiography.

6.4.6 Determination of aggregated translation products in mitochondria

Isolated mitochondria (100 µg) resuspended in 1.5x ioTL buffer and incubated shaking (600 rpm, 10min, 25°C). Translation products were labeled for 15 min with 1 µl ^{35}S-methionine (of an 11 µCi solution). Adding 25 mM methionine quenched the incorporation of radioactive methionine, and the reaction was stopped by adding 1 ml ice-cold SH buffer. For the total (T) samples, mitochondria were pelleted at 16.000 rpm, 10 min, 4°C, resuspended in loading buffer, and resuspended by shaking vigorously at 4°C for 5 minutes. Aggregated and soluble protein fractions were obtained by mitochondrial lysis (0.1% Triton X-100, 150 mM NaCl, 5 mM EDTA, 1 mM PMSF) at 4°C, 15 min shaking on the disruptor. To prevent sedimentation of ribosomes, the samples were centrifuged at 30.000 g, 15 min 4°C. The pellet (P) fraction was prepared following the total samples, and the proteins were precipitated with trichloroacetic acid (0).

6.4.7 TCA precipitation of proteins

Adding trichloroacetic acid (TCA) can precipitate proteins from a solution. Therefore, protein solutions were supplemented with 72% TCA to an end-concentration of 12% TCA. The samples were incubated overnight at -20°C or 1h at -80°C. Proteins were sedimented by centrifugation (30 min at 25,000 g at 4°C), washed with ice-cold acetone (-20°C), and pelleted (30 min at 25,000 g at 4°C). Protein pellets were dried at room temperature and resuspended in sample buffer (30 min 12,000 rpm, 25°C).

6.4.8 Autoradiography

Radioactive proteins can be detected by autoradiography. Therefore, the dried cellulose membrane was exposed to an imaging plate (Fujifilm) for phospho-imaging with the Typhoon FLA 7000 from GE Healthcare. The films were scanned in a grey-scale 8-bit format for quantification, and the quantification was performed using the ImageQuant software.

6.4.9 Sample preparation and mass-spectrometric identification of proteins

For the co-immunoprecipitation of interactors and mass spectrometry, cells were grown in SGal media, and 20 OD_{600} were harvested by centrifugation (12,000 g, 5 min) and snap-frozen in liquid nitrogen and stored at -80°C. Cell lysates were prepared in lysis buffer (50 mM Tris pH 7.5, 2% (w/v) SDS, Tablets mini EDTA-free protease inhibitor (Roche)) using a FastPrep-24 5G homogenizer (MP Biomedicals, Heidelberg, Germany) with three cycles of 30 s, speed 8.0 m/s, 120 s breaks, glass beads). For co-immunoprecipitation, Var1 mitochondria were isolated, and 500 µg of protein was lysed (10 mM Tris-HCl, pH 7.5, 150 mM sodium chloride (NaCl), 0.5 mM EDTA, 10 mM magnesium chloride ($MgCl_2$), 0.5% Triton X-100, 1 mM PMSF) for 30 min, 4°C. Cleared lysates (20000 x g, 10 min, 4°C) were diluted with dilution buffer (10 mM Tris-HCl, pH 7.5, 150 mM NaCl, 0.5 Mm EDTA; 1x cOmplete protease inhibitor cocktail, 1x PhosSTOP phosphatase inhibitor cocktail) and incubated with activated beads (ChromoTek GFP-Trap® Magnetic Agarose; monoclonal Anti-HA antibody produced in mouse (Sigma #22190322) and Amintra Protein A Resin #APA0100) and tumbled end-over-end for 1 h at 4°C. The supernatant was discarded, and beads for Pim1^{S1015}-HA and MTS-Var1-eGFP were washed twice with wash buffer I (150 mM NaCl, 50 mM Tris-HCl, pH 7.5, 5% glycerol, 0.05% Triton X-100) and all samples twice with wash buffer II (150 mM NaCl, 50 mM Tris-HCl, pH 7.5, 5% glycerol). Peptides were digested on-bead with Elution buffer I (2 M urea, 50 mM Tris-HCl, pH 7.5, 1 mM DTT, 5 ng/µl trypsin (Promega, #V5111)) for 1 h at room temperature. At room temperature, 15 ng/ µl fresh Trypsin was added for 10 min. Eluted peptides were transferred to a new tube and incubated with 50 µl elution buffer (2M urea, 50 mM Tris-HCl, pH 7.5, 5 mM chloracetamide (Sigma-Aldrich, #C0267)) overnight at room temperature in the dark. Peptides were acidified to pH <2 with Tri-4 acetic acid and desalted on homemade StageTips containing Empore C_{18} disks [200]. C18 stage tips were activated with 100 µl methanol, 100 µl buffer B (0.1% formic acid, 80% acetonitrile), and twice with 100 µl buffer A (0.1% formic acid). The acidified peptides were added onto the stage tips and washed with 100 µl buffer A. Peptides were eluted with 40-60 µl buffer B and dried down in a speed vac and resolubilized in 9 µl buffer A (0.1 % formic acid in MS grade water) and 1 µl buffer A* (2 % acetonitrile, 0.1 % tri-flouracetic acid in MS grade water). Peptides were separated using an Easy-nLC 1200 system (Thermo Scientific) coupled to a Q Exactive HF mass spectrometer via a Nanospray-Flex ion source. The analytical column (50 cm, 75 µm inner diameter (NewObjective) packed in-house with C18 resin ReproSilPur 120, 1.9 µm diameter Dr. Maisch)

was operated at a constant flow rate of 250 nl/min. Gradients of 90 minutes were used to elute peptides (Solvent A: aqueous 0.1% formic acid; Solvent B: 80 % acetonitrile, 0.1% formic acid). MS spectra with a mass range of 300–1.650 m/z were acquired in profile mode using a resolution of 60.000 [maximum fill time of 20 ms or a maximum of 3e6 ions (automatic gain control, AGC)]. Fragmentation was triggered for the top 15 peaks with charge 2–8 on the MS scan (data-dependent acquisition) with a 30 s dynamic exclusion window (normalized collision energy was 28). Precursors were isolated with a 1.4 m/z window, and MS/MS spectra were acquired in profile mode with a resolution of 15,000 (maximum fill time of 80 ms, AGC target of 2e4 ions).

For the quantitative comparison of proteomes of rho^0 and WT cells expressing MTS-Var1, 10 OD600 cells were harvested by centrifugation (12,000 g, 5 min) and snap-frozen in liquid nitrogen and stored at -80°C. Cells lysates were prepared in lysis buffer (6 M GdmCl, 10 mM TCEP, 40 mM CAA, 100 mM Tris pH 8.5) using a FastPrep-24 5G homogenizer (MP Biomedicals, Heidelberg, Germany) with 3 cycles of 30 s, speed 8.0 m/s, 120 s breaks, glass beads). Lysates were boiled for 5 min at 96°C and centrifuged (16,000 g, 2 min, 4°C). Protein concentrations were determined using the Pierce BCA Protein Assay (Thermo Scientific, #23225). For protein digestion, 25 µg of protein were diluted 1:10 with digestion buffer (10% ACN, 25 mM Tris pH 8.5); following, Trypsin and LysC were added in a 1:50 ratio, and the reaction was incubated overnight at 37°C. The next day, fresh Trypsin was added in a 1:100 ratio for 30 minutes at 37°C. The pH of samples was adjusted to pH <2 with tri-flouracetic acid. Desalting/reversed-Phase cleanup with 3x SDB-RPS StageTips. Samples were dried in speed-vac and resolubilized in 12 µl buffer A^{++} (0.1 % formic acid, 0.01 % tri-flouracetic acid in MS grade water). For the quantitative comparison of proteomes of rho^0 and WT cells expressing MTS-Var1 10 OD_{600} of cells were harvested by centrifugation (12,000 g, 5 min) and snap-frozen in liquid nitrogen and stored at -80°C. Cells lysates were prepared in lysis buffer (6 M GdmCl, 10 mM TCEP, 40 mM CAA, 100 mM Tris pH 8.5) using a FastPrep-24 5G homogenizer (MP Biomedicals, Heidelberg, Germany) with 3 cycles of 30 s, speed 8.0 m/s, 120 s breaks, glass beads). Lysates were boiled for 5 min at 96°C and centrifuged (16,000 g, 2 min, 4°C). Protein concentrations were determined using the Pierce BCA Protein Assay (Thermo Scientific, #23225). For protein digestion, 25 µg of protein were diluted 1:10 with digestion buffer (10% ACN, 25 mM Tris pH 8.5) next Trypsin and LysC were added in a 1:50 ratio, and the reaction was incubated overnight at 37°C. The next day, fresh Trypsin was added

in a 1:100 ratio for 30 min at 37°C. The pH of samples was adjusted to pH <2 with tri-flouracetic acid. Desalting/reversed-Phase cleanup with 3x SDB-RPS StageTips. Samples were dried down in speed-vac and resolubilized in 12 µl buffer A^{++} (0.1 % formic acid, 0.01 % tri-flouracetic acid in MS grade water). Peptides were separated using an Easy-nLC 1200 system (Thermo Scientific) coupled to a Q Exactive HF mass spectrometer via a Nanospray-Flex ion source. The analytical column (50 cm, 75 µm inner diameter (NewObjective) packed in-house with C18 resin ReproSilPur 120, 1.9 µm diameter Dr. Maisch) was operated at a constant flow rate of 250 nl/min. Gradients of 180 minutes were used to elute peptides (Solvent A: aqueous 0.1% formic acid; Solvent B: 80 % acetonitrile, 0.1% formic acid). MS spectra with a mass range of 300–1.650 m/z were acquired in profile mode using a resolution of 60.000 [maximum fill time of 20 ms or a maximum of 3e6 ions (automatic gain control, AGC)]. Fragmentation was triggered for the top 15 peaks with charge 2–8 on the MS scan (data-dependent acquisition) with a 30 s dynamic exclusion window (normalized collision energy was 28). Precursors were isolated with a 1.4 m/z window, and MS/MS spectra were acquired in profile mode with a resolution of 15,000 (maximum fill time of 80 ms, AGC target of 2e4 ions).

6.4.10 Analysis of mass spectrometry data

Peptide and protein identification and quantification were done using the MaxQuant software (version 1.6.10.43)[201–203] and a *S. cerevisiae* proteome database obtained from UniProt. 10plex TMT was chosen in Reporter ion MS2 quantification, up to 2 tryptic miss-cleavages were allowed, protein N-terminal acetylation and Met oxidation were specified as variable modifications, and 23 Cys carbamidomethylation as fixed modification. The "Requantify" and "Second Peptides" options were deactivated. The false discovery rate was set at 1% for peptides, proteins, and sites; the minimal peptide length was 7 amino acids. The output files of MaxQuant were processed using the R programming language. Only proteins quantified with at least 2 unique peptides were considered for the analysis. Moreover, only proteins identified in at least 2 of three MS runs were kept. A total of 3,550 proteins for the whole cell proteome and a total of 1,154 for the IP passed the quality control filters. Raw signal sums were cleaned for batch effects using limma[204] and normalized using variance stabilization normalization[205]. Proteins were tested for differential expression using the limma package for the indicated comparison of strains. A reference list of yeast mitochondrial proteins was obtained from Morgenstern *et al.,* 2017[73]. Gene set enrichment analysis was performed using

Fisher's exact test. A Benjamini-Hochberg procedure was used to account for multiple testing where this was performed[206].

6.4.11 Statistical analysis of MS data

Peptide and protein identification and quantification was done using the MaxQuant software (version 2.0.1.0) [201–203] and a *S. cerevisiae* proteome database obtained from UniProt. Protein N-terminal acetylation and Met oxidation were specified as variable modifications, and Cys carbamidomethylation as a fixed modification. The "Requantify" and "Second Peptides" options were deactivated. The false discovery rate was set at 1% for peptides, proteins, and sites, minimal peptide length was 7 amino acids. For label-free data, the LFQ normalization algorithm and second peptides was enabled. Match between runs was applied within each group of replicates. The false discovery rate was set at 1% for peptides, proteins, and sites, minimal peptide length was 7 amino acids.

The protein groups identified in each mass spectrometry data set were processed and analyzed in parallel using the R programming language (version 4.2.1, R Core Team (2018). R: A language and environment for statistical computing. R Foundation for Statistical Computing, Vienna, Austria. Available online at https://www.R-project.org/.). First, the MaxQuant output was filtered to remove contaminants, reverse hits, proteins identified by site only, and proteins identified in less than three replicates (N = 4) of every condition. This resulted in 472 (Var1- & Atp1-GFP pulldowns), 590 (Pim1-GFP pulldowns), 2093 (Hsp78-GFP pulldowns), and 4103 (whole-cell extracts) robustly identified protein groups whose label-free quantification (LFQ) intensities were log2-transformed subsequently. Lastly, missing values were imputed by sampling N = 4 values from a normal distribution (seed = 12345) and using them whenever there were no valid values in a quadruplicate of a condition. Different for each data set, the mean of this normal distribution corresponds to the 1% percentile of LFQ intensities, and its standard deviation is determined as the median of LFQ intensity sample standard deviations calculated within and then averaged over each quadruplicate.

Principal component analysis was carried out for each data set using the package *pcaMethods* [207] on the processed and standardized LFQ intensities of those protein groups with an ANOVA F-statistic p-value < 0.05 between all replicate groups to filter for proteins with a discernable degree of variance between conditions.

Protein groups were statistically analyzed using pairwise, 2-sided Welch's t-tests on the processed LFQ intensities between the replicates of respective control and treatment conditions. Only proteins with valid values in the treatment conditions were considered for comparison. Log2 fold changes were derived as the tested difference of means, and the resulting p-values were adjusted for multiple testing using the Benjamini-Hochberg procedure [208].

6.5 Immunology Methods

6.5.1 Immune decoration of cellulose membranes

Proteins transferred onto a nitrocellulose membrane were visualized by immunodecoration with specific antibodies. After staining the membrane with Ponceau S, it was incubated for one h at RT with 5% (w/v) milk in TBS buffer (10 mM Tris/HCl pH 7.5, 150 mM NaCl) to block non-specific protein binding sites. Then, the blocking solution was replaced by a solution containing the specific primary antibody (1:125 to 1:10,000 in 5% milk in TBS, prepared by immunization in rabbits). The membrane was incubated in this solution overnight at 4°C, washed three times (each 6 min) with TBS, followed by incubation with the secondary antibody (goat anti-rabbit) coupled to horseradish peroxidase (1: 10,000 in 5% milk in TBS, BioRad) for 1 h at RT. After the washing procedure with TBS, the membrane was coated with a 1:1 mix of ECL solutions (ECL 1: 100 mM Tris/HCl pH 8.5, 0.044% (w/v) luminol, 0.0066% p-coumaric acid; ECL 2: 100 mM Tris/HCl pH 8.5, 0.03% H2O2). Luminescence signals were detected on Super RX Medical X-Ray Films (Fuji) using the Optimax Type TR-developer (MS Laborgeräte). No secondary antibody was needed for the horseradish peroxidase coupled HA-antibody, and the films could be exposed directly after washing the primary antibody.

6.5.2 Antibodies

If not differently described, antibodies were raised in rabbits using recombinant purified proteins. The secondary antibody was ordered from BioRad (Goat Anti-Rabbit IgG (H+L)) - HRP Conjugate, #172- 1019, Goat Anti-Mouse IgG (H+L)-HRP Conjugate, #172-1011). The horseradish-peroxidase coupled HA antibody was ordered from Roche (Anti-HA-Peroxidase, High Affinity (3F10), #12 013 819 001) (168). The commonly used antibodies in this thesis are listed in the following table:

Table 10: Antibodies used in this study.

Name	Dilution used in 5% (w/v) milk in 1x TBS	Reference
αSod1	1:1,000	[209]
αVar1	1:500	This study
αHsp78	1:500	Thomas Langer, Max Plank Institute, Cologne
αHA	1:500	Roche, High Affinity 3F10, #12 013 819 001

6.6 Microscopy

6.6.1 Fluorescence microscopy

For microscopy, cells were grown to the mid-log phase and treated with 2 mg/ml chloramphenicol or 7.5 mg/ml cycloheximide for 2 hours before shifting cells to the indicated heat stress conditions. To express proteins under the GAL1 promotor, 0.5 % Gal was added to the medium. Cells were harvested (5 min 5000 g) to stop expression and washed twice with H_2O before resuspension in liquid media. 1 OD was harvested via centrifugation, and cell pellets were resuspended in 30 µl of H_2O. 3 µl were pipetted onto a glass slide and covered with a cover slip. Manual microscopy was performed using a Leica Dmi8 Thunder Imager. Images were acquired using an HC PL APO100x/1,44 Oil UV objective with Immersion Oil Type A 518 F for excitation of GFP 475 nm, mNeonGreen 510 nm, mScarletI, and mCherry 575 nm was used. All images were taken as Z-stacks. Image analysis was done with the LAS X software, and images were further processed in Fiji/ImageJ.

The mtCPY* and Hsp78-GFP colocalization was quantified using Fiji and the Colocalization Analysis2 Plugin (Colog2) and represented as the Pearson's correlation coefficient (PCC).

REFERENCES

[1] T. Ast and M. Schuldiner, "All roads lead to Rome (but some may be harder to travel): SRP-independent translocation into the endoplasmic reticulum," *Critical reviews in biochemistry and molecular biology*, vol. 48, no. 3, pp. 273–288, 2013.

[2] L. Krämer, C. Groh, and J. M. Herrmann, "The proteasome: friend and foe of mitochondrial biogenesis," *FEBS Letters*, vol. 595, no. 8, pp. 1223–1238, 2021.

[3] S. Rödl and J. M. Herrmann, "The role of the proteasome in mitochondrial protein quality control," *IUBMB life*, vol. 75, no. 10, pp. 868–879, 2023.

[4] J. Labbadia and R. I. Morimoto, "The biology of proteostasis in aging and disease," *Annual review of biochemistry*, vol. 84, pp. 435–464, 2015.

[5] N. Louros, J. Schymkowitz, and F. Rousseau, "Mechanisms and pathology of protein misfolding and aggregation," *Nature Reviews Molecular Cell Biology*, pp. 1–22, 2023.

[6] F. Chiti and C. M. Dobson, "Protein Misfolding, Amyloid Formation, and Human Disease: A Summary of Progress Over the Last Decade," *Annual review of biochemistry*, vol. 86, pp. 27–68, 2017.

[7] F. U. Hartl, "Protein Misfolding Diseases," *Annual review of biochemistry*, vol. 86, pp. 21–26, 2017.

[8] M. S. Hipp, P. Kasturi, and F. U. Hartl, "The proteostasis network and its decline in ageing," *Nature Reviews Molecular Cell Biology*, vol. 20, no. 7, pp. 421–435, 2019.

[9] C. B. Anfinsen, "Principles that govern the folding of protein chains," *Science (New York, N.Y.)*, vol. 181, no. 4096, pp. 223–230, 1973.

[10] T. Kiefhaber, "Protein folding kinetics," *Methods in molecular biology (Clifton, N.J.)*, vol. 40, pp. 313–341, 1995.

[11] O. S. Makin, E. Atkins, P. Sikorski et al., "Molecular basis for amyloid fibril formation and stability," *Proceedings of the National Academy of Sciences of the United States of America*, vol. 102, no. 2, pp. 315–320, 2005.

[12] C. J. Roberts, "Protein aggregation and its impact on product quality," *Current opinion in biotechnology*, vol. 30, pp. 211–217, 2014.

[13] D. Balchin, M. Hayer-Hartl, and F. U. Hartl, "In vivo aspects of protein folding and quality control," *Science (New York, N.Y.)*, vol. 353, no. 6294, aac4354, 2016.

[14] G. Kramer, A. Shiber, and B. Bukau, "Mechanisms of Cotranslational Maturation of Newly Synthesized Proteins," *Annual review of biochemistry*, vol. 88, pp. 337–364, 2019.

[15] I. Dikic, "Proteasomal and Autophagic Degradation Systems," *Annual review of biochemistry*, vol. 86, pp. 193–224, 2017.

[16] E. M. Sontag, R. S. Samant, and J. Frydman, "Mechanisms and Functions of Spatial Protein Quality Control," *Annual review of biochemistry*, vol. 86, pp. 97–122, 2017.

[17] F. U. Hartl, A. Bracher, and M. Hayer-Hartl, "Molecular chaperones in protein folding and proteostasis," *Nature <London>*, vol. 475, no. 7356, pp. 324–332, 2011.

[18] T. Saio, X. Guan, P. Rossi et al., "Structural basis for protein antiaggregation activity of the trigger factor chaperone," *Science*, vol. 344, no. 6184, p. 1250494, 2014.

[19] W. A. Houry, ed., *The Molecular Chaperones Interaction Networks in Protein*: *Folding and Degradation*, Springer, New York, NY, 2016.

[20] F. Boos, L. Krämer, C. Groh et al., "Mitochondrial protein-induced stress triggers a global adaptive transcriptional programme," *Nature cell biology*, vol. 21, no. 4, pp. 442–451, 2019.

[21] A. de Graff, D. E. Mosedale, T. Sharp et al., "Proteostasis is adaptive: Balancing chaperone holdases against foldases," *PLoS computational biology*, vol. 16, no. 12, e1008460, 2020.

[22] M. P. Mayer, "Gymnastics of molecular chaperones," *Molecular Cell*, vol. 39, no. 3, pp. 321–331, 2010.

[23] H. H. Kampinga and E. A. Craig, "The HSP70 chaperone machinery: J proteins as drivers of functional specificity," *Nature Reviews Molecular Cell Biology*, vol. 11, no. 8, pp. 579–592, 2010.

[24] C. Scheufler, A. Brinker, G. Bourenkov et al., "Structure of TPR domain-peptide complexes: critical elements in the assembly of the Hsp70-Hsp90 multichaperone machine," *Cell*, vol. 101, no. 2, pp. 199–210, 2000.

[25] M. M. Biebl and J. Buchner, "Structure, Function, and Regulation of the Hsp90 Machinery," *Cold Spring Harbor perspectives in biology*, vol. 11, no. 9, 2019.

[26] S. Reissmann, C. Parnot, C. R. Booth et al., "Essential function of the built-in lid in the allosteric regulation of eukaryotic and archaeal chaperonins," *Nature structural & molecular biology*, vol. 14, no. 5, pp. 432–440, 2007.

[27] A. F. Neuwald, L. Aravind, J. L. Spouge et al., "AAA+: A class of chaperone-like ATPases associated with the assembly, operation, and disassembly of protein complexes," *Genome research*, vol. 9, no. 1, pp. 27–43, 1999.

[28] T. Ogura and A. J. Wilkinson, "AAA+ superfamily ATPases: common structure--diverse function," *Genes to cells : devoted to molecular & cellular mechanisms*, vol. 6, no. 7, pp. 575–597, 2001.

[29] S. R. White and B. Lauring, "AAA+ ATPases: achieving diversity of function with conserved machinery," *Traffic (Copenhagen, Denmark)*, vol. 8, no. 12, pp. 1657–1667, 2007.

[30] J. P. Erzberger and J. M. Berger, "Evolutionary relationships and structural mechanisms of AAA+ proteins," *Annual review of biophysics and biomolecular structure*, vol. 35, pp. 93–114, 2006.

[31] R. Huang, Z. A. Ripstein, R. Augustyniak et al., "Unfolding the mechanism of the AAA+ unfoldase VAT by a combined cryo-EM, solution NMR study," *Proceedings of the National Academy of Sciences*, vol. 113, no. 29, E4190-9, 2016.

[32] C. Puchades, C. R. Sandate, and G. C. Lander, "The molecular principles governing the activity and functional diversity of AAA+ proteins," *Nature Reviews Molecular Cell Biology*, vol. 21, no. 1, pp. 43–58, 2020.

[33] F. den Brave, L. V. Cairo, C. Jagadeesan et al., "Chaperone-Mediated Protein Disaggregation Triggers Proteolytic Clearance of Intra-nuclear Protein Inclusions," *Cell Reports*, vol. 31, no. 9, p. 107680, 2020.

[34] S. N. Gates, A. L. Yokom, J. Lin et al., "Ratchet-like polypeptide translocation mechanism of the AAA+ disaggregase Hsp104," *Science (New York, N.Y.)*, vol. 357, no. 6348, pp. 273–279, 2017.

[35] Y. Sanchez and S. L. Lindquist, "HSP104 required for induced thermotolerance," *Science (New York, N.Y.)*, vol. 248, no. 4959, pp. 1112–1115, 1990.

[36] S. Specht, S. B. M. Miller, A. Mogk et al., "Hsp42 is required for sequestration of protein aggregates into deposition sites in Saccharomyces cerevisiae," *The Journal of cell biology*, vol. 195, no. 4, pp. 617–629, 2011.

[37] G. C. Lander, E. Estrin, M. E. Matyskiela et al., "Complete subunit architecture of the proteasome regulatory particle," *Nature <London>*, vol. 482, no. 7384, pp. 186–191, 2012.

[38] M. E. Matyskiela, G. C. Lander, and A. Martin, "Conformational switching of the 26S proteasome enables substrate degradation," *Nature structural & molecular biology*, vol. 20, no. 7, pp. 781–788, 2013.

[39] K. Lasker, F. Förster, S. Bohn et al., "Molecular architecture of the 26S proteasome holocomplex determined by an integrative approach," *Proceedings of the National Academy of Sciences*, vol. 109, no. 5, pp. 1380–1387, 2012.

[40] Y. Saeki, "Ubiquitin recognition by the proteasome," *Journal of biochemistry*, vol. 161, no. 2, pp. 113–124, 2017.

[41] C. Bashore, C. M. Dambacher, E. A. Goodall et al., "Ubp6 deubiquitinase controls conformational dynamics and substrate degradation of the 26S proteasome," *Nature structural & molecular biology*, vol. 22, no. 9, pp. 712–719, 2015.

[42] R. Spokoini, O. Moldavski, Y. Nahmias et al., "Confinement to organelle-associated inclusion structures mediates asymmetric inheritance of aggregated protein in budding yeast," *Cell Reports*, vol. 2, no. 4, pp. 738–747, 2012.

[43] D. Kaganovich, R. Kopito, and J. Frydman, "Misfolded proteins partition between two distinct quality control compartments," *Nature*, vol. 454, no. 7208, pp. 1088–1095, 2008.

[44] S. Krobitsch and S. Lindquist, "Aggregation of huntingtin in yeast varies with the length of the polyglutamine expansion and the expression of chaperone proteins," *Proceedings of the National Academy of Sciences of the United States of America*, vol. 97, no. 4, pp. 1589–1594, 2000.

[45] R. Halfmann, D. F. Jarosz, S. K. Jones et al., "Prions are a common mechanism for phenotypic inheritance in wild yeasts," *Nature*, vol. 482, no. 7385, pp. 363–368, 2012.

[46] S. M. Hill, X. Hao, B. Liu et al., "Life-span extension by a metacaspase in the yeast Saccharomyces cerevisiae," *Science (New York, N.Y.)*, vol. 344, no. 6190, pp. 1389–1392, 2014.

[47] S. B. M. Miller, C.-T. Ho, J. Winkler et al., "Compartment-specific aggregases direct distinct nuclear and cytoplasmic aggregate deposition," *The EMBO journal*, vol. 34, no. 6, pp. 778–797, 2015.

[48] D. Laporte, B. Salin, B. Daignan-Fornier et al., "Reversible cytoplasmic localization of the proteasome in quiescent yeast cells," *The Journal of cell biology*, vol. 181, no. 5, pp. 737–745, 2008.

[49] L. Krämer, N. Dalheimer, M. Räschle et al., "MitoStores: chaperone-controlled protein granules store mitochondrial precursors in the cytosol," *The EMBO journal*, vol. 42, no. 7, e112309, 2023.

[50] Q. Liu, C. E. Chang, A. C. Wooldredge et al., "Tom70-based transcriptional regulation of mitochondrial biogenesis and aging," *eLife*, vol. 11, 2022.

[51] A. Matouschek, N. Pfanner, and W. Voos, "Protein unfolding by mitochondria. The Hsp70 import motor," *EMBO reports*, vol. 1, no. 5, pp. 404–410, 2000.

[52] F.-N. Vögtle, S. Wortelkamp, R. P. Zahedi et al., "Global analysis of the mitochondrial N-proteome identifies a processing peptidase critical for protein stability," *Cell*, vol. 139, no. 2, pp. 428–439, 2009.

[53] S. G. Garg and S. B. Gould, "The Role of Charge in Protein Targeting Evolution," *Trends in Cell Biology*, vol. 26, no. 12, pp. 894–905, 2016.

[54] G. von Heijne, "Mitochondrial targeting sequences may form amphiphilic helices," *The EMBO journal*, vol. 5, no. 6, pp. 1335–1342, 1986.

[55] N. Pfanner, B. Warscheid, and N. Wiedemann, "Mitochondrial proteins: from biogenesis to functional networks," *Nature Reviews Molecular Cell Biology*, vol. 20, no. 5, pp. 267–284, 2019.

[56] D. Mokranjac, "How to get to the other side of the mitochondrial inner membrane - the protein import motor," *Biological Chemistry*, vol. 401, 6-7, pp. 723–736, 2020.

[57] N. Wiedemann and N. Pfanner, "Mitochondrial Machineries for Protein Import and Assembly," *Annual review of biochemistry*, vol. 86, pp. 685–714, 2017.

[58] H. Imachi, M. K. Nobu, N. Nakahara et al., "Isolation of an archaeon at the prokaryote-eukaryote interface," *Nature*, vol. 577, no. 7791, pp. 519–525, 2020.

[59] T. A. Williams, C. J. Cox, P. G. Foster et al., "Phylogenomics provides robust support for a two-domains tree of life," *Nature Ecology & Evolution*, vol. 4, no. 1, pp. 138–147, 2020.

[60] H. J. Muller, "THE RELATION OF RECOMBINATION TO MUTATIONAL ADVANCE," *Mutation Research/Fundamental and Molecular Mechanisms of Mutagenesis*, vol. 106, no. 1, pp. 2–9, 1964.

[61] M. Lynch, B. Koskella, and S. Schaack, "Mutation pressure and the evolution of organelle genomic architecture," *Science*, vol. 311, no. 5768, pp. 1727–1730, 2006.

[62] E. LARA, A. CHATZINOTAS, and A. G. B. SIMPSON, "Andalucia (n. gen.)--the deepest branch within jakobids (Jakobida; Excavata), based on morphological and molecular study of a new flagellate from soil," *The Journal of Eukaryotic Microbiology*, vol. 53, no. 2, pp. 112–120, 2006.

[63] P. Borst and L. A. Grivell, "The mitochondrial genome of yeast," *Cell*, vol. 15, no. 3, pp. 705–723, 1978.

[64] J. W. Taanman, "The mitochondrial genome: structure, transcription, translation and replication," *Biochimica et biophysica acta*, vol. 1410, no. 2, pp. 103–123, 1999.

[65] R. Maleszka, P. J. Skelly, and G. D. Clark-Walker, "Rolling circle replication of DNA in yeast mitochondria," *The EMBO journal*, vol. 10, no. 12, pp. 3923–3929, 1991.

[66] V. Contamine and M. Picard, "Maintenance and integrity of the mitochondrial genome: a plethora of nuclear genes in the budding yeast," *Microbiology and molecular biology reviews : MMBR*, vol. 64, no. 2, pp. 281–315, 2000.

[67] G. Michaelis, F. Michel, J. Lazowska et al., "Recombined molecules of mitochondrial DNA obtained from crosses between cytoplasmic petite mutants of Saccharomyces cerevisiae: the stoichiometry of parental DNA repeats within the recombined molecule," *Molecular & general genetics : MGG*, vol. 149, no. 2, pp. 125–130, 1976.

[68] M. W. Gray, G. Burger, R. Derelle et al., "The draft nuclear genome sequence and predicted mitochondrial proteome of Andalucia godoyi, a protist with the most gene-rich and bacteria-like mitochondrial genome," *BMC Biology*, vol. 18, no. 1, p. 22, 2020.

[69] B. F. Lang, G. Burger, C. J. O'Kelly et al., "An ancestral mitochondrial DNA resembling a eubacterial genome in miniature," *Nature*, vol. 387, no. 6632, pp. 493–497, 1997.

[70] U.-G. Maier, S. Zauner, C. Woehle et al., "Massively convergent evolution for ribosomal protein gene content in plastid and mitochondrial genomes," *Genome Biology and Evolution*, vol. 5, no. 12, pp. 2318–2329, 2013.

[71] P. Björkholm, A. Harish, E. Hagström et al., "Mitochondrial genomes are retained by selective constraints on protein targeting," *Proceedings of the National Academy of Sciences*, vol. 112, no. 33, pp. 10154–10161, 2015.

[72] K. G. Hansen, N. Aviram, J. Laborenz et al., "An ER surface retrieval pathway safeguards the import of mitochondrial membrane proteins in yeast," *Science*, vol. 361, no. 6407, pp. 1118–1122, 2018.

[73] M. Morgenstern, S. B. Stiller, P. Lübbert et al., "Definition of a High-Confidence Mitochondrial Proteome at Quantitative Scale," *Cell Reports*, vol. 19, no. 13, pp. 2836–2852, 2017.

[74] M. Bohnert, P. Rehling, B. Guiard et al., "Cooperation of stop-transfer and conservative sorting mechanisms in mitochondrial protein transport," *Current biology : CB*, vol. 20, no. 13, pp. 1227–1232, 2010.

[75] M. W. Woellhaf, F. Sommer, M. Schroda et al., "Proteomic profiling of the mitochondrial ribosome identifies Atp25 as a composite mitochondrial precursor protein," *Molecular biology of the cell*, vol. 27, no. 20, pp. 3031–3039, 2016.

[76] Y. Itoh, A. Naschberger, N. Mortezaei et al., "Analysis of translating mitoribosome reveals functional characteristics of translation in mitochondria of fungi,".

[77] M. Bode, S. Longen, B. Morgan et al., "Inaccurately assembled cytochrome c oxidase can lead to oxidative stress-induced growth arrest," *Antioxidants & Redox Signaling*, vol. 18, no. 13, pp. 1597–1612, 2013.

[78] R. O. Poyton, "Assembling a time bomb--cytochrome c oxidase and disease," *Nature Genetics*, vol. 20, no. 4, pp. 316–317, 1998.

[79] Z. Zhu, J. Yao, T. Johns et al., "SURF1, encoding a factor involved in the biogenesis of cytochrome c oxidase, is mutated in Leigh syndrome," *Nature Genetics*, vol. 20, no. 4, pp. 337–343, 1998.

[80] S. Duvezin-Caubet, M. Rak, L. Lefebvre-Legendre et al., "A "petite obligate" mutant of Saccharomyces cerevisiae: functional mtDNA is lethal in cells lacking the delta subunit of mitochondrial F1-ATPase," *Journal of Biological Chemistry*, vol. 281, no. 24, pp. 16305–16313, 2006.

[81] Y. Ohba, T. MacVicar, and T. Langer, "Regulation of mitochondrial plasticity by the i-AAA protease YME1L," *Biological Chemistry*, vol. 401, 6-7, pp. 877–890, 2020.

[82] Y. Choquet, D. B. Stern, K. Wostrikoff et al., "Translation of cytochrome f is autoregulated through the 5' untranslated region of petA mRNA in Chlamydomonas chloroplasts," *Proceedings of the National Academy of Sciences of the United States of America*, vol. 95, no. 8, pp. 4380–4385, 1998.

[83] A. Boulouis, C. Raynaud, S. Bujaldon et al., "The nucleus-encoded trans-acting factor MCA1 plays a critical role in the regulation of cytochrome f synthesis in Chlamydomonas chloroplasts," *The Plant Cell*, vol. 23, no. 1, pp. 333–349, 2011.

[84] D. U. Mick, T. D. Fox, and P. Rehling, "Inventory control: cytochrome c oxidase assembly regulates mitochondrial translation," *Nature Reviews Molecular Cell Biology*, vol. 12, no. 1, pp. 14–20, 2011.

[85] X. Perez-Martinez, S. A. Broadley, and T. D. Fox, "Mss51p promotes mitochondrial Cox1p synthesis and interacts with newly synthesized Cox1p," *The EMBO journal*, vol. 22, no. 21, pp. 5951–5961, 2003.

[86] A. Barrientos, A. Zambrano, and A. Tzagoloff, "Mss51p and Cox14p jointly regulate mitochondrial Cox1p expression in Saccharomyces cerevisiae," *The EMBO journal*, vol. 23, no. 17, pp. 3472–3482, 2004.

[87] R. Salvatori, K. Kehrein, A. P. Singh et al., "Molecular Wiring of a Mitochondrial Translational Feedback Loop," *Molecular Cell*, vol. 77, no. 4, 887-900.e5, 2020.

[88] B. B. Buchanan and S. Luan, "Redox regulation in the chloroplast thylakoid lumen: a new frontier in photosynthesis research," *Journal of Experimental Botany*, vol. 56, no. 416, pp. 1439–1447, 2005.

[89] B. B. Buchanan, "The Ferredoxin/Thioredoxin System: A Key Element in the Regulatory Function of Light in Photosynthesis," *BioScience*, vol. 34, no. 6, pp. 378–383, 1984.

[90] J. F. Allen and W. F. Martin, "Why Have Organelles Retained Genomes?," *Cell Systems*, vol. 2, no. 2, pp. 70–72, 2016.

[91] J. F. Allen, "Why chloroplasts and mitochondria retain their own genomes and genetic systems: Colocation for redox regulation of gene expression," *Proceedings of the National Academy of Sciences*, vol. 112, no. 33, pp. 10231–10238, 2015.

[92] J. M. Herrmann, M. W. Woellhaf, and N. Bonnefoy, "Control of protein synthesis in yeast mitochondria: the concept of translational activators," *Biochimica et biophysica acta*, vol. 1833, no. 2, pp. 286–294, 2013.

[93] M. Sanchirico, A. Tzellas, T. D. Fox et al., "Relocation of the unusual VAR1 gene from the mitochondrion to the nucleus," *Biochemistry and cell biology = Biochimie et biologie cellulaire*, vol. 73, 11-12, pp. 987–995, 1995.

[94] C. J. Herbert, P. Golik, and N. Bonnefoy, "Yeast PPR proteins, watchdogs of mitochondrial gene expression," *RNA Biology*, vol. 10, no. 9, pp. 1477–1494, 2013.

[95] S. R. Seshadri, C. Banarjee, M. H. Barros et al., "The translational activator Sov1 coordinates mitochondrial gene expression with mitoribosome biogenesis," *Nucleic Acids Research*, vol. 48, no. 12, pp. 6759–6774, 2020.

[96] A. R. Hibbs, K. K. Maheshwari, and S. Marzuki, "Assembly of the mitochondrial ribosomes in a temperature-conditional mutant of Saccharomyces cerevisiae defective in the synthesis of the var1 protein," *Biochimica et biophysica acta*, vol. 908, no. 2, pp. 179–187, 1987.

[97] A. V. Litvinchuk, S. S. Sokolov, A. G. Rogov et al., "Mitochondrially-encoded protein Var1 promotes loss of respiratory function in Saccharomyces cerevisiae under stressful conditions," *European Journal of Cell Biology*, vol. 92, 4-5, pp. 169–174, 2013.

[98] A. Caballero, A. Ugidos, B. Liu et al., "Absence of mitochondrial translation control proteins extends life span by activating sirtuin-dependent silencing," *Molecular Cell*, vol. 42, no. 3, pp. 390–400, 2011.

[99] L. Bertgen, T. Mühlhaus, and J. M. Herrmann, "Clingy genes: Why were genes for ribosomal proteins retained in many mitochondrial genomes?," *Biochimica et biophysica acta. Bioenergetics*, vol. 1861, no. 11, p. 148275, 2020.

[100] H. Weidberg and A. Amon, "MitoCPR-A surveillance pathway that protects mitochondria in response to protein import stress," *Science (New York, N.Y.)*, vol. 360, no. 6385, 2018.

[101] J. M. Herrmann, R. A. Stuart, E. A. Craig et al., "Mitochondrial heat shock protein 70, a molecular chaperone for proteins encoded by mitochondrial DNA," *The Journal of cell biology*, vol. 127, no. 4, pp. 893–902, 1994.

[102] C. Prip-Buus, B. Westerman, M. Schmitt et al., "Role of the mitochondrial DnaJ homologue, Mdj1p, in the prevention of heat-induced protein aggregation," *FEBS Letters*, vol. 380, 1-2, pp. 142–146, 1996.

[103] R. Dutkiewicz, B. Schilke, H. Knieszner et al., "Ssq1, a mitochondrial Hsp70 involved in iron-sulfur (Fe/S) center biogenesis. Similarities to and differences from its bacterial counterpart," *Journal of Biological Chemistry*, vol. 278, no. 32, pp. 29719–29727, 2003.

[104] S. Schmidt, A. Strub, K. Röttgers et al., "The two mitochondrial heat shock proteins 70, Ssc1 and Ssq1, compete for the cochaperone Mge1," *Journal of molecular biology*, vol. 313, no. 1, pp. 13–26, 2001.

[105] Z. Xu, A. L. Horwich, and P. B. Sigler, "The crystal structure of the asymmetric GroEL-GroES-(ADP)7 chaperonin complex," *Nature*, vol. 388, no. 6644, pp. 741–750, 1997.

[106] A. L. Horwich, S. Caplan, J. S. Wall et al., "Chapter 26 Chaperonin-mediated protein folding," in *New Comprehensive Biochemistry : Membrane Biogenesis and Protein Targeting,* W. Neupert and R. Lill, Eds., vol. 22, pp. 329–337, Elsevier, 1992.

[107] J. Ostermann, A. L. Horwich, W. Neupert et al., "Protein folding in mitochondria requires complex formation with hsp60 and ATP hydrolysis," *Nature*, vol. 341, no. 6238, pp. 125–130, 1989.

[108] E. Dibrov, S. Fu, and B. D. Lemire, "The Saccharomyces cerevisiae TCM62 gene encodes a chaperone necessary for the assembly of the mitochondrial succinate dehydrogenase (complex II)," *Journal of Biological Chemistry*, vol. 273, no. 48, pp. 32042–32048, 1998.

[109] M. Moczko, B. Schönfisch, W. Voos et al., "The mitochondrial ClpB homolog Hsp78 cooperates with matrix Hsp70 in maintenance of mitochondrial function," *Journal of molecular biology*, vol. 254, no. 4, pp. 538–543, 1995.

[110] W. Jaworek, M. Sylvester, G. Cenini et al., "Elucidation of the interaction proteome of mitochondrial chaperone Hsp78 highlights its role in protein aggregation during heat stress," *The Journal of biological chemistry*, vol. 298, no. 10, p. 102494, 2022.

[111] C. Vazquez-Calvo, V. Kohler, J. L. Höög et al., "Newly imported proteins in mitochondria are particularly sensitive to aggregation," *Acta physiologica (Oxford, England)*, vol. 238, no. 3, e13985, 2023.

[112] L. van Dyck, M. Dembowski, W. Neupert et al., "Mcx1p, a ClpX homologue in mitochondria of Saccharomyces cerevisiae," *FEBS Letters*, vol. 438, no. 3, pp. 250–254, 1998.

[113] H. Arlt, R. Tauer, H. Feldmann et al., "The YTA10-12 complex, an AAA protease with chaperone-like activity in the inner membrane of mitochondria," *Cell*, vol. 85, no. 6, pp. 875–885, 1996.

[114] J. Yang, A. S. Song, R. L. Wiseman et al., "Cryo-EM structure of hexameric yeast Lon protease (PIM1) highlights the importance of conserved structural elements," *The Journal of biological chemistry*, vol. 298, no. 3, p. 101694, 2022.

[115] S. Deshwal, K. U. Fiedler, and T. Langer, "Mitochondrial Proteases: Multifaceted Regulators of Mitochondrial Plasticity," *Annual review of biochemistry*, vol. 89, pp. 501–528, 2020.

[116] L. van Dyck, W. Neupert, and T. Langer, "The ATP-dependent PIM1 protease is required for the expression of intron-containing genes in mitochondria," *Genes & development*, vol. 12, no. 10, pp. 1515–1524, 1998.

[117] C. Deville, K. Franke, A. Mogk et al., "Two-Step Activation Mechanism of the ClpB Disaggregase for Sequential Substrate Threading by the Main ATPase Motor," *Cell Reports*, vol. 27, no. 12, 3433-3446.e4, 2019.

[118] I. Levchenko, C. K. Smith, N. P. Walsh et al., "PDZ-like domains mediate binding specificity in the Clp/Hsp100 family of chaperones and protease regulatory subunits," *Cell*, vol. 91, no. 7, pp. 939–947, 1997.

[119] C. Zhou, B. D. Slaughter, J. R. Unruh et al., "Motility and segregation of Hsp104-associated protein aggregates in budding yeast," *Cell*, vol. 147, no. 5, pp. 1186–1196, 2011.

[120] J. Krzewska, G. Konopa, and K. Liberek, "Importance of two ATP-binding sites for oligomerization, ATPase activity and chaperone function of mitochondrial Hsp78 protein," *Journal of molecular biology*, vol. 314, no. 4, pp. 901–910, 2001.

[121] J. Jumper, R. Evans, A. Pritzel et al., "Highly accurate protein structure prediction with AlphaFold," *Nature*, vol. 596, no. 7873, pp. 583–589, 2021.

[122] E. F. Pettersen, T. D. Goddard, C. C. Huang et al., "UCSF Chimera--a visualization system for exploratory research and analysis," *Journal of Computational Chemistry*, vol. 25, no. 13, pp. 1605–1612, 2004.

[123] H. Abeliovich, M. Zarei, K. T. G. Rigbolt et al., "Involvement of mitochondrial dynamics in the segregation of mitochondrial matrix proteins during stationary phase mitophagy," *Nature Communications*, vol. 4, p. 2789, 2013.

[124] K. A. Morano, C. M. Grant, and W. S. Moye-Rowley, "The response to heat shock and oxidative stress in Saccharomyces cerevisiae," *Genetics*, vol. 190, no. 4, pp. 1157–1195, 2012.

[125] M. M. Hiller, A. Finger, M. Schweiger et al., "ER degradation of a misfolded luminal protein by the cytosolic ubiquitin-proteasome pathway," *Science (New York, N.Y.)*, vol. 273, no. 5282, pp. 1725–1728, 1996.

[126] D. Vestweber and G. Schatz, "Point mutations destabilizing a precursor protein enhance its post-translational import into mitochondria," *The EMBO journal*, vol. 7, no. 4, pp. 1147–1151, 1988.

[127] M. Schmitt, W. Neupert, and T. Langer, "Hsp78, a Clp homologue within mitochondria, can substitute for chaperone functions of mt-hsp70," *The EMBO journal*, vol. 14, no. 14, pp. 3434–3444, 1995.

[128] J. Arends, M. Griego, N. Thomanek et al., "An Integrated Proteomic Approach Uncovers Novel Substrates and Functions of the Lon Protease in Escherichia coli," *Proteomics*, vol. 18, no. 13, e1800080, 2018.

[129]   I. Botos, E. E. Melnikov, S. Cherry et al., "The catalytic domain of Escherichia coli Lon protease has a unique fold and a Ser-Lys dyad in the active site," *The Journal of biological chemistry*, vol. 279, no. 9, pp. 8140–8148, 2004.

[130]   P. Simakin, C. Koch, and J. M. Herrmann, "A modular cloning (MoClo) toolkit for reliable intracellular protein targeting in the yeast Saccharomyces cerevisiae," *Microbial cell (Graz, Austria)*, vol. 10, no. 4, pp. 78–87, 2023.

[131]   D. Graifer, A. Malygin, D. O. Zharkov et al., "Eukaryotic ribosomal protein S3: A constituent of translational machinery and an extraribosomal player in various cellular processes," *Biochimie*, vol. 99, pp. 8–18, 2014.

[132]   F. Fiumara, L. Fioriti, E. R. Kandel et al., "Essential role of coiled coils for aggregation and activity of Q/N-rich prions and PolyQ proteins," *Cell*, vol. 143, no. 7, pp. 1121–1135, 2010.

[133]   J. M. Cherry, E. L. Hong, C. Amundsen et al., "Saccharomyces Genome Database: the genomics resource of budding yeast," *Nucleic Acids Research*, vol. 40, Database issue, D700-5, 2012.

[134]   Y. Xie and A. Varshavsky, "RPN4 is a ligand, substrate, and transcriptional regulator of the 26S proteasome: a negative feedback circuit," *Proceedings of the National Academy of Sciences of the United States of America*, vol. 98, no. 6, pp. 3056–3061, 2001.

[135]   L. Wrobel, U. Topf, P. Bragoszewski et al., "Mistargeted mitochondrial proteins activate a proteostatic response in the cytosol," *Nature*, vol. 524, no. 7566, pp. 485–488, 2015.

[136]   L. Wang and P. Walter, "Msp1/ATAD1 in Protein Quality Control and Regulation of Synaptic Activities," *Annual review of cell and developmental biology*, vol. 36, pp. 141–164, 2020.

[137]   C. Koch, M. Räschle, C. Prescianotto-Baschong et al., *The ER-SURF pathway uses ER-mitochondria contact sites for protein targeting to mitochondria*, 2023.

[138]   J. Song, L. Steidle, I. Steymans et al., "The mitochondrial Hsp70 controls the assembly of the F1FO-ATP synthase," *Nature Communications*, vol. 14, no. 1, p. 39, 2023.

[139] C.-T. Ho, T. Grousl, O. Shatz et al., "Cellular sequestrases maintain basal Hsp70 capacity ensuring balanced proteostasis," *Nature Communications*, vol. 10, no. 1, p. 4851, 2019.

[140] P. M. Douglas, S. Treusch, H.-Y. Ren et al., "Chaperone-dependent amyloid assembly protects cells from prion toxicity," *Proceedings of the National Academy of Sciences of the United States of America*, vol. 105, no. 20, pp. 7206–7211, 2008.

[141] J. Tyedmers, A. Mogk, and B. Bukau, "Cellular strategies for controlling protein aggregation," *Nature reviews. Molecular cell biology*, vol. 11, no. 11, pp. 777–788, 2010.

[142] M. Carrió, N. González-Montalbán, A. Vera et al., "Amyloid-like properties of bacterial inclusion bodies," *Journal of molecular biology*, vol. 347, no. 5, pp. 1025–1037, 2005.

[143] A. Ramón, M. Señorale-Pose, and M. Marín, "Inclusion bodies: not that bad…," *Frontiers in microbiology*, vol. 5, p. 56, 2014.

[144] U. Rinas, F. Hoffmann, E. Betiku et al., "Inclusion body anatomy and functioning of chaperone-mediated in vivo inclusion body disassembly during high-level recombinant protein production in Escherichia coli," *Journal of biotechnology*, vol. 127, no. 2, pp. 244–257, 2007.

[145] M. Avellaneda, K. B. Franke, B. Bukau et al., "Processive extrusion of polypeptide loops by a Hsp100 disaggregase," *Nature <London>*.

[146] E. U. Weber-Ban, B. G. Reid, A. D. Miranker et al., "Global unfolding of a substrate protein by the Hsp100 chaperone ClpA," *Nature*, vol. 401, no. 6748, pp. 90–93, 1999.

[147] A. Mogk, B. Bukau, and H. H. Kampinga, "Cellular Handling of Protein Aggregates by Disaggregation Machines," *Molecular Cell*, vol. 69, no. 2, pp. 214–226, 2018.

[148] M. J. Morten, L. Sirvio, H. Rupawala et al., "Quantitative super-resolution imaging of pathological aggregates reveals distinct toxicity profiles in different synucleinopathies," *Proceedings of the National Academy of Sciences of the United States of America*, vol. 119, no. 41, e2205591119, 2022.

[149] A. Gruber, D. Hornburg, M. Antonin et al., "Molecular and structural architecture of polyQ aggregates in yeast," *Proceedings of the National Academy of Sciences of the United States of America*, vol. 115, no. 15, E3446-E3453, 2018.

[150] S. De, D. C. Wirthensohn, P. Flagmeier et al., "Different soluble aggregates of Aβ42 can give rise to cellular toxicity through different mechanisms," *Nature Communications*, vol. 10, no. 1, p. 1541, 2019.

[151] D. Poveda-Huertes, S. Matic, A. Marada et al., "An Early mtUPR: Redistribution of the Nuclear Transcription Factor Rox1 to Mitochondria Protects against Intramitochondrial Proteotoxic Aggregates," *Molecular Cell*, vol. 77, no. 1, 180-188.e9, 2020.

[152] C. Vijayvergiya, M. F. Beal, J. Buck et al., "Mutant superoxide dismutase 1 forms aggregates in the brain mitochondrial matrix of amyotrophic lateral sclerosis mice," *The Journal of neuroscience : the official journal of the Society for Neuroscience*, vol. 25, no. 10, pp. 2463–2470, 2005.

[153] M. Bruderek, W. Jaworek, A. Wilkening et al., "IMiQ: a novel protein quality control compartment protecting mitochondrial functional integrity," *Molecular biology of the cell*, vol. 29, no. 3, pp. 256–269, 2018.

[154] L. Ruan, J. T. McNamara, X. Zhang et al., "Solid-phase inclusion as a mechanism for regulating unfolded proteins in the mitochondrial matrix," *Science advances*, vol. 6, no. 32, eabc7288, 2020.

[155] T. Bender, I. Lewrenz, S. Franken et al., "Mitochondrial enzymes are protected from stress-induced aggregation by mitochondrial chaperones and the Pim1/LON protease," *Molecular biology of the cell*, vol. 22, no. 5, pp. 541–554, 2011.

[156] K. Rottgers, N. Zufall, B. Guiard et al., "The ClpB homolog Hsp78 is required for the efficient degradation of proteins in the mitochondrial matrix," *The Journal of biological chemistry*, vol. 277, no. 48, pp. 45829–45837, 2002.

[157] A. Göke, S. Schrott, A. Mizrak et al., "Mrx6 regulates mitochondrial DNA copy number in Saccharomyces cerevisiae by engaging the evolutionarily conserved Lon protease Pim1," *Molecular biology of the cell*, vol. 31, no. 7, pp. 527–545, 2020.

[158] J. Wei and F. Sherman, "Sue1p is required for degradation of labile forms of altered cytochromes C in yeast mitochondria," *The Journal of biological chemistry*, vol. 279, no. 29, pp. 30449–30458, 2004.

[159] W. L. Fangman, J. W. Henly, and B. J. Brewer, "RPO41-independent maintenance of rho- mitochondrial DNA in Saccharomyces cerevisiae," *Molecular and cellular biology*, vol. 10, no. 1, pp. 10–15, 1990.

[160] R. Gupta, M. Kanai, T. J. Durham et al., "Nuclear genetic control of mtDNA copy number and heteroplasmy in humans," *Nature*, vol. 620, no. 7975, pp. 839–848, 2023.

[161] Y. Oma, Y. Kino, N. Sasagawa et al., "Intracellular localization of homopolymeric amino acid-containing proteins expressed in mammalian cells," *Journal of Biological Chemistry*, vol. 279, no. 20, pp. 21217–21222, 2004.

[162] B. Westermann, B. Gaume, J. M. Herrmann et al., "Role of the mitochondrial DnaJ homolog Mdj1p as a chaperone for mitochondrially synthesized and imported proteins," *Molecular and cellular biology*, vol. 16, no. 12, pp. 7063–7071, 1996.

[163] C. Klanner, W. Neupert, and T. Langer, "The chaperonin-related protein Tcm62p ensures mitochondrial gene expression under heat stress," *FEBS Letters*, vol. 470, no. 3, pp. 365–369, 2000.

[164] K. Klann and C. Münch, "Quantitative Translation Proteomics Using mePROD," *Methods in molecular biology (Clifton, N.J.)*, vol. 2428, pp. 75–87, 2022.

[165] R. Banerjee, V. Trauschke, N. Bertram et al., *mtHsp70 converts mitochondrial proteostasis distress into impaired protein import*, 2022.

[166] J. Sethuraman, A. Majer, N. C. Friedrich et al., "Genes within genes: multiple LAGLIDADG homing endonucleases target the ribosomal protein S3 gene encoded within an rnl group I intron of Ophiostoma and related taxa," *Molecular biology and evolution*, vol. 26, no. 10, pp. 2299–2315, 2009.

[167] A. G. Korovesi, M. Ntertilis, and V. N. Kouvelis, "Mt-rps3 is an ancient gene which provides insight into the evolution of fungal mitochondrial genomes," *Molecular Phylogenetics and Evolution*, vol. 127, pp. 74–86, 2018.

[168] R. R. Cupo and J. Shorter, "Skd3 (human ClpB) is a potent mitochondrial protein disaggregase that is inactivated by 3-methylglutaconic aciduria-linked mutations," *eLife*, vol. 9, 2020.

[169] S. B. Wortmann, S. Ziętkiewicz, M. Kousi et al., "CLPB mutations cause 3-methylglutaconic aciduria, progressive brain atrophy, intellectual disability, congenital neutropenia, cataracts, movement disorder," *American journal of human genetics*, vol. 96, no. 2, pp. 245–257, 2015.

[170] S. Lee, S. B. Lee, N. Sung et al., "Structural basis of impaired disaggregase function in the oxidation-sensitive SKD3 mutant causing 3-methylglutaconic aciduria," *Nature Communications*, vol. 14, no. 1, p. 2028, 2023.

[171] P. Risiglione, F. Zinghirino, M. C. Di Rosa et al., "Alpha-Synuclein and Mitochondrial Dysfunction in Parkinson's Disease: The Emerging Role of VDAC," *Biomolecules*, vol. 11, no. 5, 2021.

[172] M. Vicario, D. Cieri, F. Vallese et al., "A split-GFP tool reveals differences in the sub-mitochondrial distribution of wt and mutant alpha-synuclein," *Cell death & disease*, vol. 10, no. 11, p. 857, 2019.

[173] J. Shorter, "The mammalian disaggregase machinery: Hsp110 synergizes with Hsp70 and Hsp40 to catalyze protein disaggregation and reactivation in a cell-free system," *PLoS ONE*, vol. 6, no. 10, e26319, 2011.

[174] P. Seneci, "Chapter 6 - Targeting Assembly and Disassembly of Protein Aggregates: A Raggle-taggle Bunch with High Hopes," in *Chemical modulators of protein misfolding and neurodegenerative disease,* P. Seneci, Ed., pp. 173–228, Academic Press, Amsterdam, London, 2015.

[175] J. He, C.-C. Mao, A. Reyes et al., "The AAA+ protein ATAD3 has displacement loop binding properties and is involved in mitochondrial nucleoid organization," *The Journal of cell biology*, vol. 176, no. 2, pp. 141–146, 2007.

[176] D. F. Bogenhagen, D. Rousseau, and S. Burke, "The layered structure of human mitochondrial DNA nucleoids," *Journal of Biological Chemistry*, vol. 283, no. 6, pp. 3665–3675, 2008.

[177] K. N. Truscott, B. R. Lowth, P. R. Strack et al., "Diverse functions of mitochondrial AAA+ proteins: protein activation, disaggregation, and degradation," *Biochemistry and cell biology = Biochimie et biologie cellulaire*, vol. 88, no. 1, pp. 97–108, 2010.

[178] S. Karlin and C. Burge, "Trinucleotide repeats and long homopeptides in genes and proteins associated with nervous system disease and development," *Proceedings of the National Academy of Sciences of the United States of America*, vol. 93, no. 4, pp. 1560–1565, 1996.

[179] M. M. Albà and R. Guigó, "Comparative analysis of amino acid repeats in rodents and humans," *Genome research*, vol. 14, no. 4, pp. 549–554, 2004.

[180] R. van der Lee, M. Buljan, B. Lang et al., "Classification of intrinsically disordered regions and proteins," *Chemical reviews*, vol. 114, no. 13, pp. 6589–6631, 2014.

[181] A. Baryshnikova, M. Costanzo, S. Dixon et al., "Synthetic genetic array (SGA) analysis in Saccharomyces cerevisiae and Schizosaccharomyces pombe," *Methods in enzymology*, vol. 470, pp. 145–179, 2010.

[182] D. M. Walther, P. Kasturi, M. Zheng et al., "Widespread Proteome Remodeling and Aggregation in Aging C. elegans," *Cell*, vol. 161, no. 4, pp. 919–932, 2015.

[183] E. W. J. Wallace, J. L. Kear-Scott, E. V. Pilipenko et al., "Reversible, Specific, Active Aggregates of Endogenous Proteins Assemble upon Heat Stress," *Cell*, vol. 162, no. 6, pp. 1286–1298, 2015.

[184] J. Carroll, M. C. Altman, I. M. Fearnley et al., "Identification of membrane proteins by tandem mass spectrometry of protein ions," *Proceedings of the National Academy of Sciences of the United States of America*, vol. 104, no. 36, pp. 14330–14335, 2007.

[185] K. Klann, G. Tascher, and C. Münch, "Functional Translatome Proteomics Reveal Converging and Dose-Dependent Regulation by mTORC1 and eIF2α," *Molecular Cell*, vol. 77, no. 4, 913-925.e4, 2020.

[186]   B. Lorber, F. Fischer, M. Bailly et al., "Protein analysis by dynamic light scattering: methods and techniques for students," *Biochemistry and molecular biology education : a bimonthly publication of the International Union of Biochemistry and Molecular Biology*, vol. 40, no. 6, pp. 372–382, 2012.

[187]   W. M. Babinchak and W. K. Surewicz, "Studying Protein Aggregation in the Context of Liquid-liquid Phase Separation Using Fluorescence and Atomic Force Microscopy, Fluorescence and Turbidity Assays, and FRAP," *Bio-protocol*, vol. 10, no. 2, 2020.

[188]   J. A. J. Housmans, G. Wu, J. Schymkowitz et al., "A guide to studying protein aggregation," *The FEBS journal*, vol. 290, no. 3, pp. 554–583, 2023.

[189]   M. J. Casadaban and S. N. Cohen, "Analysis of gene control signals by DNA fusion and cloning in Escherichia coli," *Journal of molecular biology*, vol. 138, no. 2, pp. 179–207, 1980.

[190]   M. Meselson and R. Yuan, "DNA restriction enzyme from E. coli," *Nature*, vol. 217, no. 5134, pp. 1110–1114, 1968.

[191]   M. Ralser, H. Kuhl, M. Ralser et al., "The Saccharomyces cerevisiae W303-K6001 cross-platform genome sequence: insights into ancestry and physiology of a laboratory mutt," *Open biology*, vol. 2, no. 8, p. 120093, 2012.

[192]   B. D. Gambill, W. Voos, P. J. Kang et al., "A dual role for mitochondrial heat shock protein 70 in membrane translocation of preproteins," *The Journal of cell biology*, vol. 123, no. 1, pp. 109–117, 1993.

[193]   S. Backes, S. Hess, F. Boos et al., "Tom70 enhances mitochondrial preprotein import efficiency by binding to internal targeting sequences," *The Journal of cell biology*, vol. 217, no. 4, pp. 1369–1382, 2018.

[194]   B. Westermann and W. Neupert, "Mitochondria-targeted green fluorescent proteins: convenient tools for the study of organelle biogenesis inSaccharomyces cerevisiae," *Yeast (Chichester, England)*, vol. 16, no. 15, pp. 1421–1427, 2000.

[195] D. Mumberg, R. Müller, and M. Funk, "Yeast vectors for the controlled expression of heterologous proteins in different genetic backgrounds," *Gene*, vol. 156, no. 1, pp. 119–122, 1995.

[196] C. Janke, M. M. Magiera, N. Rathfelder et al., "A versatile toolbox for PCR-based tagging of yeast genes: new fluorescent proteins, more markers and promoter substitution cassettes," *Yeast (Chichester, England)*, vol. 21, no. 11, pp. 947–962, 2004.

[197] K. J. Livak and T. D. Schmittgen, "Analysis of relative gene expression data using real-time quantitative PCR and the 2(-Delta Delta C(T)) Method," *Methods (San Diego, Calif.)*, vol. 25, no. 4, pp. 402–408, 2001.

[198] U. K. Laemmli, "Cleavage of structural proteins during the assembly of the head of bacteriophage T4," *Nature*, vol. 227, no. 5259, pp. 680–685, 1970.

[199] J. Kyhse-Andersen, "Electroblotting of multiple gels: a simple apparatus without buffer tank for rapid transfer of proteins from polyacrylamide to nitrocellulose," *Journal of biochemical and biophysical methods*, vol. 10, 3-4, pp. 203–209, 1984.

[200] J. Rappsilber, M. Mann, and Y. Ishihama, "Protocol for micro-purification, enrichment, pre-fractionation and storage of peptides for proteomics using StageTips," *Nature protocols*, vol. 2, no. 8, pp. 1896–1906, 2007.

[201] J. Cox and M. Mann, "MaxQuant enables high peptide identification rates, individualized p.p.b.-range mass accuracies and proteome-wide protein quantification," *Nature biotechnology*, vol. 26, no. 12, pp. 1367–1372, 2008.

[202] J. Cox, N. Neuhauser, A. Michalski et al., "Andromeda: a peptide search engine integrated into the MaxQuant environment," *Journal of proteome research*, vol. 10, no. 4, pp. 1794–1805, 2011.

[203] S. Tyanova, T. Temu, and J. Cox, "The MaxQuant computational platform for mass spectrometry-based shotgun proteomics," *Nature protocols*, vol. 11, no. 12, pp. 2301–2319, 2016.

[204] M. E. Ritchie, B. Phipson, Di Wu et al., "limma powers differential expression analyses for RNA-sequencing and microarray studies," *Nucleic Acids Research*, vol. 43, no. 7, e47, 2015.

[205] W. Huber, A. von Heydebreck, H. Sültmann et al., "Variance stabilization applied to microarray data calibration and to the quantification of differential expression," *Bioinformatics (Oxford, England)*, 18 Suppl 1, S96-104, 2002.

[206] Y. Benjamini and Y. Hochberg, "Controlling the False Discovery Rate: A Practical and Powerful Approach to Multiple Testing," *Journal of the Royal Statistical Society: Series B (Methodological)*, vol. 57, no. 1, pp. 289–300, 1995.

[207] W. Stacklies, H. Redestig, M. Scholz et al., "pcaMethods--a bioconductor package providing PCA methods for incomplete data," *Bioinformatics (Oxford, England)*, vol. 23, no. 9, pp. 1164–1167, 2007.

[208] Y. BENJAMINI and Y. HOCHBERG, *CONTROLLING THE FALSE DISCOVERY RATE: A PRACTICAL AND POWERFUL APPROACH TO MULTIPLE TESTING*.

[209] C. Klöppel, C. Michels, J. Zimmer et al., "In yeast redistribution of Sod1 to the mitochondrial intermembrane space provides protection against respiration derived oxidative stress," *Biochemical and biophysical research communications*, vol. 403, no. 1, pp. 114–119, 2010.

ABBREVIATIONS

°C   Grade Celsius

5-FOA   5- Fluoroorotic acid

µg   Microgram

µl   Microliter

µM   Micromolar

AAA+   ATPases Associated with Diverse Cellular Activities

Amp   Ampicillin

Asn   Asparagine

ATP   Adenosine triphosphate

ADP   Adenosine diphosphate

Cam   Chloramphenicol

CES   control by epistasis of synthesis

CIP   Calf intestine alkaline phosphatase

CoRR   Colocation for redox regulation

ddH$_2$O   Double distilled water

DMSO   Dimethyl sulfoxide

DNA   Deoxyribonucleic acid

DTT   Dithiothreitol

DUMP   Deposits of unfolding mitochondrial proteins

E. coli   *Escherichia coli*

ECL	Enhanced chemiluminescence
EDTA	Ethylene diamine tetraacetate
ER	Endoplasmic reticulum
ERAD	ER-associated degradation
EtOH	Ethanol
FRAP	Fluorescence recovery after photobleaching
g	Gravity of earth
GFP	Green fluorescent protein
NG	mNeonGreen
GO	Gene Ontology
h	Hours
HA	Hemagglutinin
HEPES	4-(2-hydroxyethyl)-1-piperazine-ethane sulfonic acid
HF	High fidelity
HSE	Heat shock element
HSP	Heat shock protein
IDR	Intrinsically disordered region
IMiQ	Intramitochondrial protein quality control
IM	Inner mitochondrial membrane
IMS	Intermembrane space
INQ	Intranuclear quality control aggregates

IPOD	insoluble protein deposits
JUNQ	juxtanuclear quality control aggregates
Kan	Kanamycin
kDa	Kilodalton
LB	Lysogeny broth media
LLPS	Liquid-liquid phase separation
M	Molarity
MAD	Mitochondria-associated degradation
mg	Milligram
min	Minute
ml	Milliliter
mM	Millimolar
MPP	Mitochondrial processing peptidase
MRP	Mitochondrial ribosomal protein
mtCPR	Mitochondrial compromised protein import response
mtDNA	mitochondrial DNA
MTS	Matrix targeting signal
NEF	Nucleotide exchange factor
nm	Nanometer
OD_{600}	Optical density at 600 nm
OM	Outer mitochondrial membrane

P	Pellet aggregated fraction
PACE	Proteasome associated control element
PAGE	Polyacrylamide gel electrophoresis
PCR	Polymerase chain reaction
PDRE	Pleiotropic drug reporter element
PEG	Polyethylene glycol
PK	Proteinase K
polyA	poly alanine
polyN	poly asparagine
polyQ	poly glutamine
RNA	Ribonucleic acid
rpm	Revolutions per minute
Proteostasis	Protein homeostasis
RT	Room temperature
s	Seconds
S	Soluble fraction
S. cerevisiae	*Saccharomyces cerevisiae*
SDS	Sodium dodecyl sulfate
T	Total
TA	Tail-anchored
TBS	Tris-buffered saline

TCA	Trichloroacetic acid
TIM	Translocase of the inner membrane
TMT	Tandem Mass Tag
TOM	Translocase of the outer membrane
TR	Tandem repeats
TPR	Tetratricopeptide repeats
Tris	Tris-(hydroxymethyl)-aminomethane
U	Units
UPR	Unfolded protein response
UPR^{am}	Unfolded protein response activated by mistargeted proteins
UPR^{mt}	Mitochondrial unfolded protein response
UPS	Ubiquitin-proteasome system
w/v	Weight per volume
WT	Wild type
YFP	Yellow fluorescent protein

Table 11: List of S3 proteins used for Figure 23C.

Organism	Protein	N content
Mitochondrial, mitochondrially encoded		
Candida castellii	*YP_002836201.1*	*26.6%*
Candida glabrata	*NP_818776.1*	*31.3%*
Cyberlindnera mrakii	*P47906.1*	*18.7%*
Cyberlindnera suaveolens	*YP_008475117.1*	*19.4%*
Eremothecium gossypii	*NP_987081.1*	*24.8%*
Geotrichum candidum	*YP_009110266.1*	*22.1%*
Kazachstania unispora	*YP_009444501.1*	*20.4%*
Kluyveromyces lactis	*YP_054503.1*	*24.5%*
Komagataella phaffii	*CCA41182.2*	*19.1%*
Lachancea mirantina	*CCW77454.1*	*24.1%*
Magnusiomyces capitatus	*YP_009029705.1*	*22.9%*
Nakaseomyces bacillisporus	*YP_002836209.1*	*29.6%*
Saccharomyces cerevisiae	*NP_009320.1*	*31.9%*
Saccharomycodes ludwigii	*APD14981.1*	*31.4%*
Torulaspora pretoriensis	*AJG03009.1*	*25.9%*
Wickerhamomyces canadensis	*NP_038223.1*	*22.8%*
Wickerhamomyces pijperi	*YP_008475099.1*	*21.6%*
Monosiga brevicollis	*Q9G9H1_MONBE*	*14.8%*
Malawimonas jakobiformis	*Q9G889_MAJA*	*10.7%*
Cyanidioschyzon merolae	*Q9ZZN7_CYAME*	*9.9%*
Arabidopsis thaliana	*RT03_ARATH*	*5%*

Chloroplast, plastid-encoded

Cyanidioschyzon merolae	*RR3_CYAM1*	*3.4%*
Arabidopsis thaliana	*RR3_ARATH*	*5%*
Nicotiana tabacum	*RR3_TOBAC*	*4.1%*

Mitochondrial, nuclear-encoded

Danio rerio	NP_001018518.1	1.8%
Drosophila melanogaster	NP_524476.1	3.6%
Homo sapiens	NP_114403.1	1.8%
Rattus norvegicus	NP_001071127.1	1.8%

Bacterial

Bacillus cereus	WP_098545547.1	3.2%
Escherichia coli	HDS0101445.1	3.0%
Mycobacterium tuberculosis	WP_050185982.1	2.2%
Rickettsia prowazekii	NP_221017.1	5.5%

```
Var1         1 MKLKLLNMILSMMNKTNNNNNIIINNTLDSLMNKKLLLKNMLLDMNNKKM    50
               |||||||||||||||..:|.|||  |||||||||||||||||||..|||
Var1-N       1 MKLKLLNMILSMMNKTLTDNKIII--TLDSLMNKKLLLKNMLLDMTKKKM    48


Var1        51 NNMKRMLNNNNMNPAGANPVVHRIGPAGNINNKLQHLNNMNNWNTQIYNY   100
               |||||||.||.||||| |||||||||||||..|||||||||.:|||||||||
Var1-N      49 --MKRMLNNKNMKPAGA-PVVHRIGPAGNIGTKLQHLNNMYSWNTQIYNY    95


Var1       101 NKNMEIMNTMNDKLINKLLYKMMTLKLNNMNINKIIMSKTINQHSLNKLN   150
               ||.|||||||||||.||||||||.||||||||||||||||||||||||
```

110

```
Var1-N            96  NKTMEIMNTMNDKLINTLLYKMMTLKLLNMNINKIIMSKTINQHSLNKLN    145


Var1             151  IKFYYYNNDINNNNNNNNNNNYYMNMMNKLMNIMNNNMNNNLCNILSYYYK    200
                      ||||||||||||.|||..:|||||.|||||||||..||||.|||||||||
Var1-N           146  IKFYYYNNDINNMNNNQLDNYYMTMMNKLMNIMTINMNNYLCNILSYYYK    195


Var1             201  KKVTIEPIKLSYIYLNSDIFSKYISLNDMDKYNNGILTNYQRMLNNIMPK    250
                      |||||||||||||||||||||||||.||||||.|||||||||||.|||||
Var1-N           196  KKVTIEPIKLSYIYLNSDIFSKYISLLDMDKYNIGILTNYQRMLNIMPK    245


Var1             251  LNDHNISMNYINNINNINNNKYNNMINLLNNNNNINNNNNYNNNNNNYIG    300
                      |||||||||||||||..||.|||||||.||||..:|        .:.|||
Var1-N           246  LNDHNISMNYINNIYLINKNKYNNMILLLNNTLSI---------MSYYIG    286


Var1             301  NINNIYNNMTIDNIPMDILMYKYLVGWSIKFKGRLSNNNGRTSTTNLLNG    350
                      ||.|||.:||||||||||||||||||||||||||::.||||||.||||
Var1-N           287  NITNIYKSMTIDNIPMDILMYKYLVGWSIKFKGRLSSSKGRTSTTKLLNG    336


Var1             351  TFNNKKYLWSNINNNYKLNYIPSNHNLYNNSNINKNGKYNIKVKLNFI-    398
                      ||||||||||||||||||||||||||||||.||||||||||||||||||
Var1-N           337  TFNNKKYLWSNINNNYKLNYIPSNHNLYNLSNINKNGKYNIKVKLNFI*   385
```

Figure 39: Alignment of Var1 and Var1 with a lower asparagine content (Var1-N). Amino acid sequence of Var1 (top row) and a mutant with deleted and exchanged amino acids in non-conserved regions to reduce the asparagine content to 18.5%. Alignment was done with EMBOSS Needle.

ACKNOWLEDGMENTS

hat. Egal ob spontane Yoga-Zooms, lustige Fotoshootings, der epische Kampf gegen deine Balkon-Taube, die Zeit mit dir hat mir immer auf das neue Kraft gegeben. Ich bin sehr dankbar dafür, dass ich in schönen und schwierigen Momente immer auf deine Unterstützung bauen konnte. **Tamara**, für dich gibt es scheinbar keine Hürde, die nicht zu meistern wäre. Deine entspannte Art und Positivität sind einfach ansteckend. Deswegen hätte es auch mit keinem anderen so viel Spaß gemacht, die Entwicklermaschine von Algen zu befreien und anschließend wieder mit giftigen Chemikalien zu füttern. Ich schätze deine ehrliche Rückmeldung, besonders dann, wenn ich über das Ziel hinausschieße! Ich hoffe, dass wir unsere gemeinsamen Dance-Pausen und Rotweinabende noch viele Länder und Städte sehen werden! Und danke dafür, dass du mich überzeugt hast, mir ein Rennrad zuzulegen. (Auch wenn ich jetzt verstehe, warum es ein Risikosport ist.) Einen Riesen Dank gilt dir **Carina**! Deine Willensstärke und kreativen Ideen inspirieren mich immer wieder. Deine Selbstsicherheit und dein Durchsetzungsvermögen und direkte Art, Probleme anzugehen sind ein großes Vorbild für mich. Außerdem war es immer wieder spannend, mit dir Nachmittags auf zufällige Themen zu stoßen, über die man ewig diskutieren konnte. Deine Art, die Dinge anzupacken, ist bewundernswert!

Christian, Danke für die Hilfe beim Auswerten meiner Proteomics-Daten. Auf deine Unterstützung konnte ich vertrauen, nicht nur bei R-Fragen. Egal ob ich auf der Suche nach Englisch-Vokabeln oder einem speziellen Paper war, du wusstest immer einen guten Rat. Deine Meinung habe ich immer geschätzt. Ich bin dankbar dafür, dass wir den Weg unseres PhDs gemeinsam gehen konnten.

Anna-Lena, ich finde es schön, dass du Katzen so sehr liebst- vielleicht sogar mehr als ich. Die täglichen Katzen-Snaps zaubern mir immer ein Lächeln ins Gesicht und versüßen mir den Tag! Ich finde es beeindruckend, wie du deinen Weg von deinem Master zur PhD-Studentin meisterst und bin dankbar dafür, dich bei diesem Weg begleitet zu haben. Weiter so! Ich werde es vermissen, morgens mit dir über das Leben, und alles was dazugehört zu plaudern.

Katha, ich habe die Zeit mit dir genossen. Deine Kreativität, deine Liebe zur Fotografie und Tieren haben mich immer wieder beeindruckt. Ich bin dankbar dafür, mit dir unseren Abenteuer- oder auch Albtraum Campingausflug gemacht zu haben. Unvergesslich!

Anna Probst, ich freue mich darüber, dass du mir damals schon in deiner Bachelorarbeit beim Zurechtfinden in der BioTech geholfen hast und wir uns anschließend immer wieder über den

Weg gelaufen sind. Danke für Abende mit Sushi, Heimwege und andere Gelegenheiten; immer mit tollen Gesprächen!

Yura I am glad that you joined our group in Kaiserslautern. I really appreciate your guidance and support in finding my way in science.

Connie, Simone, Sabine, Vera, Andrea ohne euch wäre die Zellbiologie nicht das, was sie ist. **Connie**, es ist wunderbar, jeden Morgen mit deiner positiven Stimmung begrüßt zu werden. **Simone** ohne deine Unterstützung wäre ich hilflos in den ganzen Anträgen und Formularen untergegangenen. **Sabine**, du ist ein ganz besonderer Ruhepol, ich finde es toll, wie du dich für so viele Themen begeistern kannst. Danke, dass ich deine Hühner kennenlernen durfte, das hat mir sehr viel Freude bereitet. **Vera**, ich bin froh, mit dir ein Labor geteilt zu haben, egal wie spontan, du hast mich immer bei meinen Experimenten tatkräftig unterstützt. **Andrea**, die Sorge um das Grundpraktikum hat uns zusammengeschweißt. Gute Kommunikation ist unser Ding. Danke dafür, dass du immer den Zeitplan im Blick hattest, alles bis ins kleinste Detail geplant und mir dadurch auch den Rücken freigehalten hast! Danke euch allen für eine tolle Zeit!

Saskia danke dafür, dass du aus einer vollen Schale immer wieder die schärfste Paprika gefunden hast, und die mentale Unterstützung beim Plasma-Spenden, wenn auch beides nicht immer zu deiner Freude war. Ich möchte mich außerdem für dein offenes Ohr und unsere gemeinsame Radtour bedanken!

Senvja, ich bin so dankbar, dass du für mich so manchen Studenten übernommen hast und beeindruckt mit welcher Geduld du dich ihnen gewidmet hast. Außerdem finde ich es toll, mit welcher Motivation du täglich bei der Quiz-Runde dabei ist.

Büsra, deine Freude und Luftsprünge sind ansteckend. Behalte das bei!

Azkia and **Nikita**, thank you so much for the culinary treats you brought to the lab. I really enjoyed it. **Azkia,** I am very thankful for your open ear and helpful advice regarding microscopy and my future. Dear **Nikita**, I am so grateful you did not snap my neck, even though you would find it satisfying. I really enjoyed joking around with you. **Pavel,** you are one of a kind. It took some time to get to know your sense of humor. But thank you very much for teaching us all about non-verbal communication.

Danke **Lorenz** dafür, dass du unsere tägliche Quiz-Runde im Labor eingeführt hast. Von „Quess The Audio" zu „Wordle", dadurch hat sich eine tolle Teambuilding-Aktivität gebildet. Außerdem bin ich froh, dass du uns alle vom Swingolfen überzeugen konntest. Und sich daraus noch ein toller Abend in der Stadt ergeben hat.

Ein Dank an alle Studenten, die ich Betreuen durfte. Ich habe so viel dadurch gewonnen. **Uli**, ich habe es genossen, dich im Master zu begleiten, deine Umsicht und Sorge für die Ausbildung von anderen konnte ich immer wieder wertschätzen. **Tim**, ich danke dir für die Unterstützung an meinem Projekt. **Basti**, auch wenn du nur für eine kurze Zeit bei uns in der Zellbiologie verbracht hast, hat es mich beeindruckt, wie du immer alles gibst.

Als letztes möchte ich meiner ganzen Familie von Herzen danken, die mich immer auf meinem Lebensweg unterstützt hat. Ganz besonders möchte ich meiner Mutter danken. Ich schätze mich glücklich darüber, dass du mich immer ermutigt hast, meinen eigenen Weg zu suchen und das zu tun, was mir Freude bereitet. Ich bin dankbar dafür, dass du uns immer alle Optionen offengehalten hast und uns beide bei jedem Schritt unserer Reise begleitet hast.

CURRICULUM VITAE

Lea Tamara Bertgen

Place of birth   Neustadt/Weinstraße, Germany

Education

Since 11/2019   **PhD Studies**, University of Kaiserslautern

Cell Biology

Supervisor: Prof. Dr. Johannes Herrmann

"*Distinct types of intramitochondrial protein aggregates protect mitochondria against proteotoxic stress*"

10/2017 – 09/2019   **Master of Science**, University of Kaiserslautern

Molecular Cell Biology

Cell Biology

Supervisor: Prof. Dr. Johannes Herrmann

"*Aggregationsverhalten des mitochondrial kodierten Proteins Var1 in Saccharomyces cerevisiae*"

10/2014 – 08/2017   **Bachelor of Science**, University of Kaiserslautern

Biowissenschaften

Cell Biology

Supervisor: Prof. Dr. Johannes Herrmann

"*Konplementierung einer mitochondrialen Deletion durch nukleäre Lokalisierung des Gens*"

08/2006 – 07/2014   **Allgemeine Hochschulreife**,

Käthe-Kollwitz-Gymnasium, Neustadt/Weinstraße

Secondary school diploma qualifying for university admission

Other scientific training

2019 – present	**Supervision**, University of Kaiserslautern
	Cell Biology
	Supervision of practical courses, bachelor and master students.
02/2017	**Internship**, Julius Kühn-Institut Siebeldingen
	Mycology

Awards

11/2022	**Best Poster Award**
	ISF Workshop Mitochondria Past, Present Evolution, Proteostasis, Dynamics and Disease